PHOTOMETRIC STUDIES OF STARBURST GALAXIES

A Thesis Submitted to

The Gujarat University

in partial fulfillment

for

THE DEGREE OF DOCTOR OF PHILOSOPHY

in

PHYSICS

by

APARNA A. CHITRE

PHYSICAL RESEARCH LABORATORY
NAVRANGPURA
AHMEDABAD 380 009
INDIA

March 1999

CERTIFICATE

I hereby declare that the work presented in this thesis is original and has not formed the basis for the award of any degree or diploma by any University or Institution.

A. Chitre

Aparna A.Chitre

(Author)

Astronomy and Astrophysics Division
Physical Research Laboratory
Navrangpura
Ahmedabad - 380 009 (India)

CERTIFIED BY

U.C. Joshi

Prof. Joshi U.C.

(Thesis Supervisor)
Associate Professor
Astronomy and Astrophysics Division
Physical Research Laboratory
Navrangpura
Ahmedabad - 380 009 (India)

To Aai-Baba...

Contents

Acknowledgements

I would like to thank my thesis supervisor Prof. U.C. Joshi for introducing me to the joys of observational astronomy. He has patiently observed with me on several nights in Mt. Abu and Nainital and trained me in the basics of data reductions. His enthusiasm has been a great source of inspiration. He was always ready to answer my questions no matter how busy he was with other comittments. I also wish to thank Prof. M.R. Deshpande for generous allocation of telescope time. Shashi has been a great help during observations and I am grateful to him. I am grateful to Mr. N.M. Vadher for maintaining the CCD camera in top shape and helping out with any problems and Mr A.B. Shah for software related aspects of the instrument. I thank Dr. Bruno Guiderdoni of IAP, Paris, for providing the model spectra and for the useful discussions I had with him in person and over e-mail. Our librarian, Mrs. Uma Desai has helped a lot in procuring the latest bibliographic material.

I acknowledge the staff at PRL and particularly at Thaltej for their co-operation. Thanks are due to the staff at the observatory in Mt. Abu.

Friends at PRL have always been very helpful. I am grateful to my dear friends, Kunu and Kamath for standing by me through thick and thin. Their support has always been a morale booster and helped me go on through difficult times. Watson has been a great senior, always ready to help. I thank him for his help and for the number of useful discussions I had with him. Nandu's enthusiasm never failed to cheer me up. I had a pleasant time with Nandu and Muthu. I thank Poulose for help with programming during the initial stages. Outings and movies with friends have been the bright spots in the otherwise monotonous life of this research scholar. I enjoyed all the functions and celebrations at the PRL hostel.

Without the encouragement and support of my family, this thesis would not have been possible. Last but not the least, I thank Anil for being by my side.

List of Tables

List of Figures

Chapter 1

Introduction

Haro initiated a new fundamental direction in astrophysics with his discovery of several galaxies with compact regions showing large uv excess in the continuum and strong emission lines (Haro 1956). Following Haro's methods and using the 1-m Schmidt at the Byurakan observatory, Markarian and his co-workers conducted an objective prism survey and compiled an optical sample of 1500 objects with blue excess and a strong uv continuum; published as 15 lists (Markarian 1983 and references therein). A photometric study by Weedman (1973) of Markarian galaxies selected from the first four lists showed that only those objects classified as Seyferts emit significant nonthermal continua from their nuclei. The strong blue and uv continua emitted by the remaining large fraction of objects is thermal in origin, as indicated by narrow low-ionization emission lines. This implies that these galaxies have a large population of hot, blue stars. The term "starburst" was first coined by Weedman (1973) to describe such galaxies experiencing episodes of star formation that are too intense to be sustained over the lifetime of the galaxy. In these galaxies, the rate of star formation is much higher as compared to that in normal galaxies (Larson 1987). The burst of star formation produces a large number of massive stars which completely dominate the luminosity of the galaxy. Massive stars emit copiously in the ultraviolet. Radiation from massive stars can be absorbed by dust and re-emitted in the form of IR radiation. Observationally, starburst galaxies are typically selected on the basis of their emission-line spectrum (Sargent & Searle 1970), their blue optical colours (Balzano 1983) or their infrared colours (Soifer et al. 1987). Starbursts are characterized by strong HII line emission and a stellar

continuum dominated by O and B stars in the blue wavelengths. Huchra (1977a), in his aperture photometric studies on a sample of non-Seyfert Markarian galaxies found that they were bluer for their morphological types and they generally get bluer towards their center, unlike other galaxies. He also put forth the idea that the UBV colours of these galaxies could be explained by superimposing a burst of star formation on an old galaxy population. Larson & Tinsley (1978) were the first to suggest that "bursts of star formation" could be triggered as a result of tidal forces in interacting galaxies.

Markarian galaxies are more luminous in the far-infrared than normal spirals and their infrared luminosities are well correlated with L_B and $H\alpha$ suggesting that they are a sub-set of the infrared selected galaxies and happen to be relatively dust free along the line of sight but not necessarily in other directions (Deutsch & Willner 1986).

1.1 *The Starburst Phenomena*

The essential characteristic of a starburst is the conversion of a large amount of gas into stars in a time much shorter than the evolutionary timescale. For a starburst to occur in a galaxy, two conditions have to be necessarily satisfied, one being the reduction in the timescale for star formation and the other being an increase in the efficiency. Durations as short as 20 Myr have been inferred for starbursts in galaxies (Larson & Tinsley 1978; Kennicutt et al. 1987). In some of the best studied starbursts like M82, it has also been inferred that most of the gas in the burst region is consumed by star formation, at least if a normal IMF is used. The star formation timescale is inversely proportional to the mass surface density while the SFR per unit area is directly proportional to the mass surface density and inversely proportional to the timescale. Hence, the star formation rate per unit area becomes directly proportional to the square of the mass surface density. A reduction in the timescale by two orders of magnitude as has been inferred for many starburst

would require an increase in the mass surface density by two orders of magnitude to at least 1000 $M_{\odot}/pc^2$. The best evidence for global populations of young stars comes from IRAS. Much of the recent work on starbursts was prompted not by the optical surveys but by the discovery of a large number of IR luminous galaxies by IRAS. The infrared luminosities and L/M ratios of some of the galaxies discovered by IRAS appeared to be too high to be sustained over their lifetimes. Rieke & Low (1975) carried out a detailed mapping and photometric study of the nucleus of the nearby starburst galaxy, NGC 253. They were the first to conclude that the near infrared flux was generated by stars. They found the M/L ratio in the nucleus to be significantly less than 1 and concluded that if the IR emission was powered by thermonuclear burning of the mass, the present level of emission could not be sustained for the life of this galaxy. They also proposed that the strong IR emission from this and many other spirals may be occurring in episodes. Rieke et al. (1980) constructed a grid of models for starbursts and used their NIR data along with other published data on M82 and NGC 253 to constrain starburst models of the energetic nuclear sources in these galaxies. The high energy photons from the massive stars heat the surrounding interstellar dust, and this radiation is re-emitted in the thermal infrared, in the spectral region 10-300 μm. Since the absorption cross-section of the dust is strongly peaked in the ultraviolet, this far infrared (FIR) emission can be a sensitive tracer of the star formation rate (SFR) and is responsible for the high FIR luminosities observed for these IR selected galaxies.

1.2 *Triggers of the starburst*

The search for environmental factors that might trigger a burst of star formation has a long observational and theoretical history (Sulentic et al. 1990). A variety of mechanisms have been proposed to explain the starburst phenomenon (Schweizer 1986; Scalo & Struck-Marcell 1986). Much of the effort has focussed on the role of galaxy-galaxy interactions in giving rise to activity in the galactic nucleus. Global non-axisymmetric perturbations can play a key role in channeling gas to the central

regions and feeding the activity. Theoretical models have contributed substantially to our understanding of how it is possible to build up enormous concentration of gas in the centers of merger remnants (Barnes & Hernquist 1992; Mihos & Hernquist 1994). The onset of a starburst in the central regions of galaxies requires a high concentration of gas in this region, which in turn requires a large-scale dynamical disturbance to cause the gas in the galaxy to lose angular momentum and fall rapidly towards the center. Numerical simulations indicate that gas flows towards the centers of galaxies in response to tidal perturbations and the resulting dissipation of angular momentum (see Barnes & Hernquist 1992 and references therein). In their numerical simulations of disk galaxies which accrete a low-mass dwarf companion, Mihos & Hernquist (1994) find that in response to the tidal perturbations of an in falling satellite galaxy, the disk galaxy develops a strong two-armed spiral structure, which in turn drives large quantities of disk gas into its central regions. They find that the global star formation rate remains constant during the early stages of the accretion, before rising rapidly by an order of magnitude when the central density becomes very large and gives rise to a compact starburst. Gravitational interactions and mergers seem to play a major role in triggering starbursts, but violently interacting galaxies are not necessarily the seat of starbursts (Bushouse 1986) and most starbursts seem to be isolated (Coziol et al. 1997). Besides tidal interactions, the presence of other non-axisymmetric gravitational perturbations like those produced by stellar bars or oval distortions can also induce radial gas flows. If an Inner Lindblad Resonance (ILR) exists, the flow of the gas towards the center is halted and funneled into a ring at this location. Numerical simulations have confirmed the effectiveness of both tidal interactions (Icke 1985; Noguchi & Ishibashi 1986) and bars (Schwarz 1984, Combes & Gerin 1985). Such mechanisms to explain the inflow of gas have been discussed by Simkin et al. (1980); Friedli & Benz (1993) and Heller & Shlosman (1994). Shlosman et al. (1989) proposed bars and bars within bars as possible mechanisms for fueling the central region in AGN. Secondary bars have been observationally detected by de Vaucouleurs (1974) in NGC 1291 and NGC 1326. Heraudeau et al. (1996) have also

detected bars in the central regions of galaxies from NIR surface photometry. Fully consistent 3D simulations by Friedli & Martinet (1993), have also revealed the formation of misaligned secondary bars within the primary bar. Small curved dust lanes or molecular bars close to the nucleus might also indicate the presence of a non-axisymmetric gravitational field. In all cases, a departure from axial symmetry in the mass distribution produces gravitational torques that alter the angular momentum distribution of the gas, allowing matter to flow inwards. Combes (1998) gives a detailed discussion of the various triggers giving rise to a starburst.

Toomre & Toomre (1972) put forward the idea of the production of elliptical galaxies through the mergers of disks and since then several attempts have been made to study the characteristics of merger remnants and compare them with ellipticals (Dressler 1984). A number of models based on numerical simulations of mergers of disk galaxies were able to reproduce fine structure like ripples or faint shells that have been observed in many ellipticals (Schweizer 1983).

1.3 *Optical studies of starburst galaxies*

In the optical region, starburst galaxies are identified by their emission line spectra resembling HII regions. Aperture photometric studies of Huchra (1977a) showed that these galaxies generally get bluer towards their centers. However, aperture photometry is only capable of providing information about the integrated properties of the galaxy. No information about the spatial distribution of the star forming regions or the structure of the galaxy hosting the burst can be derived from this kind of data. A spatially resolved study through various spectral bands is necessary to study the detailed photometric properties of the galaxies, the locations and the distribution of the star forming regions with respect to the underlying galaxy and the structure of the galaxy hosting the starburst phenomenon. A spectrophotometric survey of starburst nuclei from the Markarian sample was conducted by Balzano (1983) wherein she studied the spectra of the nuclear regions and reported

the emission line fluxes in the nuclear regions of Markarian galaxies with a nuclear starburst. However, this does not include a few starburst cases like Mrk 332 which show intense extra nuclear star formation. Contini et al. (1998) present optical long-slit spectroscopic observations of barred Markarian starburst galaxies and find that 62% of starburst nuclei are isolated and show no sign of gravitational interactions. A detailed morphological study of a large sample of starburst galaxies is required to identify the triggering phenomena in these objects. In terms of distance, luminosity and level of interaction, these galaxies are intermediate between HII galaxies and luminous IR galaxies. Images of ultraluminous IRAS galaxies have shown that many of these galaxies undergoing a starburst are interacting and show the presence of tails, bridges and other features indicative of a merger or an interaction.

1.4 Multiwavelength studies

Starburst galaxies emit radiation almost at all frequencies right from radio to X-ray. The spectral energy distribution of starbursts from X-ray to radio and the spectral features characteristic of starburst galaxies can be found in the detailed review by Moorwood (1996).

Radio emission from starburst galaxies is a mixture of free-free continuum from HII regions and synchrotron radiation from supernova generated electrons interacting with the interstellar magnetic field (Condon et al. 1982; Mass-Hesse & Kunth 1991). Condon & Dressel (1978) noticed that the compact radio sources tend to occur more frequently in paired galaxies and they suggested that an existing nucleus is triggered into activity by the gravitational interaction. Hummel (1980) found that the radio continuum in the nuclei of interacting galaxies was enhanced by a factor of 2-3 as compared to isolated spirals. Condon et al. (1982) interpreted the radio continuum morphology of a class of "bright radio spiral galaxies" as

evidence for powerful nuclear starbursts; the majority of which seemed to be triggered by galaxy-galaxy interactions. Observations of Markarian galaxies by Chini (1987) at 1.3 mm show that the luminosity of the starburst follows $L \propto M_g^{0.72}$; where M_g is the gas mass. This implied that the basic parameter for the strength of the activity is the gas mass.

IRAS has revealed a class of extraordinarily luminous interacting galaxies that appear to be starbursts (Soifer et al. 1984; Lonsdale et al. 1984). Surveys of interacting galaxies in the mid-infrared (Joseph et al. 1984; Lonsdale et al. 1984; Cutri & McAlary 1985) revealed an enhancement (by a factor of 2-3) of infrared emission in interacting systems as compared to isolated galaxies. Joseph & Wright (1985) identified a subset of advanced mergers in the Arp atlas with extremely strong mid-infrared emission that they described as "ultraluminous" infrared galaxies. They argued that super starbursts may occur in the evolution of most mergers. Starburst galaxies are found to have a tight correlation between the FIR and the radio luminosities (Wunderlich et al. 1987; van den Driel et al. 1991; Franceschini et al. 1988; Condon et al. 1991). Stine (1992) studied a sample of Markarian starburst galaxies at 6cm and 20 cm and found that the correlation between the global radio and IR emission for this sample is strongest at 25 and 60 μm wavelengths in which the warm dust dominates. Deutsch & Willner (1987) studied a sample of Markarian starburst galaxies in the FIR and they found that these galaxies are more luminous and have higher colour temperatures than normal spirals. They also found that the FIR emission correlates well with the total blue luminosity, the nuclear blue luminosity and the nuclear Hα luminosity. In the near infrared, starbursts are characterized by strong recombination lines of hydrogen (Brγ at 2.166 μm) and helium (2.06 μm). The shape of the continuum is like that of a late-type giant or supergiant star with a deep CO band absorption at 2.3 μm. The J band contains Paβ (1.282 μm) in strong emission and the H band is dominated by [FeII]λ 1.644 μm usually attributed to supernova remnants. The uv continuum is dominated by massive OB stars and P-Cyg profiles are seen. Starburst regions without any sign of P Cygni profiles are attributed to less massive, later type O or B stars.

The X-ray emission in starburst galaxies comes from the contributions of the massive binaries, supernova remnants, starburst driven winds and inverse Compton scattering of farinfrared photons by relativistic electrons which are all strongly correlated with the supernova rate. X-ray observations of peculiar galaxies by Fabbiano et al. (1982) show that the emission is extended in nature and the fluxes are compatible with the levels of massive star formation implied by ultraviolet and optical data.

1.5 *Modelling studies*

Since the late 1970's, evolutionary synthesis models have been used for interpreting the observed colours, spectra, chemical composition etc. of galaxies. Evolutionary population synthesis models aim at predicting the observed properties of a stellar population at different times of its evolution. Model stellar atmospheres along with stellar evolution theory are used to follow the evolution of a population of stars with a certain IMF and the resultant properties like the spectrum, the line strengths, the magnitudes and colours are predicted. These are compared with the observed values for any particular object to estimate the age of an observed burst in a galaxy. The first generation of evolutionary models of stellar population was based on colours of stars and gave the integrated colours of the galaxies. These photometric models were introduced by Tinsley (1972) and Searle et al. (1973), to interpret the visible colours of galaxies in the Hubble sequence. An interpretation of peculiar blue galaxies by a burst of star formation superimposed on an old galaxy was given by Larson & Tinsley (1978). They showed that the colours of Markarian starburst galaxies could be explained by the superposition of a young burst on an old galaxy and derived star formation rates for a large sample of isolated and interacting galaxies from UBV colours.The models were improved by predicting a nebular component (Huchra 1977b), with a metal-deficiency effect and far UV colours (Rocca-Volmerange et. al 1981). Worthey (1994) constructed detailed sets of models for intermediate age and old stellar populations. Leonardi

& Rose (1996) present a technique for accurately determining the ages of starbursts in post starburst galaxies. They use the strength of the CaIIH + Hϵ absorption feature relative to that of CaIIK to separate effects of burst strength from burst age. A detailed review on evolutionary synthesis from UV to IR is given by Bruzual (1996).

1.6 *This investigation*

The aim of this work is to investigate the photometric and structural properties of starburst galaxies. A spatially resolved study has been conducted to explore the morphological structure and the locations of star forming regions with respect to the underlying galaxy. This has been studied using surface photometry of the objects through various pass bands. We present, in detail, the morphological study of a sample of 19 starburst galaxies of the Markarian survey, based on $UBVRI$ and Hα imaging. The contour maps of the galaxies are presented in different bands to study the morphological appearance of the galaxies at different wavelengths. Colour maps were constructed to shed light on the distribution of various stellar populations, namely the young stellar population and the old underlying population in the galaxy and to map the dust. The spatial distribution of regions of massive star formation has been explored through Hα narrow band imaging. The global radial distribution of star forming sites was studied by performing simulated concentric aperture photometry on the Hα images. Pseudo equivalent widths were derived to estimate the ratio of the current to recent past star formation rates on a global scale as well as their distribution with increasing distance from the nucleus.

The surface brightness distribution of the galaxies in various pass bands was derived by fitting elliptical isophotes to the galaxy images. The structural properties of the starburst galaxies were studied to derive information about the underlying galaxy. Structural details were investigated using isophotal analysis.

The colour profiles were used to study the global distribution of the star forming regions. Faint fine structure was extracted from the galaxy images to get information about non axisymmetric structures, vestiges of mergers or interaction induced alterations in the galaxy structure which could be possible causes of triggering the starburst. A variety of techniques were used for the analysis of the data and the interpretation of the results. Structural parameters like half-light radii and disk scale lengths were derived.

Composite models were constructed to estimate the ages of the burst and the mass contribution to the burst. This involved the superposition of an instantaneous burst on an old galaxy. Two models were constructed for the old galaxy. In one case, the old population was taken to be coeval and in the other case, the old population was an actively evolving one. The age and strength of the burst in each galaxy was estimated.

Chapter 2

Observations and Data Reduction

Summary

In this chapter, the details of the CCD and the filter system used for observations are described. We discuss the criteria for sample selection and outline the general observing procedure. The basic data reduction and calibration procedures are explained. We also discuss the photometric accuracy and the limiting magnitudes reached by our photometry. In addition to this, procedures used for correcting the data for galactic extinction and the reddening within the program galaxy are also explained.

2.1 *The sample*

The sample of starburst galaxies for the present study was drawn exclusively from the Markarian lists. Starburst galaxies with visual magnitudes brighter than $14^m.5$ were selected. The visual magnitude constraint was put so that frames with a good signal-to-noise ratio could be obtained with the 1.2m telescope and the broad band filters used with reasonable integration times. No consideration was made for any particular morphological type. Thus, the sample is unbiased towards the Hubble type or any other morphological features. The other criterion was the angular extent of the object. Galaxies having angular sizes smaller than 20″ were not considered as with the given plate scale, a galaxy of diameter 20″ would occupy less than 30 pixels and meaningful surface photometry could not be performed at this scale and this would render the detection of structures on smaller scales difficult. The perception of the morphology is dependent on the redshift. So we constrained ourselves to a redshift less than 0.02. The sample of galaxies is presented in Table 2.1 along with some global properties of the galaxies namely the co-ordinates, the morphological type, the redshift and the linear scale of the galaxy in pc per arcsec.

2.2 *Instruments*

Thanks to the availability of modern instruments, advances were possible in the morphological analysis of galaxy images. Observational improvements are of four types : improved angular resolution, improved wavelength coverage due to the construction of detectors sensitive at different wavelengths, the linearity and the large dynamic range given by the CCD detectors. CCD cameras, with their large dynamic range and higher sensitivities have become the most popular instruments for imaging purposes. Since CCDs are linear detectors over a very large dynamic range, they permit the simultaneous imaging of the very high surface brightness as well as low surface brightness regions. Starburst galaxies generally have a

Table 2.1: Sample of starburst galaxies

GALAXY	α (2000)	δ (2000)	TYPE[a]	z	Linear scale[b] pc/″
Mrk 14	08:10:59.1	72:47:41	S0?	0.0105	203
Mrk 87	08:21:41.2	73:59:23	SB0/a	0.0094	182
Mrk 190	11:51:47.0	48:40:53	S0/E	0.0033	64
Mrk 213	12:31:20.5	57:57:47	SBa	0.0105	203
Mrk 332	23:59:25.6	20:45:15	SBc	0.008	155
Mrk 363	01:50:58.0	21:59:50	Scp	0.0099	192
Mrk 439	12:24:35.8	39:22:56	Sa	0.0035	68
Mrk 449	13:11:30.8	36:16:52	Sap	0.0037	72
Mrk 602	02:59:50	02:46:17	SBbc	0.0095	184
Mrk 603	03:08:57.3	-02:57:07	E	0.0090	174
Mrk 708	09:42:11.3	04:40:24	SB	0.0059	114
Mrk 743	11:38:12.9	12:06:43	E0p	0.0033	64
Mrk 781	12:53:50.7	09:42:33	SBc	0.0094	182
Mrk 799	14:00:45.6	59:19:42	dbl	0.0094	182
Mrk 1002	01:37:17.5	05:52:38	E1	0.0105	203
Mrk 1134	23:46:58.5	29:27:34	I0	0.0172	333
Mrk 1194	05:11:46.2	05:12:01	SB0	0.0158	306
Mrk 1308	11:54:12.2	00:08:11	S0	0.0035	68
Mrk 1379	14:17:40.3	-07:25:03	SBbc dbl	0.0094	183

[a] Markarian catalog (downloaded from CDS)

[b] Calculated using H_0=75 $kms^{-1}Mpc^{-1}$

Table 2.2: Filter details.

Band	Components (thickness in mm)	Central Wavelength μm
U	UG 1 (1) + S86 12 (2) + FILL (2)	0.36
B	BG 37 (3) + BG 39 (1) + GG 395 (1)	0.43
V	BG 40 (3) + CG 495 (2)	0.55
R	OG 570 (3) + KG 3 (2)	0.66
I	RG 9 (2) + FILL (3)	0.84

very high surface brightness nucleus, while the outer regions of the galaxy and the underlying structures have a low surface brightness. Therefore, the large dynamic range of a CCD can be used to advantage in imaging starburst galaxies. Mean radial profiles in these cases can have sufficiently high signal-to-noise ratio, such that the effects of bars, spiral arms, dust, warps and asymmetrical rings of star formation can modulate their radial luminosity profiles appreciably. We used a thinned, back illuminated Tektronix 1024x1024 pixels CCD chip for imaging the program objects. The efficiency of back-illuminated CCDs is greater than the front-illuminated ones. Thinning the substrate increases the sensitivity of back-illuminated CCDs in blue which is required for the present program since the we wanted to study the strong blue continuum in these starburst galaxies. However, thinning reduces the sensitivity in the red.

The sample of galaxies for this thesis were observed at the Cassegrain focus of the 1.2 m telescope at Gurushikhar, Mt.Abu. The f-ratio of this telescope at the Cassegrain focus is f/13 , giving a plate scale of $15''\text{mm}^{-1}$ at the focal plane of the telescope. There is a provision to operate the CCD at various sensitivities. We used two sensitivity settings: The high sensitivity setting, with a gain of $0.8e^{\ominus}$/ADU was used for observations between October 1996 and December 1996, while the low sensitivity option with a gain of $4e^{\ominus}$/ADU was used for all subsequent observations. The resolution of the CCD is computed to be $0.317''pixel^{-1}$. On chip binning of 2x2 was employed keeping in mind the data storage requirements. The final resolution was $0.634''pixel^{-1}$ and the typical seeing was between 1.2"-2" so, the point spread function (PSF) was sampled appropriately. The field of view provided by the chip was 5'.2× 5'.2. Broad-band UBV Johnson's filters and RI Kron-Cousins filters with diameters of 50 mm were used for the observations. The response curves of the filters are given in Fig. 2.1. The response of the filters was combined with the response of the CCD and the resultant response curves are presented in Table 2.2. For Hα imaging, both on-band filters for sampling the line emission and off-band filters for estimating the underlying continuum were used. Narrow band filters with FWHM $80A^{o}$ were used for the on-band and off-band

measurements.

2.3 *Observing procedure*

CCD images were obtained for the sample galaxies during several observing runs between October 1996 and April 1997 through broad band $UBVRI$ and narrow band Hα filters. The observations were carried out under photometric conditions with typical seeing of 1.5". Each observation through each filter was broken up in to 3 to 5 separate exposures. The exposure times for a single exposure ranged typically from 120 seconds to 300 seconds. The total integration times are presented in Table 2.3 along with the dates of observation. Standard stars were observed throughout the night sandwiched between galaxy observations to cover a large range in airmass. The FWHM of the redshifted Hα filter was 80 A^o , so contamination by [NII] λ 6548-84 emission was unavoidable. For obtaining the pure line emission, the underlying stellar continuum has to be correctly estimated and subtracted. For this, off-band observations were made in addition to the on-band observations. Bias frames were taken in groups of 25 frames at a time and combined to construct the average bias. Combining a large number of frames reduces the read noise by a factor of $(1/(\sqrt{n}))$ where n stands for the number of frames combined. Sky flats were taken every night during twilight for each observing run. A minimum of 15 flats were taken in each filter. The exposure time was set so as to get more than 10,000 counts per pixel. A master flat was constructed using all the flats taken during the observing run which was typically 4-5 days.

2.4 *Notes on individual galaxies*

The appearance of the galaxies in the direct images is described below:

1. **Mrk 14** : This S0 galaxy appears smooth without any apparent signs of distortions.

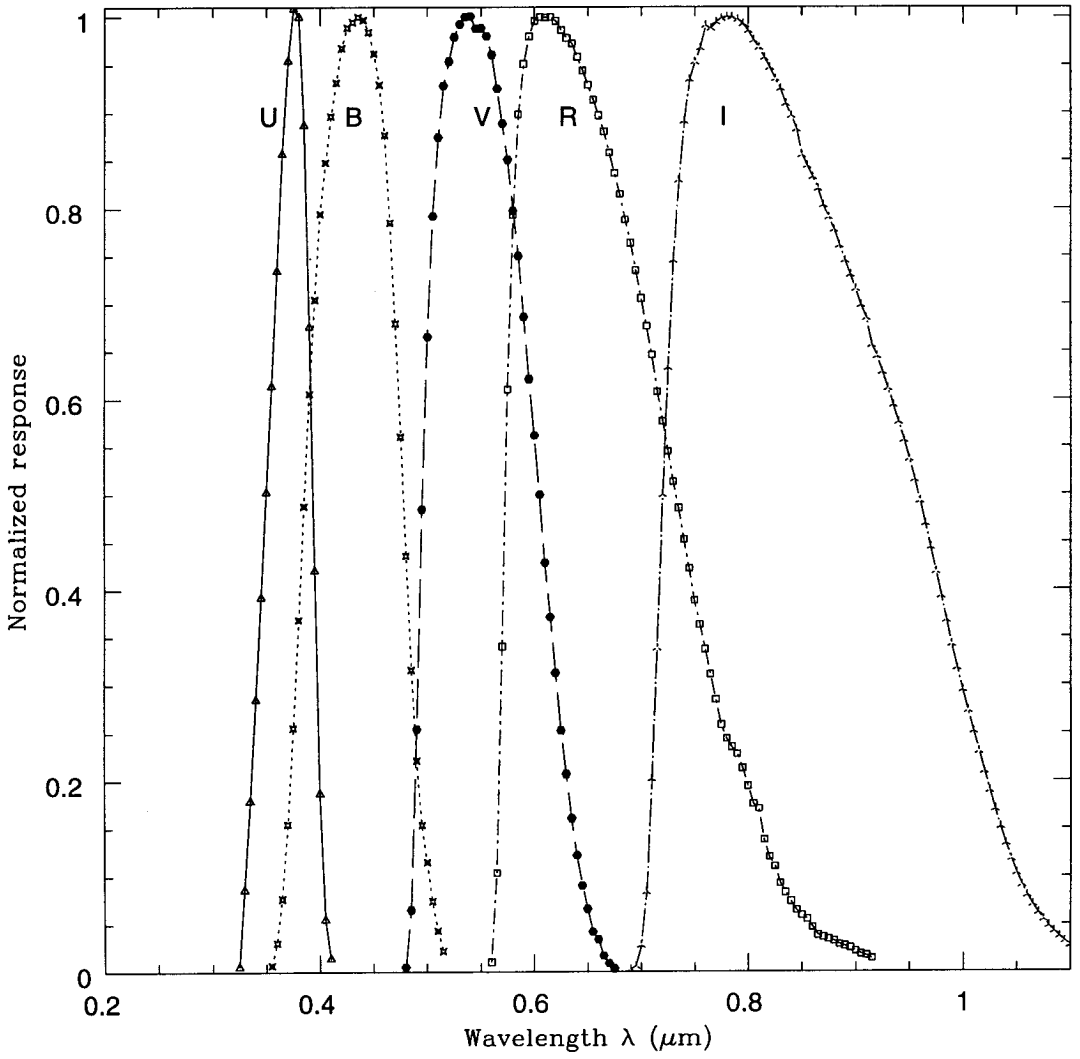

Figure 2.1: The response curves of the U, B, V, R, I filters used. These represent the response of the filters for this CCD+filter combination together.

2. **Mrk 87** : This is a barred galaxy with a ring surrounding the bar. A companion is seen towards its NE.

3. **Mrk 190** : The galaxy image appears smooth and nearly circular.

4. **Mrk 213** : This SBa galaxy shows a thin spiral arm emerging from the south eastern end and curving around towards the north western side where it is attached to an almost stellar condensation.

5. **Mrk 332** : This spiral galaxy has been classified variously as barred and unbarred in different catalogues. It shows two distinct and bright spiral arms with a number of condensations in them.

6. **Mrk 363** : This galaxy has been classified as a peculiar spiral.

7. **Mrk 439** : This is a peculiar spiral galaxy.

8. **Mrk 449** : This edge-on spiral shows a dust lane at an angle to the minor axis.

9. **Mrk 602** : This is a spiral with a prominent bar.

10. **Mrk 603** : This is a member of a nest of interacting galaxies.

11. **Mrk 708** : This is an elongated spiral galaxy with many superimposed stars.

12. **Mrk 743** : This peculiar E0 galaxy shows the presence of two nuclei surrounded by a common envelope.

13. **Mrk 781** : This is a barred spiral. It is the only flocculent spiral in our sample.

14. **Mrk 799** : This barred spiral shows asymmetric and distorted spiral arms. A superassociation exists at one end of the bar. A small satellite galaxy is seen near the southern side of this galaxy.

15. **Mrk 1002** : This E/S0 galaxy appears smooth. A foreground star is present near its north eastern edge.

16. **Mrk 1134** : This irregular galaxy lies at the end of one of the spiral arms of a larger spiral galaxy forming a M51 type of system.

17. **Mrk 1194** : This is a barred spiral with a high inclination to the line of sight.

18. **Mrk 1308** : This is a small nearby galaxy of S0 type extending about half an arc minute. It has a small linear companion located at 30″ towards the west.

19. **Mrk 1379** : This galaxy is a VV object (Vorontsov-Velyaminov 1977), with nests of interacting objects. It is a barred spiral galaxy.

2.5 *Data Reduction*

The CCD data was reduced using various tasks in IRAF[1] on the IBM-6000 RISC system at PRL, Ahmedabad. The bias frames and the flats were used to determine the read noise and the gain of the system in $e^{\ominus}$/ADU using the FINDGAIN task within IRAF. All the data were reduced using the same basic procedure, a detailed explanation of which can be found in Massey & Jacoby (1992). First, an average bias frame was constructed using ZEROCOMBINE and subtracted from all the frames to compensate for the bias level. Master flats were constructed in each filter by combining and scaling the individual flats using FLATCOMBINE. All the images were flat fielded using the task CCDRED. After correcting for bias and flat-fielding, the images were cleaned of cosmic rays using the task COSMIC in IRAF. The sidereal time of observation was computed using the UT and the latitude and longitude of the observatory within the package ASTTIMES. The airmass was determined from these values and the co-ordinates (RA and DEC) of the object. Corrections for the airmass were applied using the extinction coefficient obtained from the transformation equations (see Section 2.6).

After the individual object and the standard star frames were processed using CCDRED, the separate exposures were aligned. For observations taken at a stretch on the same night, the frames were first aligned using IMSHIFT which shifts the frames in the x and y direction using foreground stars in the frame. In case of observations taken on different nights, the frames were first corrected for small rotations that could have been introduced while remounting the instrument on the telescope. This was done using GEOMAP, a task which computes the centroids of the stars in the galaxy frame and then rotates and shifts the images according to the given reference image. The IMCOMBINE task was then used to median combine the images by filter, using average sigma clipping to remove bad pixels. In cases where we had only two usable images in a filter, averaging of the

[1]IRAF is distributed by National Optical Astronomy Observatories, which is operated by the Association of Universities Inc. (AURA).

Table 2.3: Journal of observations.

Galaxy	Date observed	Exposure time (secs)					
Mrk		U	B	V	R	I	Hα
14	4,5FEB97	2640	1380	660	480	600	2100
87	7APR97	1500	1200	360	360	360	1420
190	5APR97	1800	800	480	360	720	1800
213	4,5FEB97	3000	1500	720	660	660	2100
332	4NOV96	3600	1160	360	300	300	1800
363	6NOV96	1500	1020	360	360	320	1500
439	5MAR97	1400	510	360	360	360	1600
449	6APR97	1800	900	450	450	600	1800
602	9DEC96	1620	1320	360	240	600	2040
603	4FEB97	900	900	200	320	240	1200
708	9DEC96	2400	2000	1200	1300	400	1500
743	7APR97	1800	800	450	420	360	1500
781	6FEB97	1200	800	600	520	560	1200
799	27JAN,6FEB97	3000	3000	2400	1950	1800	2400
1002	4NOV96	2400	1200	550	300	300	1200
1134	8DEC96	1500	720	240	360	360	1320
1194	6APR97	2400	900	600	300	300	1200
1308	6APR97	1800	800	450	360	480	1800
1379	7FEB97	1320	1000	360	360	520	1200

two frames was done. Co-adding of frames improves the signal-to-noise ratio of the observations. The combined images were scaled by exposure and the mean exposure times of the resultant images were noted. The sky background was computed from the mode of the histogram of each image. Since the field of view was large enough as compared with the program objects, the histogram was sky dominated. After sky correction, the images were scaled to one second exposure before transforming them to the standard system.

In case of Hα images, the off-band and the on-band images were also shifted, combined and scaled to 1 second exposure using the same procedure as that for the broad band images. To account for small changes in the transmission of the on and the off-band filters, the mean ratio of the intensities of the foreground stars in the on and off-band images was determined. About 5 to 6 stars were used for determining this mean value. This was used to scale the off-band image. This image was then subtracted from the on-band image to give a pure emission-line image, free of underlying continuum light. Care was taken to smooth the images to the same PSF before subtraction to avoid spurious positive or negative regions in the final image. A final image with properly removed stars i.e. with neither positive nor negative residuals at the locations of stars is an indication of an accurate continuum subtraction.

2.6 *Photometric Calibrations*

Standard stars from Landolt (1992) were observed throughout the night for calibrating the broad-band data. In order to sample a wide range in magnitudes and colours, care was taken to choose standard stars ranging from $8^m.0 < V < 15^m.0$ and $-0.20 < (B-V) < +1.00$, so that the colour dependence term in the transformation equations could be accurately calibrated. Fifteen stars were selected in this way for each observing run. After performing the basic reductions of bias and flat correction and cosmic ray removal, the airmass was determined as described in the

previous section. These frames were ready for analysis. The standard stars were first identified using DAOFIND. When there were many stars in the frame, this was done interactively. The radial profile of each star was first plotted to confirm that it had not saturated or drifted during the exposure. Aperture photometry was performed on these stars using the PHOT task in IRAF. Apertures ranging from 3 x FWHM to 5 x FWHM were centered on the star and an annular region was taken around the star for estimation of the sky background. The mode of the pixel values in the sky annulus was determined and this sky level was subtracted from the total counts in the aperture. A PHOT instrumental magnitude was computed using the equation :

$$m_{phot} = -2.5\log[\Sigma(C/t)] + m_0 \tag{2.1}$$

where C are the residual counts within the aperture after subtracting the sky value, t is the exposure time and m_0 is the arbitrary zero point value which we set to 25. The PHOTCAL package was used to set up the configuration file and the transformation equations. The form of the transformation equations is :

$$\begin{aligned}
mu &= U + u1 + u2 * Xu + u3 * (U - B) + u4 * (U - B) * Xu \\
mb &= B + b1 + b2 * Xb + b3 * (B - V) + b4 * (B - V) * Xb \\
mv &= V + v1 + v2 * Xv + v3 * (B - V) + v4 * (B - V) * Xv \\
mr &= R + r1 + r2 * Xr + r3 * (V - R) + r4 * (V - R) * Xr \\
mi &= I + i1 + i2 * Xi + i3 * (R - I) + i4 * (R - I) * Xi
\end{aligned} \tag{2.2}$$

where mu, mb, mv, mr, mi correspond to the instrumental magnitudes; $u1, b1, v1, r1, i1$ are constants; $u2, b2, v2, r2, i2$ are the extinction coefficients; Xu, Xb, Xv, Xr, Xi correspond to the airmass at which the observations were taken in U, B, V, R, I respectively ; $u3, b3, v3, r3, i3$ are the colour dependent coefficients; $u4, b4, v4, r4, i4$ are the second order colour terms which are very small and are assumed to be zero in the present analysis. The upper cases stand for the standard values of magnitudes and colours. Least squares fitting was done to transform the instrumental values to the standard values. The mean values of the coefficients are tabulated in

Table 2.4: Transformation Coefficients

coeff	3-6Nov96	7-10Dec96	4-6Feb97	5Mar97	5-7Apr97
u1	4.07	6.36	6.40	6.65	6.79
u2	0.65	0.65	0.74	0.74	0.74
u3	-0.14	-0.12	-0.21	-0.16	-0.16
b1	1.77	4.07	4.05	4.26	4.29
b2	0.4	0.4	0.52	0.52	0.542
b3	0.04	-0.13	-0.05	-0.05	0.01
v1	1.36	3.54	3.56	3.78	3.84
v2	0.15	0.15	0.3	0.3	0.3
v3	-0.07	-0.07	-0.05	-0.04	-0.09
r1	1.29	3.45	3.39	3.60	3.66
r2	0.10	0.10	0.33	0.33	0.33
r3	-0.08	-0.10	-0.09	-0.05	-0.05
i1	1.55	3.73	3.73	3.99	3.97
i2	0.07	0.07	0.24	0.24	0.24
i3	-0.04	-0.08	-0.03	-0.06	0.14

Table 2.4. In Table 2.4, the coefficients obtained for the first run (3-6Nov96) differ from the coefficients obtained in the subsequent runs because the CCD was operated at a different sensitivity setting during the first run as described in Section 2.2. The dominant contribution to the galaxy images in the U band is from star forming regions. Also, the extinction is high in U. Hence the U band images show a patchy structure and were not used in deriving global properties and comparing with the images at other wavelengths. The typical errors in the transformed magnitudes are 0.03 in B, 0.03 in V, 0.02 in R and 0.04 in I. The Hα images were obtained only for tracing the regions of massive star formation and to study the relative intensities of the emission with respect to the underlying continuum. Hence, no absolute calibration was performed for these images.

2.7 *Interstellar Extinction and Inclination Corrections*

The light suffers extinction as it travels through interstellar space in our galaxy as well as within the program galaxy. The observed magnitudes are thus fainter due to this extinction. Corrections for interstellar extinction have been made as follows: The extinction within our galaxy is dependent on the galactic latitude (b) of the object. The values for galactic extinction in B (A_B) and the reddening E(B-V) were taken from Burstein & Heiles (1984). For galaxies which did not have values tabulated, we calculated (A_B) using the following equation from Aaronson et al. (1980).

$$A_B = 0.133[\csc(b) - 1] \tag{2.3}$$

The extinction in other wavebands can be calculated using this value and the standard extinction curve (Seaton 1979). The extinction within the program galaxy is determined using the relation from Tully (1988).

$$A_B^i = -2.5\log\left\{ f(1 + e^{-\tau \sec i}) + \frac{(1-2f)(1-e^{-\tau \sec i})}{\tau \sec i} \right\}$$
$$\tau = 0.55; f = 0.25 \tag{2.4}$$

where i is the inclination of the galaxy to the line of sight.

2.8 *Photometry limits*

The mean values of the sky was found by considering boxes of 5×5 pixels at various locations of the blank sky. For each frame the sky brightness was determined by averaging these mean values measured within several areas around the galaxy. The typical values of sky brightness are 20, 19.5, 18.9, 17.3 mag/arcsec^2 in B, V, R and I bands respectively. The rms noise in the sky sets the limits on the depth of the photometry. The rms noise in the sky corresponded to 24.5, 23.9, 23.8 and 23.0 mag/arcsec^2 in the B, V, R and I bands respectively.

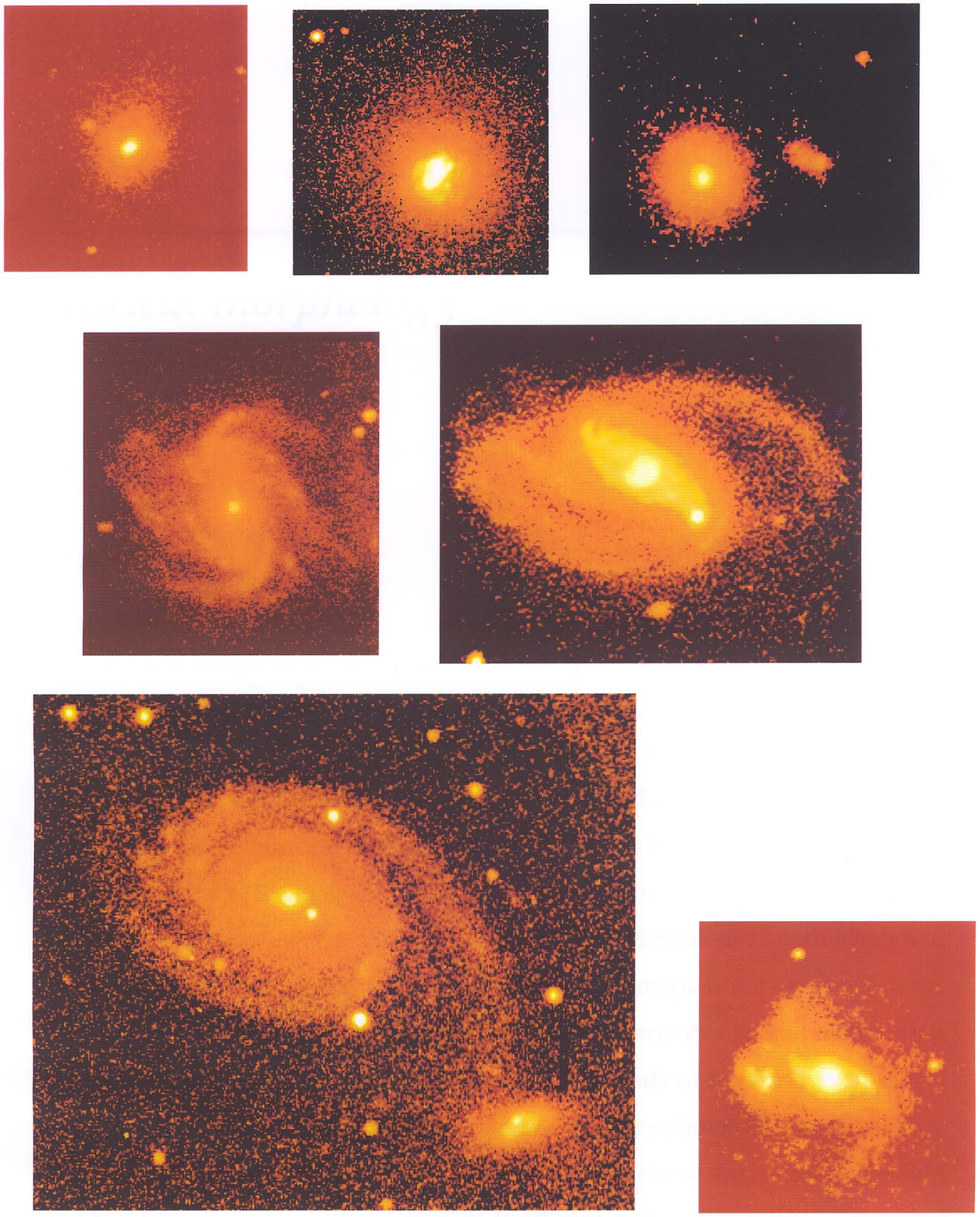

Figure 2.2: Some of the sample galaxies depicting the varied morphologies. Left to right: Top panel: Mrk 14, Mrk 439, Mrk 1308; Middle panel: Mrk 781 and Mrk 799; Bottom panel: Mrk 1134 and Mrk 1379. North is at the top and East to the left.

Chapter 3

Optical morphology

Summary

Optical CCD images of the sample of starburst galaxies from the Gurushikhar 1.2 m telescope are presented in the form of contour maps and colour images. The emission line Hα images are also presented. We discuss the morphology of the starburst region and the underlying host galaxy based on the analysis of the contour maps, the colour and Hα images. We can broadly group the galaxies into three types : S0's/E's, spirals and irregulars/peculiars based on their morphology. The contours of most of the galaxies show some distortions in their isophotes. The presence of young stars as traced by the colour maps is not confined to the nuclear region alone but their distribution shows a variety of spatial distribution in the form of blue rings, superassociations at the ends of bars and even global star formation. The Hα emission shows a variety of morphologies and we classify them into four basic types and describe the characteristics of the emission. We find that in a few cases, the peak of emission is off-centered with respect to the optical nucleus.

3.1 *Optical Morphology*

Starburst galaxies are a very inhomogeneous morphological class of galaxies where the common property is the dominant starburst component. Observations of star forming galaxies reveal an obvious relation between the star formation rate and dynamical features. The possible association between nuclear activity and galaxy morphology has interested many workers (Sersic & Pastoriza 1967; Heckman 1978; Simkin et al. 1980). The dynamical processes experienced by a galaxy get reflected in its morphology. Thus the study of the morphology of a galaxy is basically a study of its dynamical history. Since most of the visible light in a galaxy is produced by stars, the morphology traces the stellar populations and its appearance varies at different wavelengths, depending on the stellar populations contributing to the luminosity in that waveband. For instance, in the R and the NIR bands, a spiral galaxy appears smooth, while in the U and B bands, the spiral arms look thinner, ragged and show clumpy star forming regions. An inspection of a photographic atlas of barred galaxies reveals a variety of unique star formation properties - star forming knots concentrated along the bar or in spiral arms emanating from the bar. Giant HII regions are often present at the extremities of bars or in conspicuous hot spots in nuclear or resonance rings. The association of nuclear starbursts with stellar bars strongly suggests that it arises as a consequence of a bar-related phenomenon e.g. a resonance. The inner Lindblad resonance (ILR) in particular, is expected to be the site of enhanced molecular cloud density and star formation in the central region of barred spiral galaxies (Combes & Gerin 1985). The location of the ILR depends on the form of the mass distribution and is expected to be closest to the nucleus in galaxies with the highest central mass concentration.

It has been observed that nuclear starbursts occur preferentially in early-type barred spirals (Devereux & Hameed 1997). Elmegreen et al. (1990) present evidence that radial mass-transfer and star formation during an encounter can

change an unbarred late-type galaxy into a barred early-type galaxy. This might explain why nuclear star formation is so rare in late-type spirals. They give statistical evidence to prove that galaxy interactions produce strong spirals, which because of their torques lead to bar formation and a significant mass inflow in the disk. For a prolonged encounter, the mass inflow can apparently change a non-barred galaxy of intermediate Hubble-type Sbc-Scd, to a barred galaxy of early Hubble type SBa-SBb by increasing the density in the inner region and by removing a significant amount of the gas mass and star formation from the outer disk. The most spectacular starbursts occur in tidally interacting galaxies and mergers. Interactions with companion galaxies or merger processes leave their signature in the form of peculiar structures like distortions in the galaxy isophotes, tails, bridges, double nuclei, etc. Dynamical interactions and mergers can be responsible for periods of enhanced star formation (Larson & Tinsley 1978; Sharp & Jones 1980). Theoretical models have added substantially to our understanding of the merger process, in particular by demonstrating how it is possible to build up enormous concentrations of gas in the centers of merger remnants. The numerical simulations of Toomre & Toomre (1972) were successful in reproducing the tails observed in the Antennae by considering gravitational interactions and tidal forces. Numerical simulations now reproduce many features seen in starburst galaxies, including their disturbed morphologies and gas inflows fueling the starburst. Tidal forces have bipolar symmetry in the perturbed galactic disk which represent the differences of attraction forces from the companion over the whole disk. An attraction excess on one side and a corresponding lack on the other disrupt the disk. When the two interacting galaxies have equal masses, the two internal spiral features form a bridge, which will soon be accreted by one of the galaxies, the two external spiral arms will spread out in the form of two antennae, which will subsist in 1 or 2 million years (Combes 1987). Two famous examples are The Antennae (NGC 4038-9) and The Mice (NGC 4676 A-B).

Though many of the optically selected starburst galaxies show peculiar morphologies, there are many cases where neither apparent evidence of interaction nor

the presence of non-axisymmetric structures like bars or oval distortions is evident on visual inspection. A detailed morphological study of the underlying galaxy and its structure is essential in addressing such cases and determining the cause of the burst especially in such cases where no apparent signatures are seen. A spatially resolved study of a sample of starburst galaxies will aid in understanding the underlying structure of the galaxy hosting the starburst. The morphology of the star forming regions can provide insights into the triggering mechanisms, while the morphology of the underlying component gives an indication of the nature of the gravitational potential well in which the starburst occurs.

3.1.1 Morphology of the sample objects

As mentioned in Chapter 2, we have selected the sample objects with a variety of Hubble types. A visual inspection of the direct images reveals that the objects show a number of morphological peculiarities. The early type galaxies generally show smooth outer structure. Many of them like Mrk 190 and Mrk 439 appear circular in long exposures. However, their inner regions show a variety of non axisymmetric structures or clumpy central regions. These structures are clearly brought out in the contour maps presented in Fig. 3.1a-s . A double nucleus is seen in one of the galaxies, Mrk 743. Non concentric outer envelopes are also seen in many of the objects belonging to this class. Such non concentric isophotes around galaxies present the strongest evidence for perturbations resulting from tidal interactions between galaxies. Using N-body simulations, Borne (1984) and Aguilar & White (1986) have shown that strong asymmetric envelope distortions can result from tidal interactions between galaxies. A displacement of the nucleus from the center of its envelope will quickly decay away and thus, this must reflect recent tidal perturbations.

Our sample contains 10 spirals. Of these, 8 are barred spirals. The spirals generally show disturbed, asymmetric spiral arms or sometimes, as in the case of Mrk 799, three spiral arms. Mrk 332 and Mrk 449 are the two spirals which show

neither a companion nor the presence of a bar. The appearance of the isophotes changes at different wavelengths. At shorter wavelengths, they appear clumpy due to the presence of star forming regions and dust, while they have a smoother appearance at longer wavelengths.

The irregulars/peculiars show highly distorted isophotes especially in the central regions. Some objects like Mrk 1134 show a clumpy structure throughout the body.

We discuss the morphological characteristics of each of the objects in detail in Section 3.4.

3.2 *Colour Maps*

Colour maps are good tracers of the stellar populations in a galaxy. Broad band photometry is relatively easy to obtain and gives an immediate impression of the spectral energy distribution of the galaxy. The star formation rates at two different epochs, namely a period about 10^9 years ago and the present time can be traced by the B luminosity and the Hα luminosity respectively. Hence, a comparison of broad band colour images like $(B-V)$ or $(B-I)$ and the Hα images can lead to an estimation of how the recent star formation history of a galaxy has taken place in different regions (Márquez & Moles 1994). The $UBVR$ colours are dominated by the mixture of the intermediate mass main sequence stars ($\sim$ 5-10 $M_\odot$) and disk giants ($\sim$ 0.8-3 $M_\odot$). Colours have been used to estimate the stellar population of galaxies (Searle et al. 1973; Tinsley & Danly 1980; Frogel 1985; Peletier & Valentijn 1989; Silva & Elston 1994). The spatial distribution of colours can be used to trace the locations of enhanced star formation activity, dust and stellar populations. The spatial organization of the star forming complexes can be a clue to the mechanism controlling the burst. A spatially resolved study through various passbands will help us understand the physical processes controlling star formation in such a dynamic environment. Previous studies by Hodge (1975) and Keel et. al (1985)

indicate a tendency for star formation to be concentrated around the nuclear region in interacting galaxies, although there are cases where there is significant star formation taking place at other locations.

3.2.1 *Construction and interpretation of colour maps*

The colour maps were constructed by dividing the intensity images in two bands and calibrating them using the transformation equations described in Section 2.6. To conduct a spatially resolved study of the stellar populations and the distribution of dust, we constructed $(B-V)$, $(V-R)$ and $(B-I)$ colour maps. The colour maps were constructed after matching the PSFs in the two bands to avoid artifacts. This was achieved by degrading the better of the PSFs in the two bands by using a gaussian smoothing filter. The colour maps thus obtained were examined to identify features like star forming regions, dust lanes, etc. and study their photometric properties and their locations with respect to the underlying galaxy. The $(B-I)$ colour map is presented in the fourth panel in Figs. 3.1a-s. The grey scales have been chosen to maximize the contrast over the range of colour indices. Nearly all the galaxies in our sample show a blue nucleus indicating relatively higher star formation in this region as compared to the rest of the galaxy. In some cases, the nucleus does not appear blue which may be due to obscuration by dust or a dominant redder population, but the presence of massive stars in this regions can be deduced from the presence of Hα emission (which suffers lesser attenuation) in this region. Mrk 363 and Mrk 1134 show global star formation while Mrk 332 shows intense star formation in the spiral arms and Mrk 799 shows intense star formation at one end of the bar, in addition to the nucleus. In general, the galaxies show more small-scale irregularities in the B band. This is due to two causes : (a) The distribution of young stellar population, which is distributed imhomogeneously in general and is more emissive in the blue and (b) the non-uniform distribution of dust, more effective in producing blue extinction than red. The colour maps convey two types of information whose combination can make interpretation quite

complex. The redder regions correspond to either an older population or obscuration by dust. Qualitatively, it is often possible to distinguish between these two effects (Prieto et al. 1992a,b) using the results of the ellipse fitting analysis, which will be dealt with in the next chapter.

3.3 *Hα images*

The Hα emission from giant HII regions is a good tracer of OB star formation. The presence of Hα emission from gas is a sign-post indicating that at least one massive star has formed there recently. Massive stars emit Lyman continuum photons which ionize the surrounding hydrogen. In the subsequent recombination process, Balmer photons are emitted. Measurement of the integrated Balmer photon flux provides a direct estimate of the Lyman continuum luminosity and the corresponding OB star formation rate (SFR). These regions show Hα in emission, which has been used extensively by Kennicutt (1983) to derive SFRs in spirals. The regions of emission, thus delineate the location of star forming giant molecular clouds and the gas involved in star formation. Their locations can be used to detect the effects of perturbing forces which is supposed to be responsible for the anomalously high gas densities , subsequently leading to the triggering of the burst. In particular, the HII regions reflect the recent dynamic influence on the gas because of their short lifetimes (Hodge 1975).

3.3.1 *Spatial distribution of star forming regions*

The sample of galaxies was observed with appropriately red shifted narrow band filters which were centered at red-shifted Hα. The large scale patterns of star formation were studied using continuum subtracted emission line images. A visual inspection of continuum subtracted Hα images shows that all the galaxies except Mrk 439 and Mrk 1194 show the nuclear region intensely in emission, signaling the presence of massive stars in the central region. On the basis of the emission-line

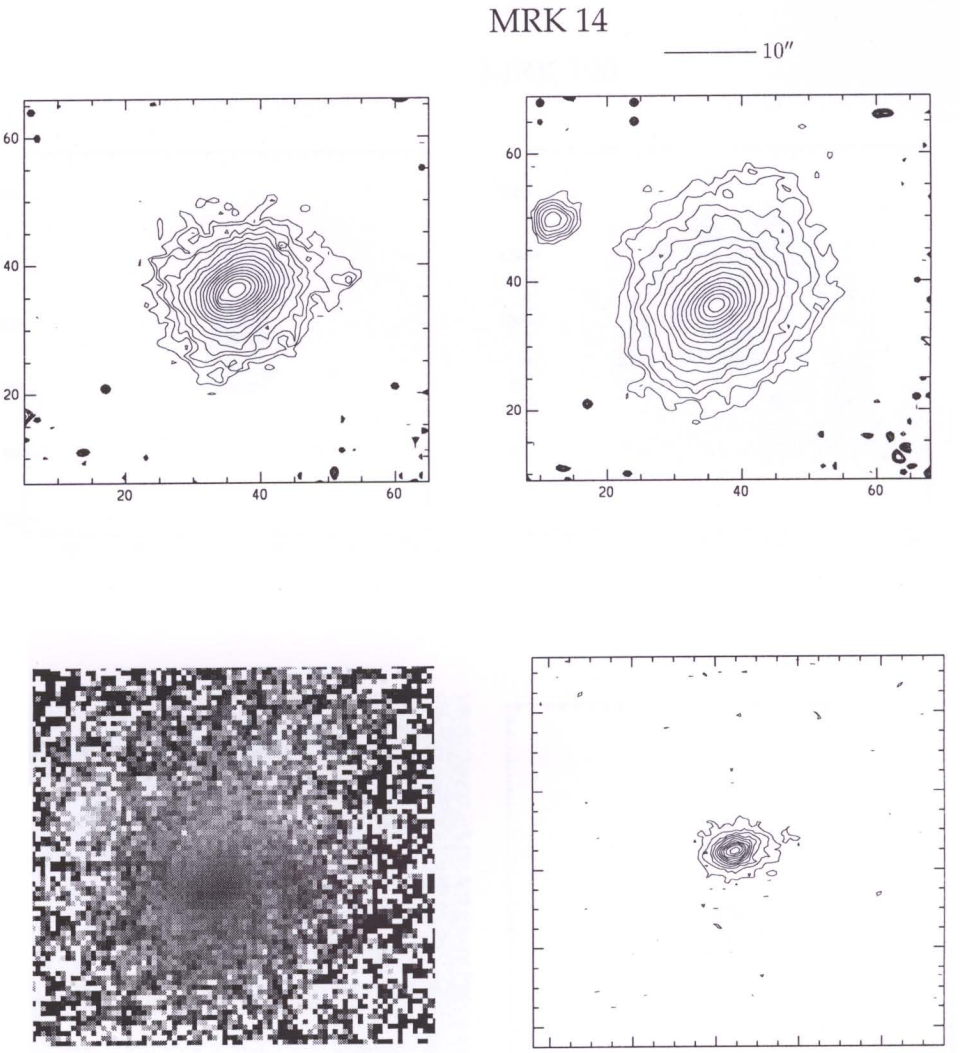

Figure 3.1a

Figure 3.1: Top row : left: B isophotal contours, right: I isophotal contours. Bottom row : left : $(B-I)$, right : Hα isophotal contours. North is at the top and East is to the left. Contours are plotted at intervals of $0^m.25$ with the faintest one at 3σ of the background. The same order is followed in the figures (a) to (s).

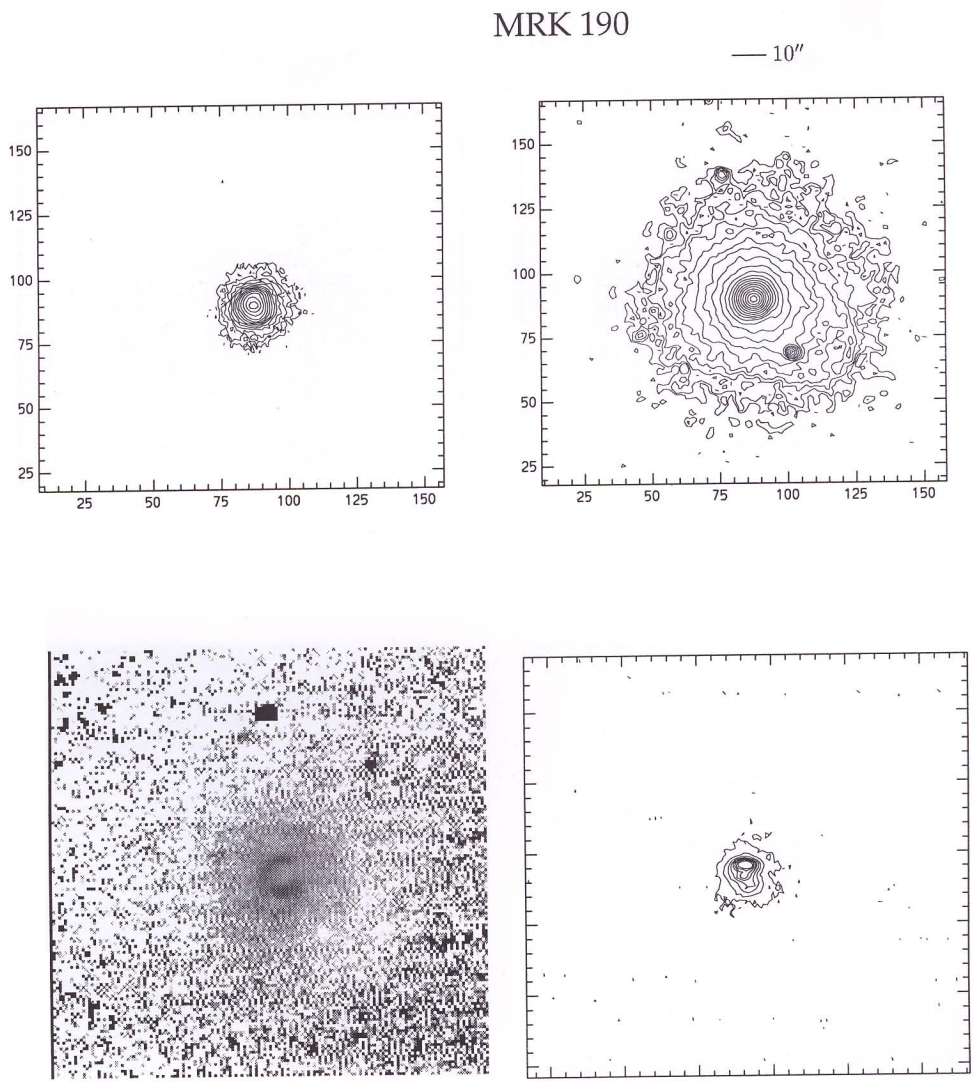

Figure 3.1b

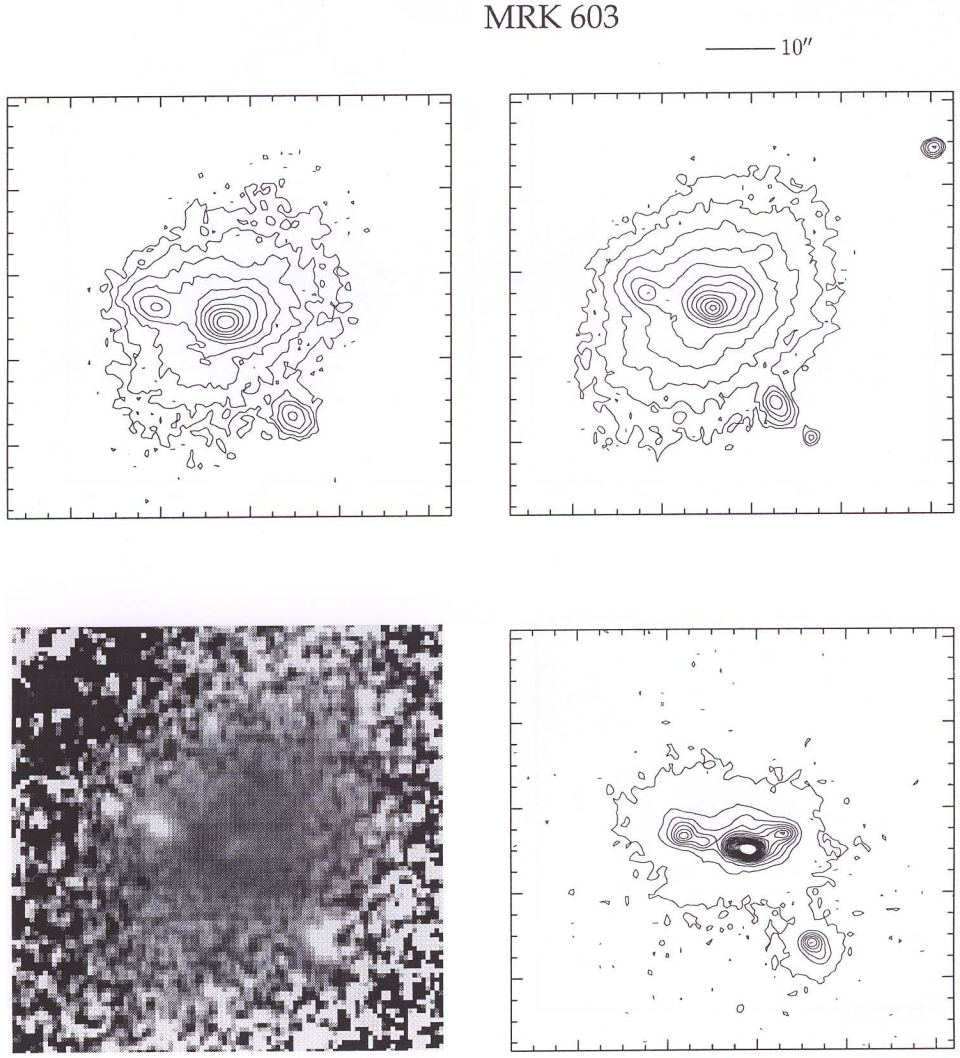

Figure 3.1c

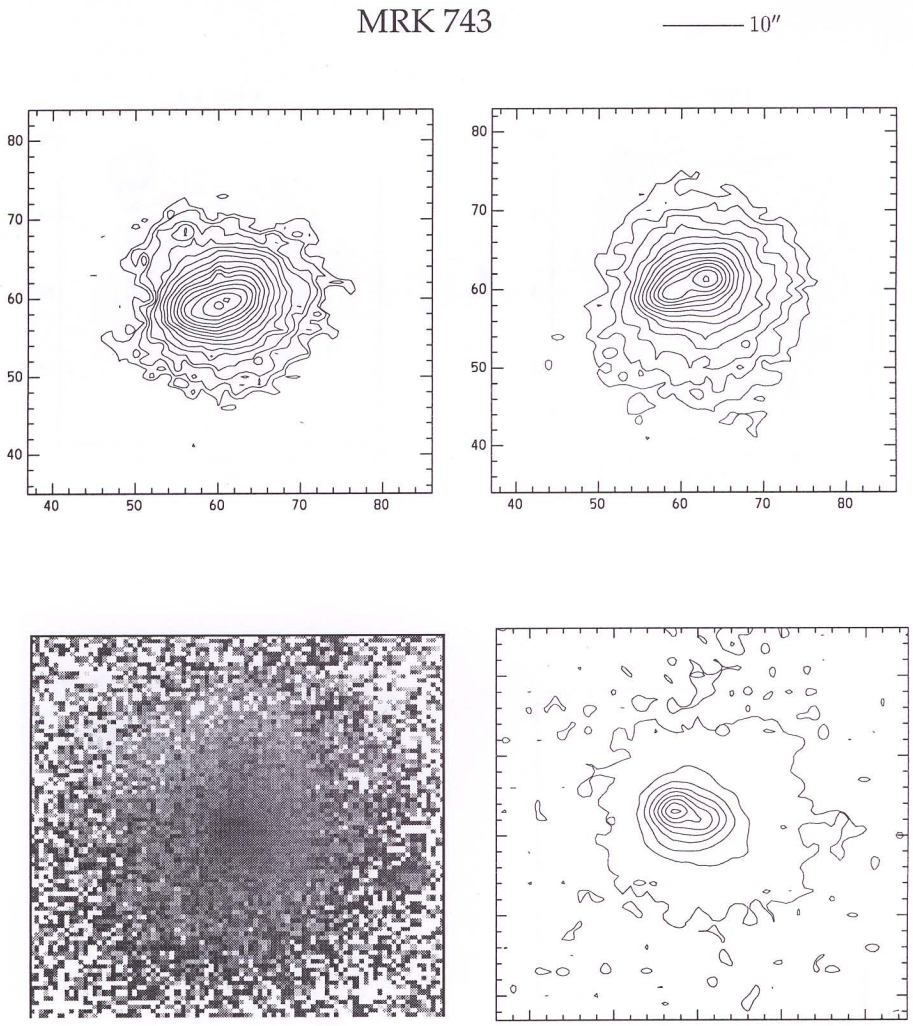

Figure 3.1d

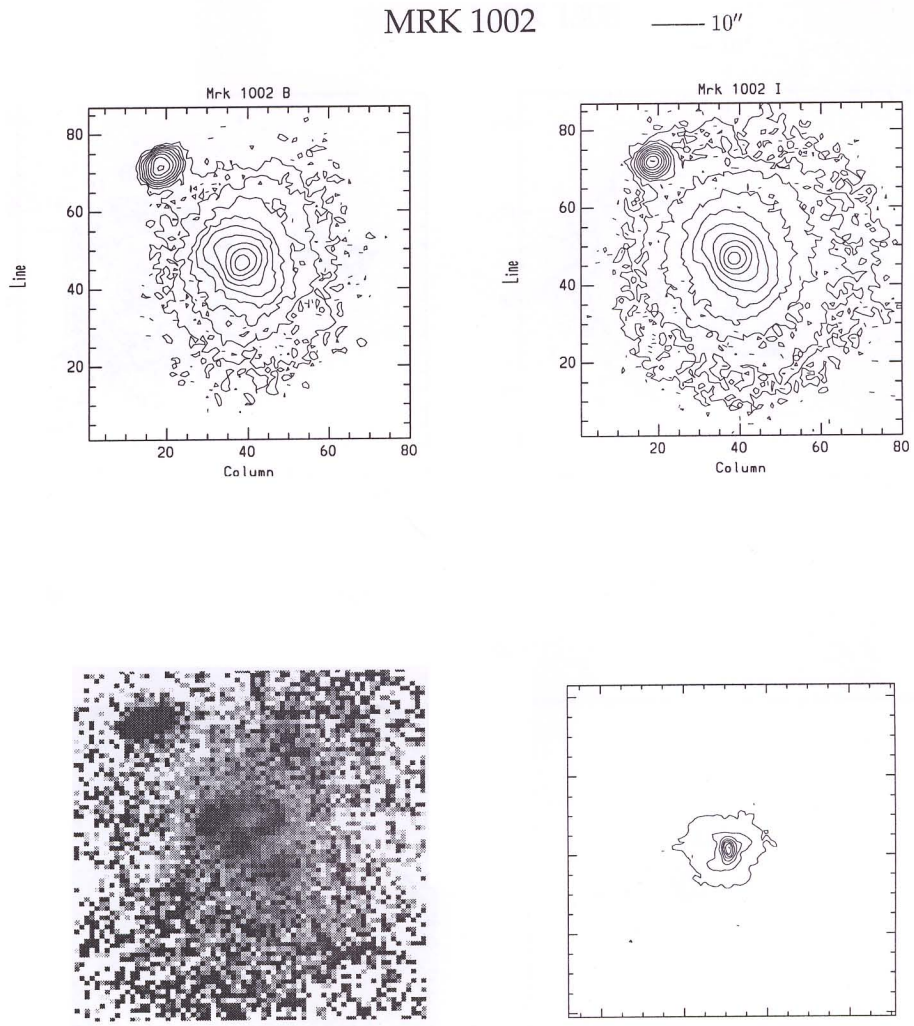

Figure 3.1e

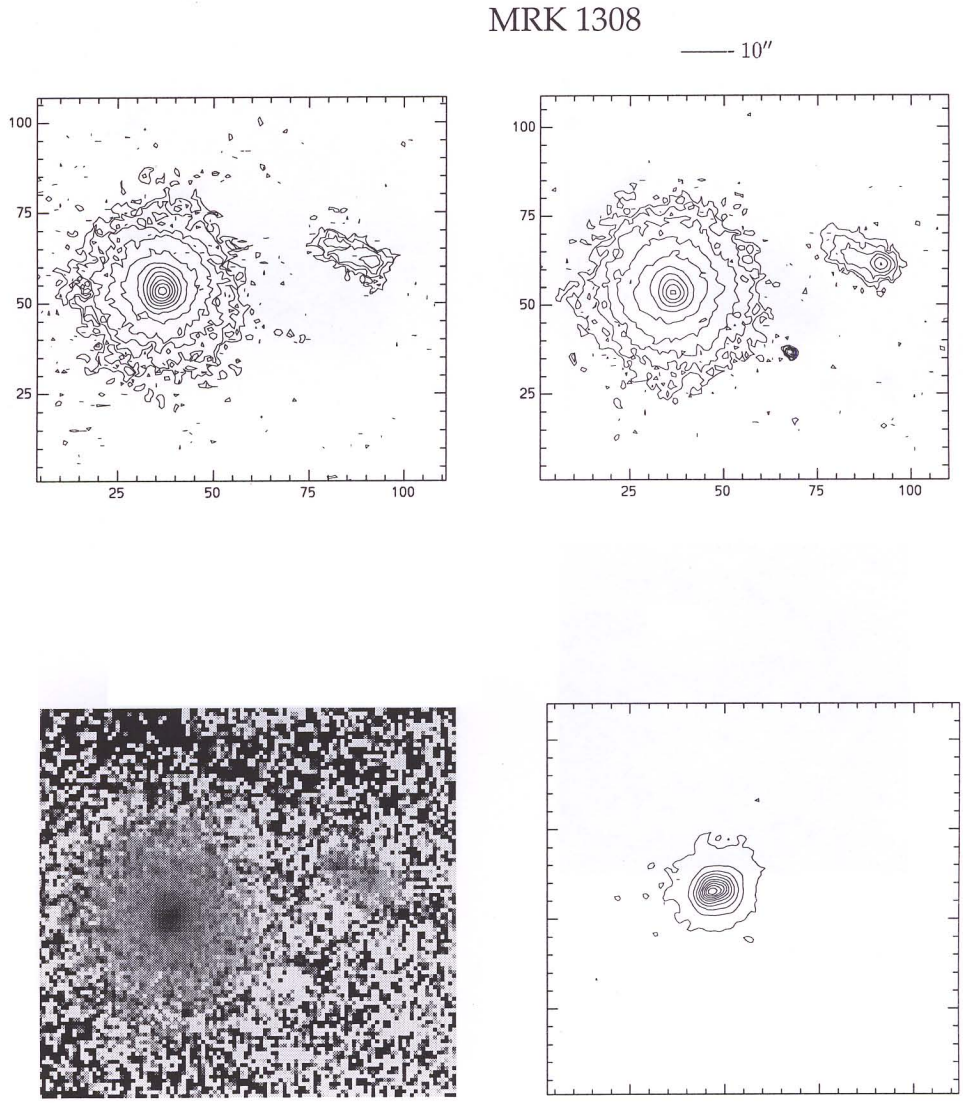

Figure 3.1f

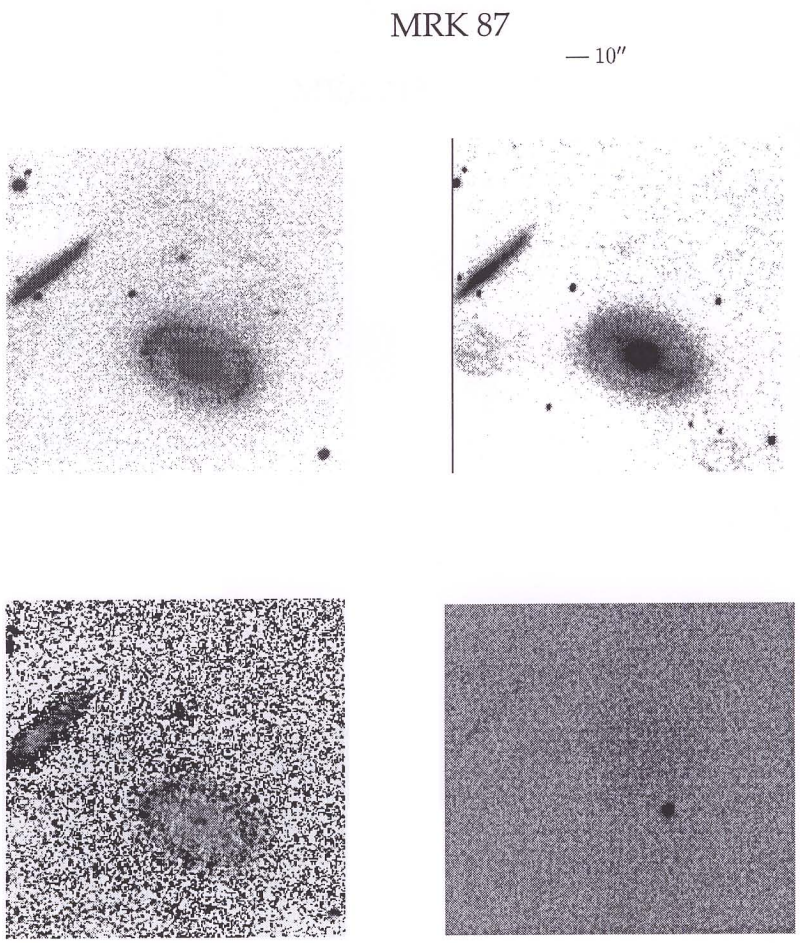

Figure 3.1g: Direct images in B, I and Hα are shown instead of the isophotal contours to clearly bring out the ring. The locations of the figures is the same as in all others.

MRK 213 —— 10″

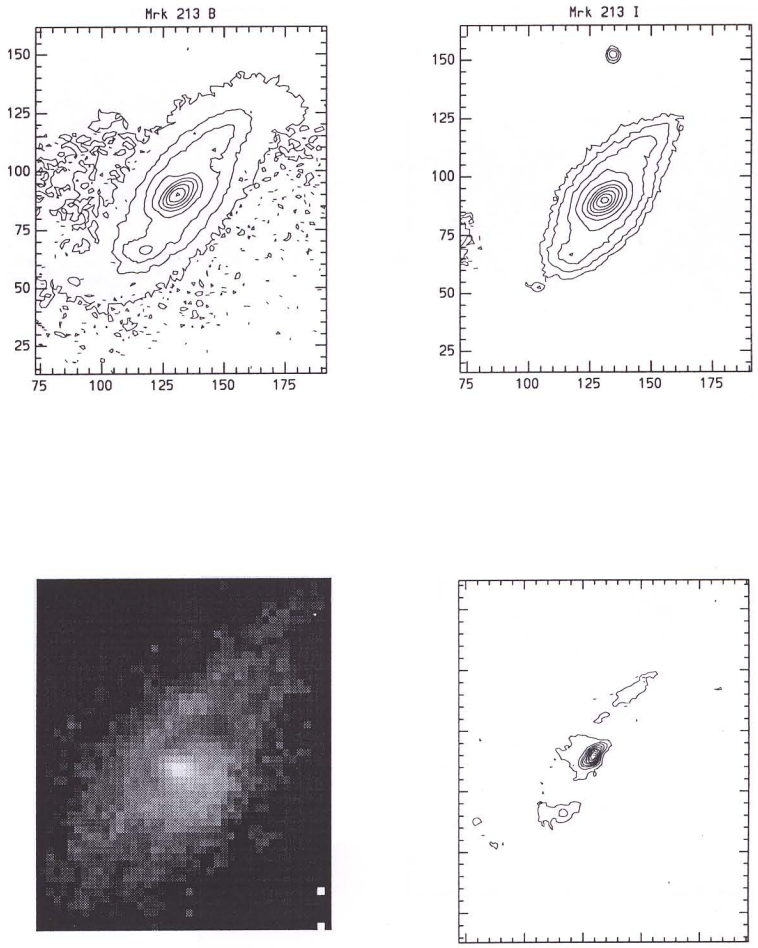

Figure 3.1h

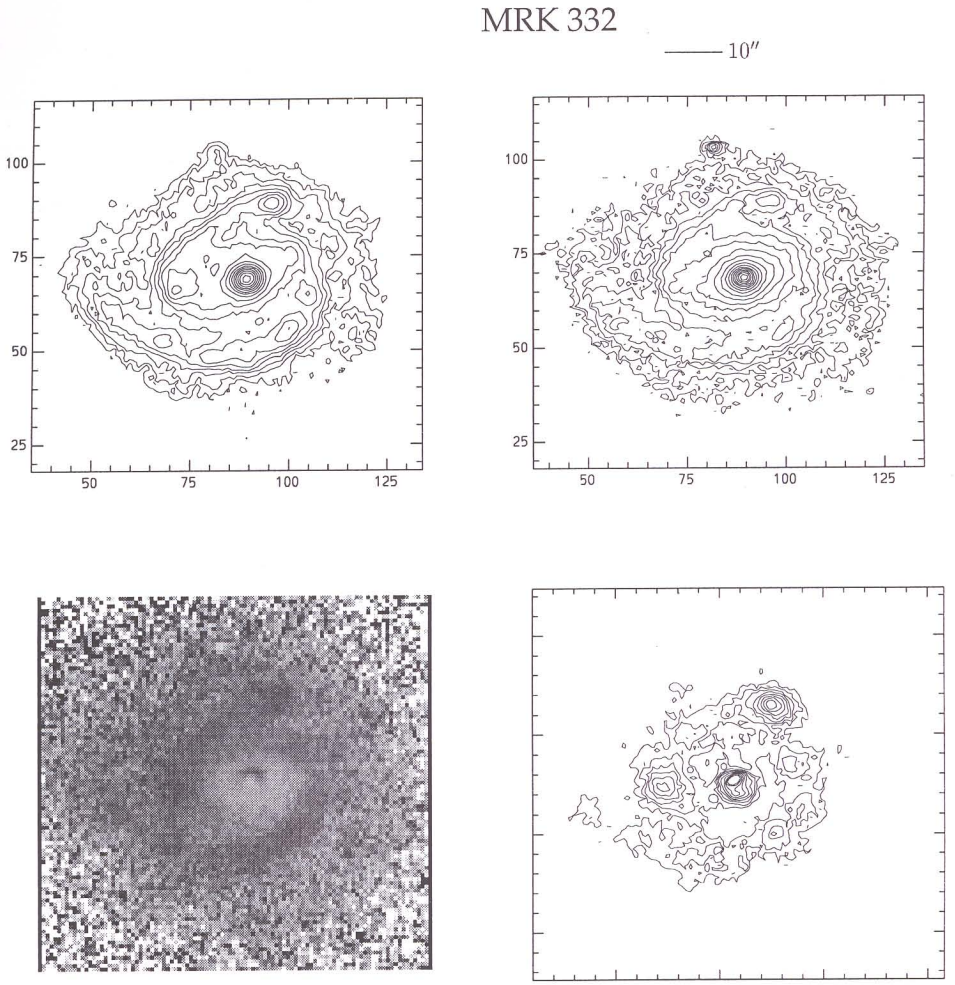

Figure 3.1i

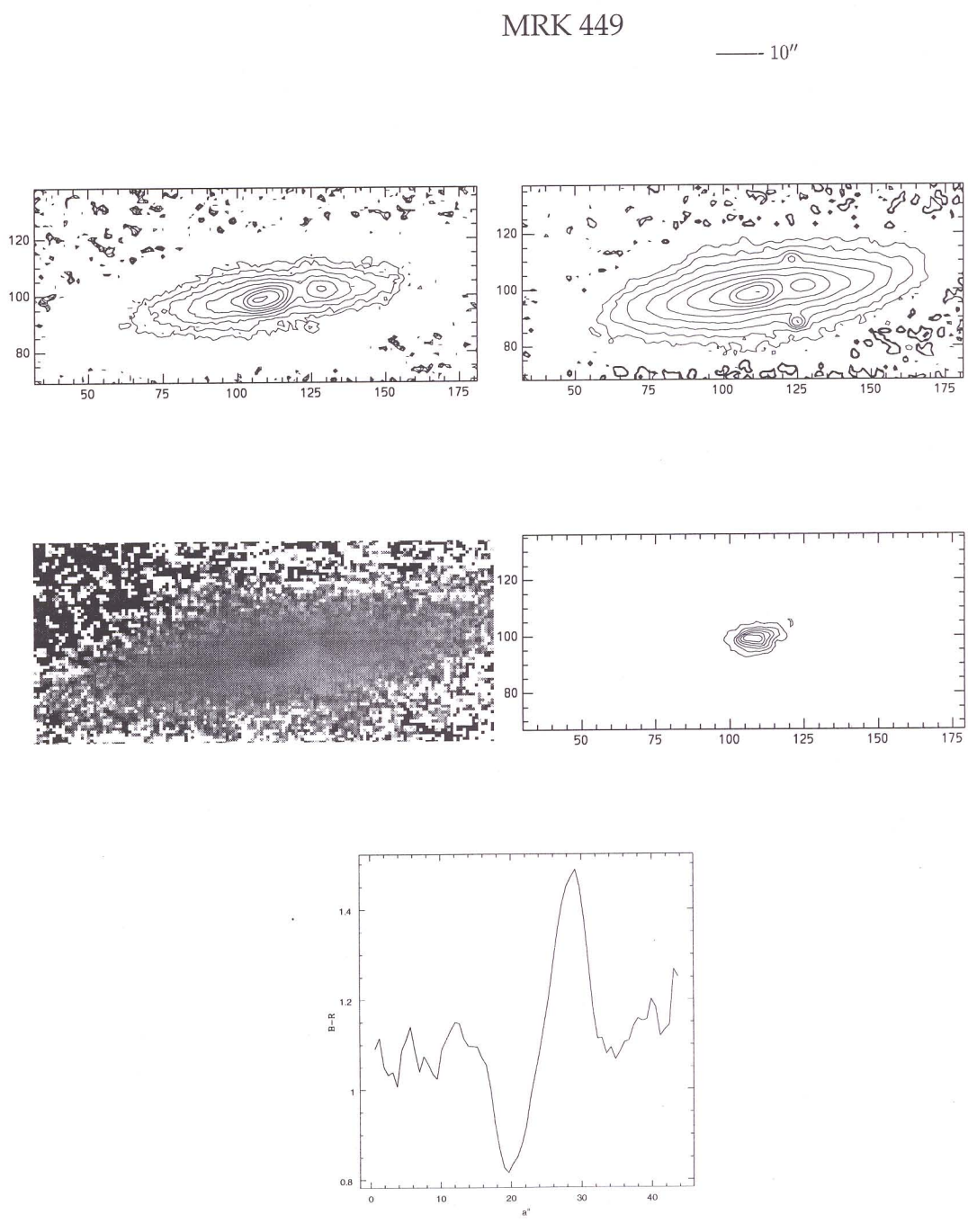

Figure 3.1j: The bottom panel shows the variation in $(B - R)$ along a cut through the nucleus and dust lane at a position angle of 97^o

The figures at the top and in the middle are in the same order as the rest of the figures.

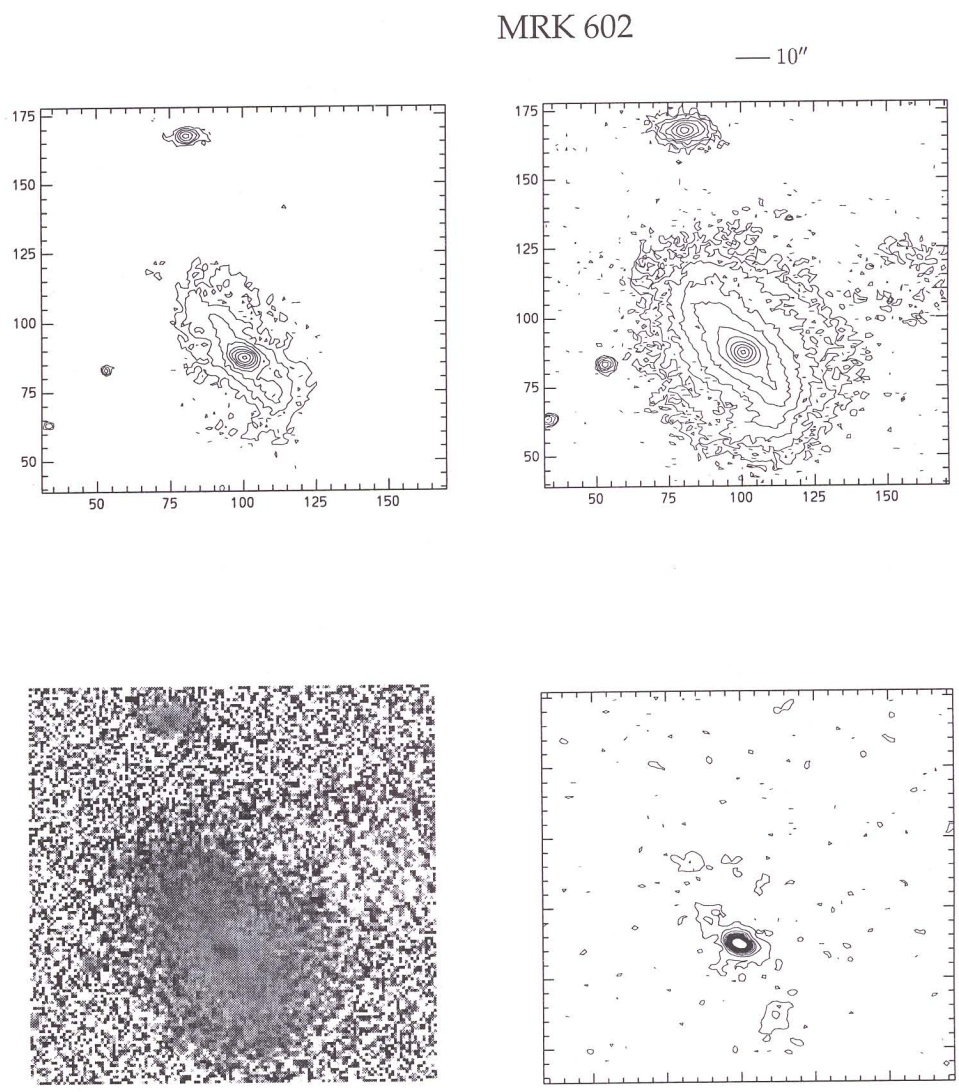

Figure 3.1k

MRK 708

— 10″

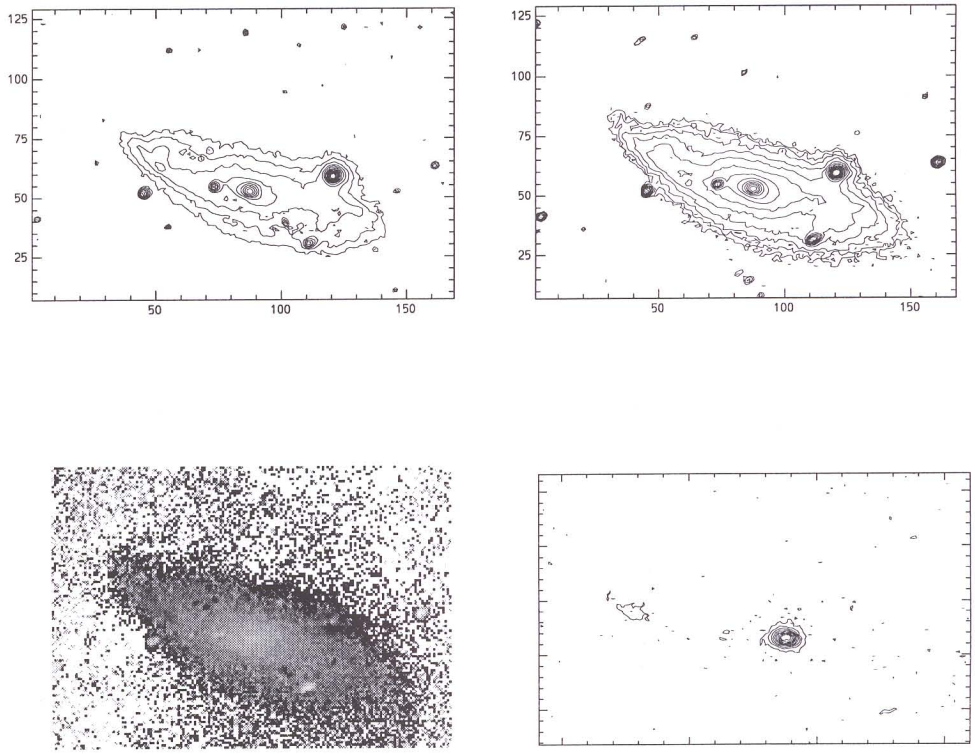

Figure 3.11

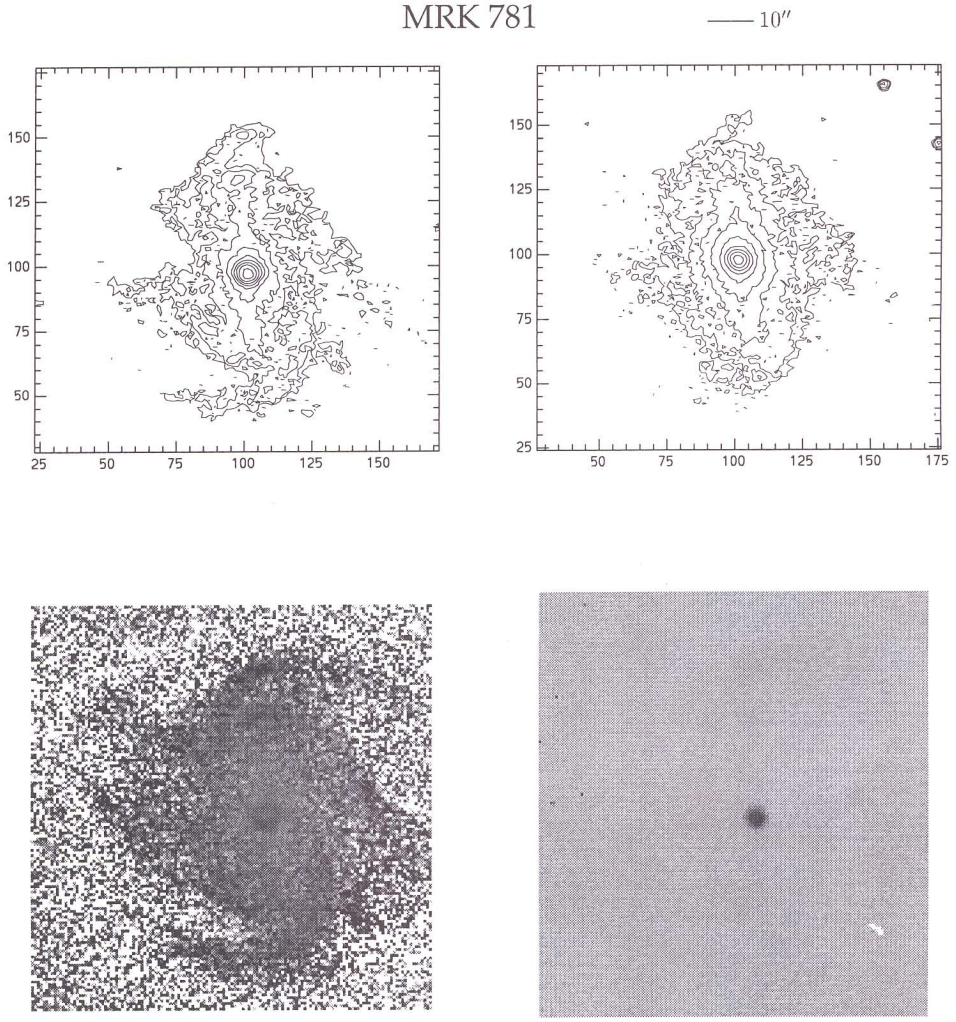

Figure 3.1m: The continuum subtracted Hα image is shown instead of the isophotes in the fourth panel.

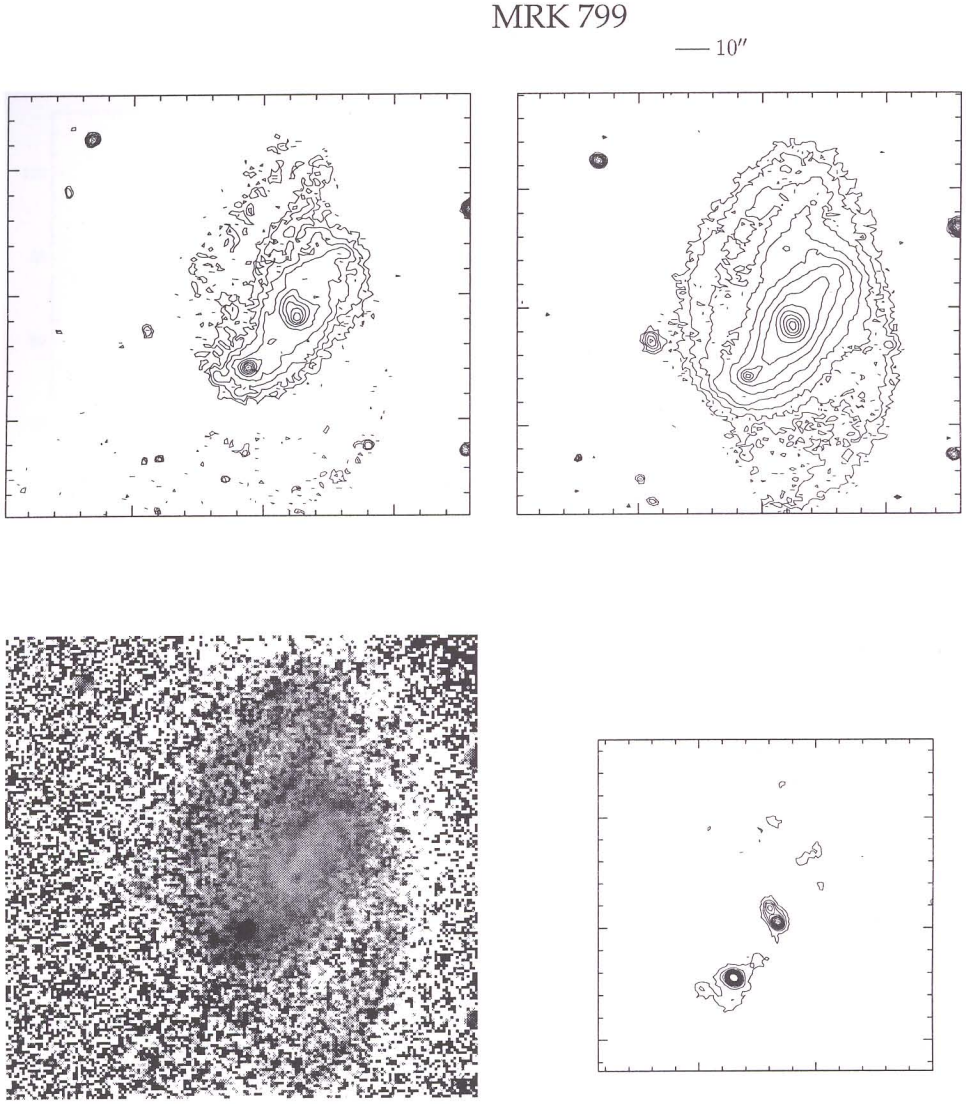

Figure 3.1n

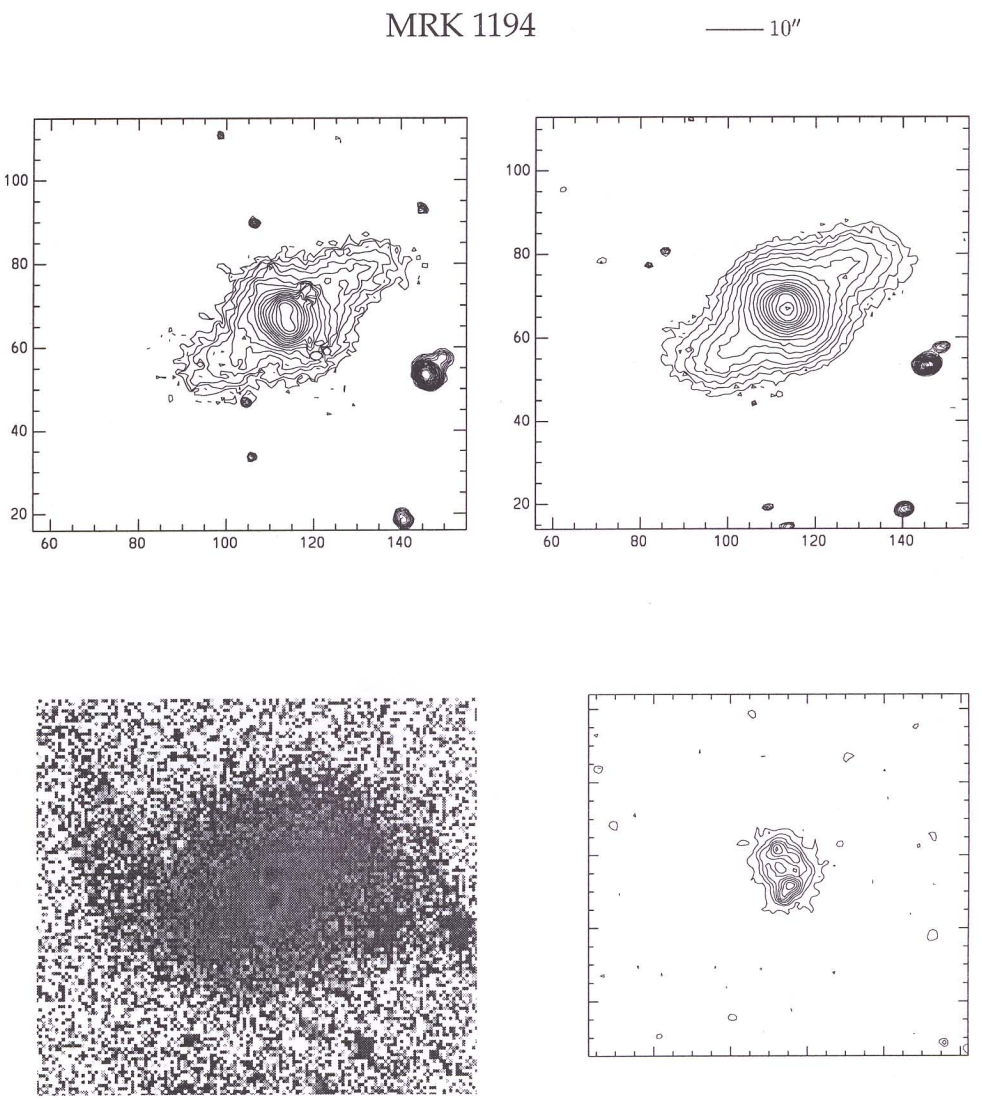

Figure 3.1o

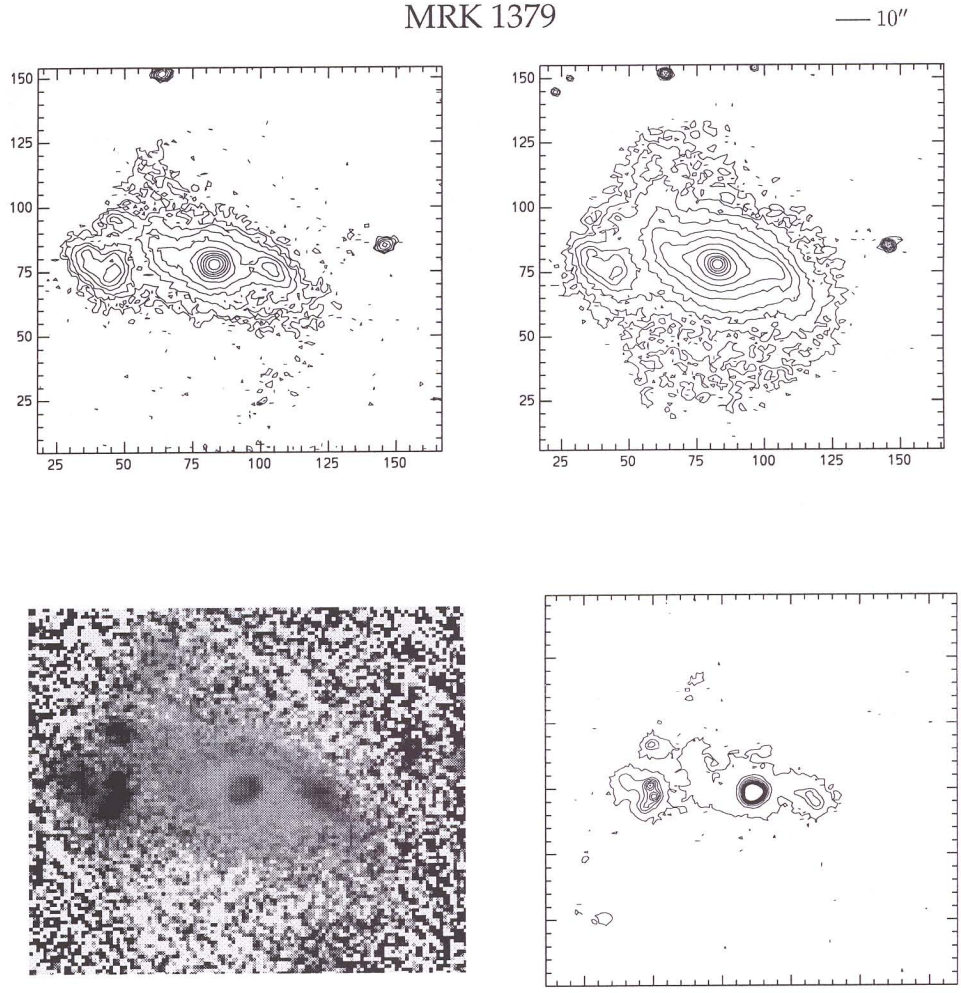

Figure 3.1p

morphologies, we have divided the sample into the following four subclasses.

1. Galaxies showing Hα emission in the central region only. Mrk 1308, Mrk 14, Mrk 87, Mrk 449 and Mrk 1002 belong to this class.

2. Galaxies showing extended Hα emission or galaxies with extranuclear emission, in addition to nuclear star formation. This includes most of the spirals which show emission from either one or both the ends of the bar, or along the bar (e.g. Mrk 213, Mrk 1379, Mrk 799 and Mrk 602), Mrk 190 which shows extended emission in the nuclear region, Mrk 332 and Mrk 781, with emission in the spiral arms, are also included in this group. The ellipticals like Mrk 743 and Mrk 603 also have extended regions in emission.

3. Galaxies with global massive star formation. Line emission is observed throughout the body of the galaxy in Mrk 363 and Mrk 1134, indicating a global starburst. The fact that massive star formation in starburst galaxies is not always confined to the nuclear region alone is best illustrated in these cases. Their strong stellar continuum at longer wavelengths (R and I bands) points to the fact that they are not young systems experiencing their first phase of star formation, but are old systems with a younger burst of star formation.

4. The last class includes starburst galaxies with peculiar emission-line morphologies. Mrk 439 and Mrk 1194 belong to this class. Mrk 439 shows extended Hα emission along a bar which is misaligned with the optical continuum isophotes, while Mrk 1194 shows no emission from the central region but clearly shows a circumnuclear ring of massive star formation.

The radial distribution of the Hα emission was studied by synthetic aperture photometry in the regions of emission. The central intensity was normalized and the radial profiles thus obtained are shown in Fig. 3.2. A majority of the objects have a Hα distribution that is centrally peaked and falls off at a more or less exponential rate with increasing radius. A few cases like Mrk 1379 and Mrk 363 have Hα distributions that show a different behaviour. The fall-off in the line intensity with radial

Table 3.1: Characteristics of Hα emission

Galaxy	Global pseudo E.W.	emission morphology
Mrk 14	0.909	extended
Mrk 87	-	central
Mrk 190	0.537	central,resolved
Mrk 213	0.208	central,end of bar
Mrk 332	0.440	central,spiral arms
Mrk 363	1.127	global
Mrk 439	0.399	along a misaligned bar
Mrk 449	0.524	nuclear
Mrk 602	0.6918	central,along bar,ends of bar
Mrk 603	1.706	global
Mrk 708	0.812	nuclear, eastern end of bar
Mrk 743	1.374	extended
Mrk 781	1.374	central,spiral arms
Mrk 799	0.380	central,end of bar
Mrk 1002	0.565	central
Mrk 1134	0.490	global
Mrk 1194	0.709	along a ring
Mrk 1308	0.812	nuclear
Mrk 1379	1.025	central,end of bar

distance is much smoother in Mrk 1379, while in Mrk 363, the peak is off-centered from the nucleus.

3.3.2 *Pseudo equivalent widths of Hα*

To study the regions of current star formation relative to the underlying continuum contributed by old stars, a pseudo equivalent width (p E.W.) of Hα was computed. This was done by dividing the Hα intensity by the stellar continuum intensity estimated from the scaled off-band continuum image. This is not a true equivalent width, however, it can be used to compare relative levels from galaxy to galaxy. It provides a measure of the current star formation rate relative to the recent past star formation rate, since the line emission is due to massive stars with ages $<10^7$ years while the stellar continuum at these wavelengths is due to G and K giants which

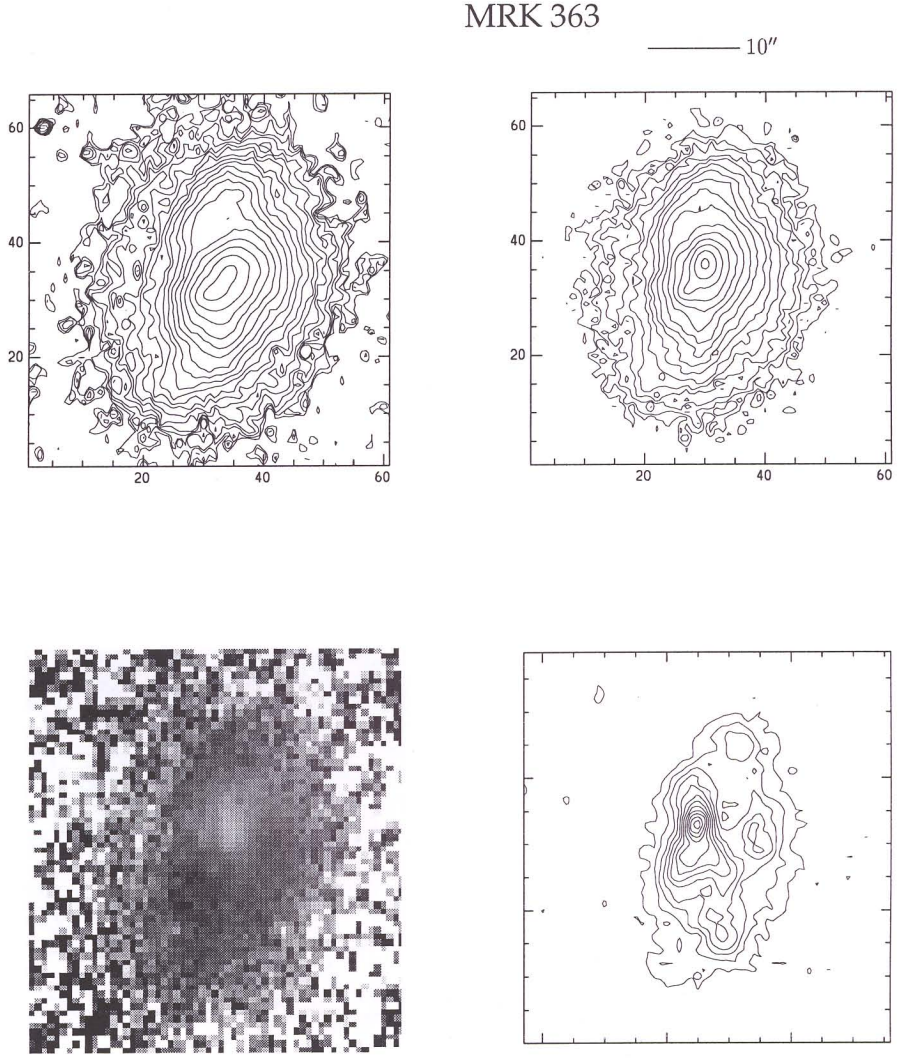

Figure 3.1q

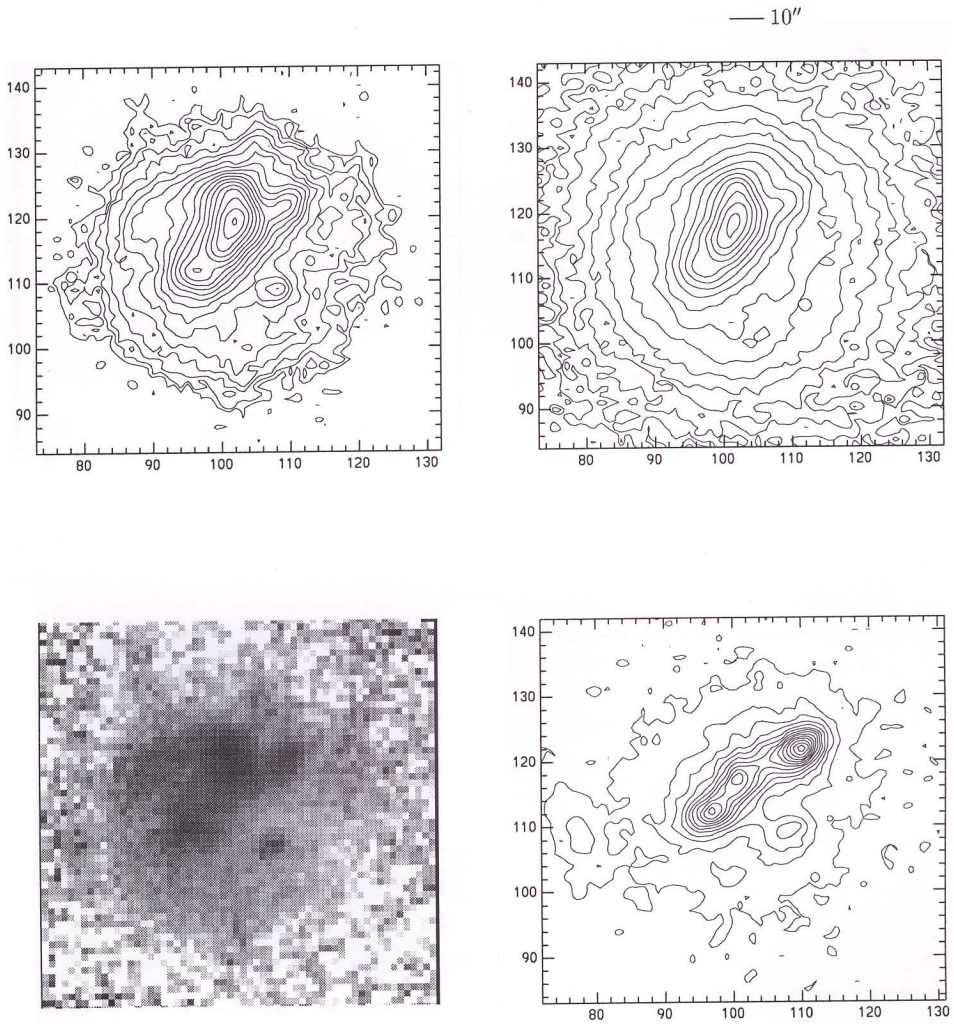

Figure 3.1r

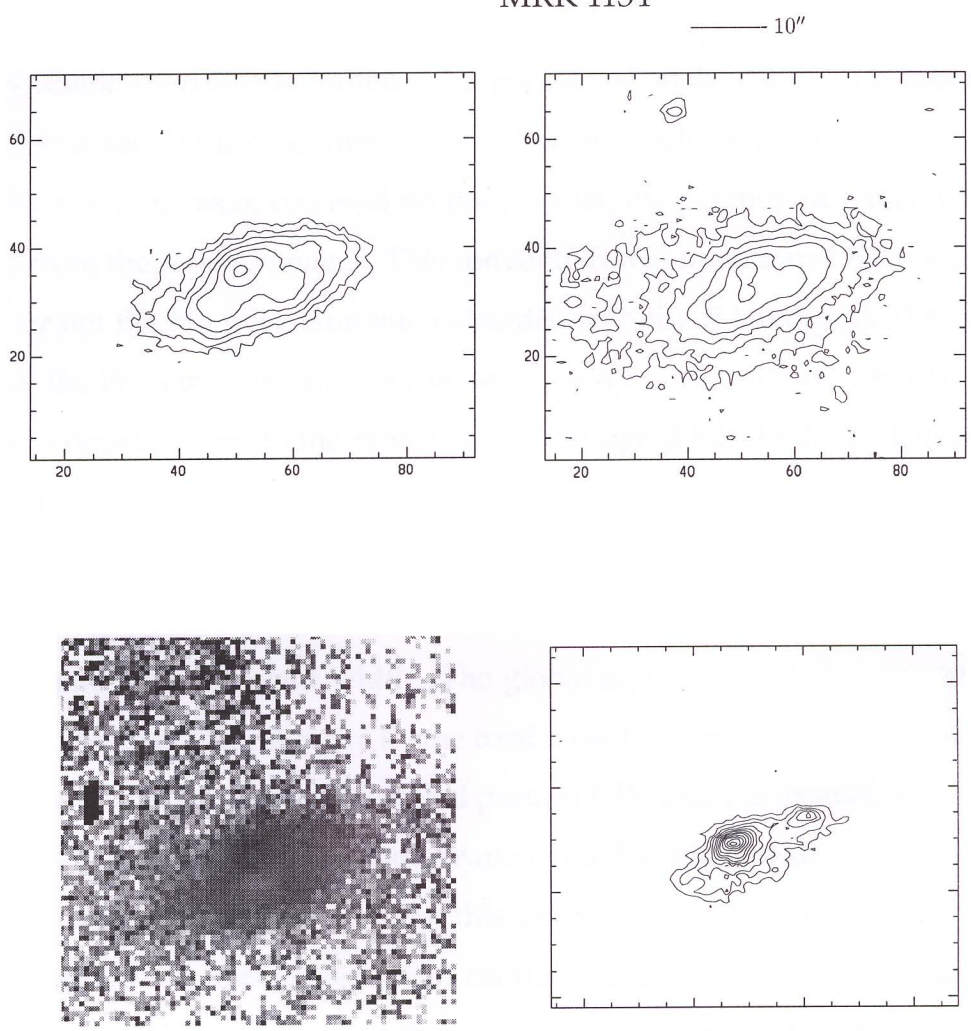

Figure 3.1s

are typically a few billion years of age (Huchra 1977b; Kennicutt 1983). Since we are interested only in the relative contributions, the units are arbitrary. Bushouse (1986) uses a similar approach to derive pseudo equivalent widths for a sample of interacting galaxies. However, he uses the total flux in the R band while we use the flux in the scaled off-band images. Global and radially dependent pseudo equivalent widths were derived by the following procedure :

Synthetic aperture photometry was performed on the continuum subtracted Hα images to derive the brightness distribution through concentric circular apertures. The apertures were centered on the nucleus, the position of which was determined from the R band images. This convention was maintained irrespective of whether or not the Hα peak emission coincides with the R band peak. The radial profiles of the line emission intensity were derived in this manner. Circular apertures were considered up to the radius where the signal falls to the 3σ level of the background value in the line images. The same scaled images that were used for continuum subtraction served to derive a similar radial profile for the continuum in the emitting region. The ratio of the two intensities gives the radial distribution of the pseudo equivalent width. The global equivalent width was obtained by dividing the total line intensity by the total scaled continuum intensity over the emitting region. Table 3.1 lists the global pseudo E.W. and the locations of the Hα emission. In Mrk 87, the signal to noise ratio in the Hα image was poor, so we did not deduce the global pseudo E.W. for this galaxy. The radial dependence of the intensity distribution normalized to the central intensity plotted on a logarithmic scale and the radial dependence of the pseudo equivalent width (p E.W.) are presented in Fig. 3.2 for a few representative cases. The intensity is maximum at the center and falls of smoothly outwards. Many of the galaxies show an exponential decline in the Hα intensity. Mrk 332 is an exceptional case in which the intensity shows a marked increase at 10", corresponding to the star forming regions along the spiral arms. It was noted that the radial distribution of pseudo E.W. does not follow the same behaviour as that of the intensity profiles. The radial dependence of the pseudo equivalent widths can be grouped into the following types :

- Peaking in the central region and falling off steadily outwards as in Mrk 14, Mrk 213, Mrk 743.

- Peaking near the nucleus, but off-centered from it as in Mrk 1379, Mrk 1308, Mrk 439, Mrk 603 and Mrk 363.

- Showing multiple peaks as in Mrk 1002, Mrk 332. One of the peaks is close to the nuclear region and the other at a large distance from the center.

The global pseudo E.W. listed in Table 3.1 was compared with the pseudo E.W. in the central region. It was found that the central pseudo E.W. was higher than the global value in nearly all cases. This suggests that the star formation is more enhanced with respect to the underlying population in the central regions of these starburst galaxies. A few cases like Mrk 363, Mrk 439 and Mrk 332 showed that the ratio of the central pseudo E.W. to its global value was less than unity. All these three galaxies show a considerable amount of extranuclear star formation.

3.4 *Individual galaxies*

The sample can be divided into three broad morphological types : early type galaxies namely S0's and E's; spirals; and irregulars and ellipticals.

3.4.1 *S0's and E's*

The isophotal contours and colour maps of the galaxies belonging to this group are presented in Fig. 3.1a-f.

- **Mrk 14 :**
  This galaxy has been classified as likely to be an S0 by Huchra (1977a) while it forms a part of the sample of distant irregulars in a study conducted by Hunter & Gallagher (1986). The contours in the outer regions look disturbed

(Fig. 3.1a). Keel & van Soest (1992) find no candidate companions near this galaxy. The only significant feature in the colour maps is the blue nucleus. The $(B-I)$ colour map does not show any features like dust lanes. On the whole, the colours get redder outwards. A sharp change is seen in the inner 8"; $(B-V)$ changes steeply from 0.15 to 0.75 in this region. Beyond this, the change is more gradual. The Hα image shows extended emission peaking in the nuclear region. The pseudo E.W. also shows a peak in the nuclear region and falls off smoothly with radial distance.

- **Mrk 190 :**

  This galaxy has been classified as S0/E. The outer contours appear smooth and almost circular (Fig. 3.1b). The isophotes in the B band show the presence of an inner structure lying along east-west and a faint indication of spiral arms in the north-south direction. van den Bergh (1980) describes it as a very small face-on spiral with a bright core of extent 8" and a disk 29" in diameter. The U band contours show a double structure in the central region.

  Towards longer wavelengths, the contours become smoother and are nearly circular. The colour maps show a blue ring straddling the nuclear region, 400 pc wide with a $(B-V)\sim0.5$ which is bluer by $0^m.2$ as compared to the nuclear region. Li et al. (1994) have found from aperture synthesis observations of HI and CO that it does not show a central HI depression or an inner/outer HI ring. Most of the HI emission is within the de Vaucouleur's radius. They find no indications for the nuclear burst to be a recent merger or interaction and suggest that it could be occurring periodically. Our Hα image shows that the emission is extended, consistent with Wrobel & Heeschen (1991) finding extended radio emission in Mrk 190.

- **Mrk 603 :**

  Mrk 603 along with its two companions forms a triple system. It has been studied extensively by Petrosian & Burenkov (1993). They deduce the presence of about 3×10^5 OB stars which photoionize the gas. They also detect

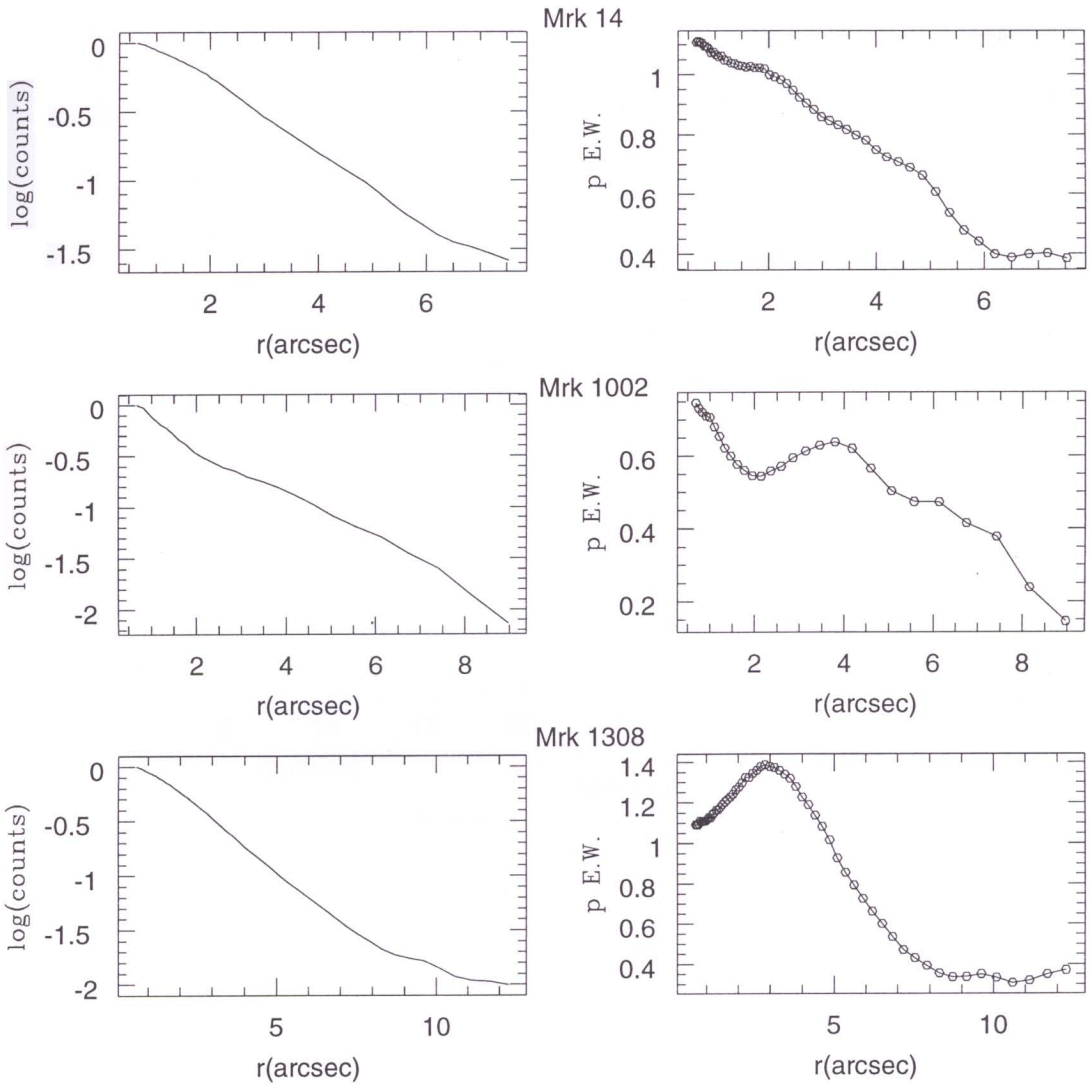

Figure 3.2:

The left panel shows the radial variation of the normalised Hα intensity plotted on a logarithmic scale and the right panel shows the radial variation of the pseudo equivalent width (p E.W.)

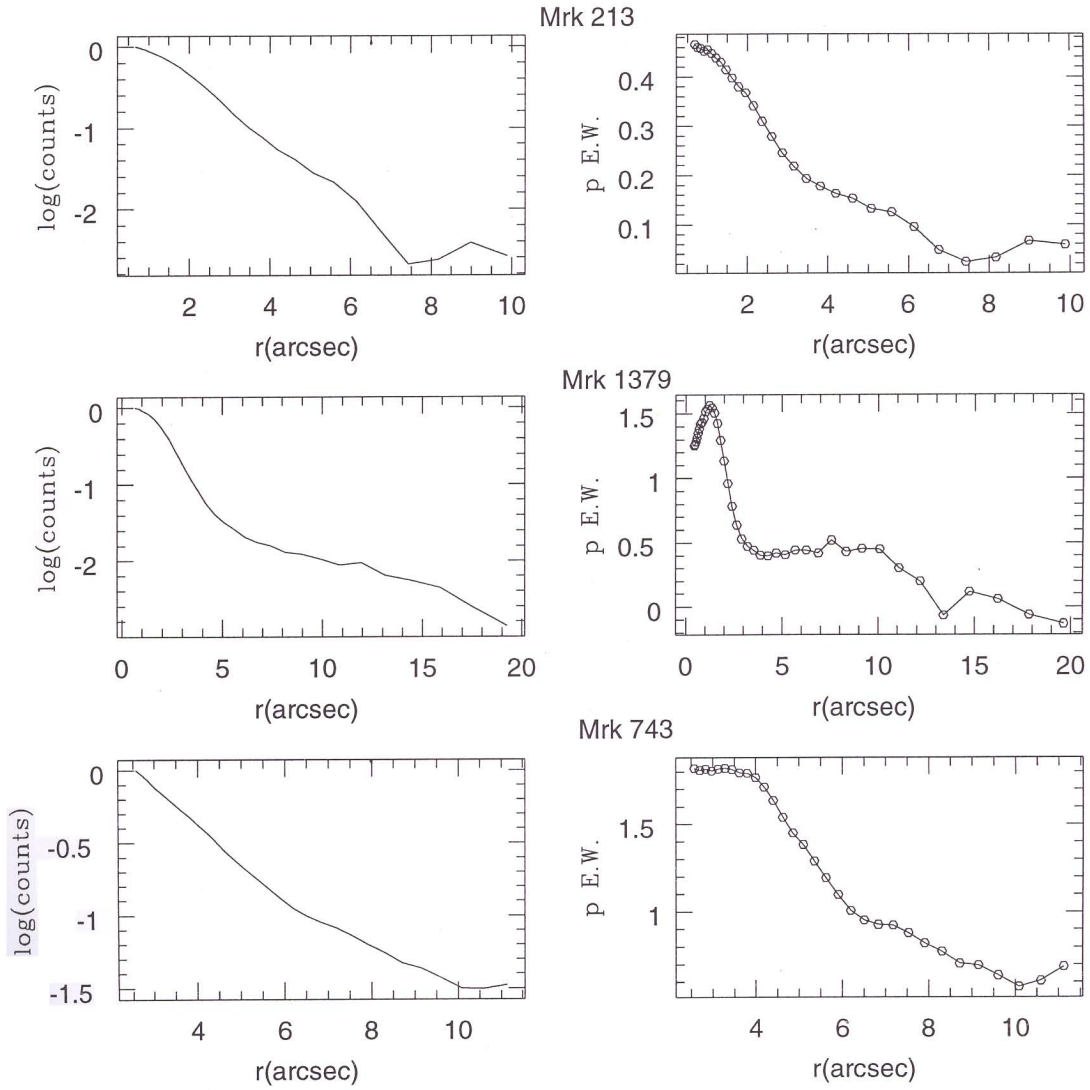

Figure 3.2 (contd.)

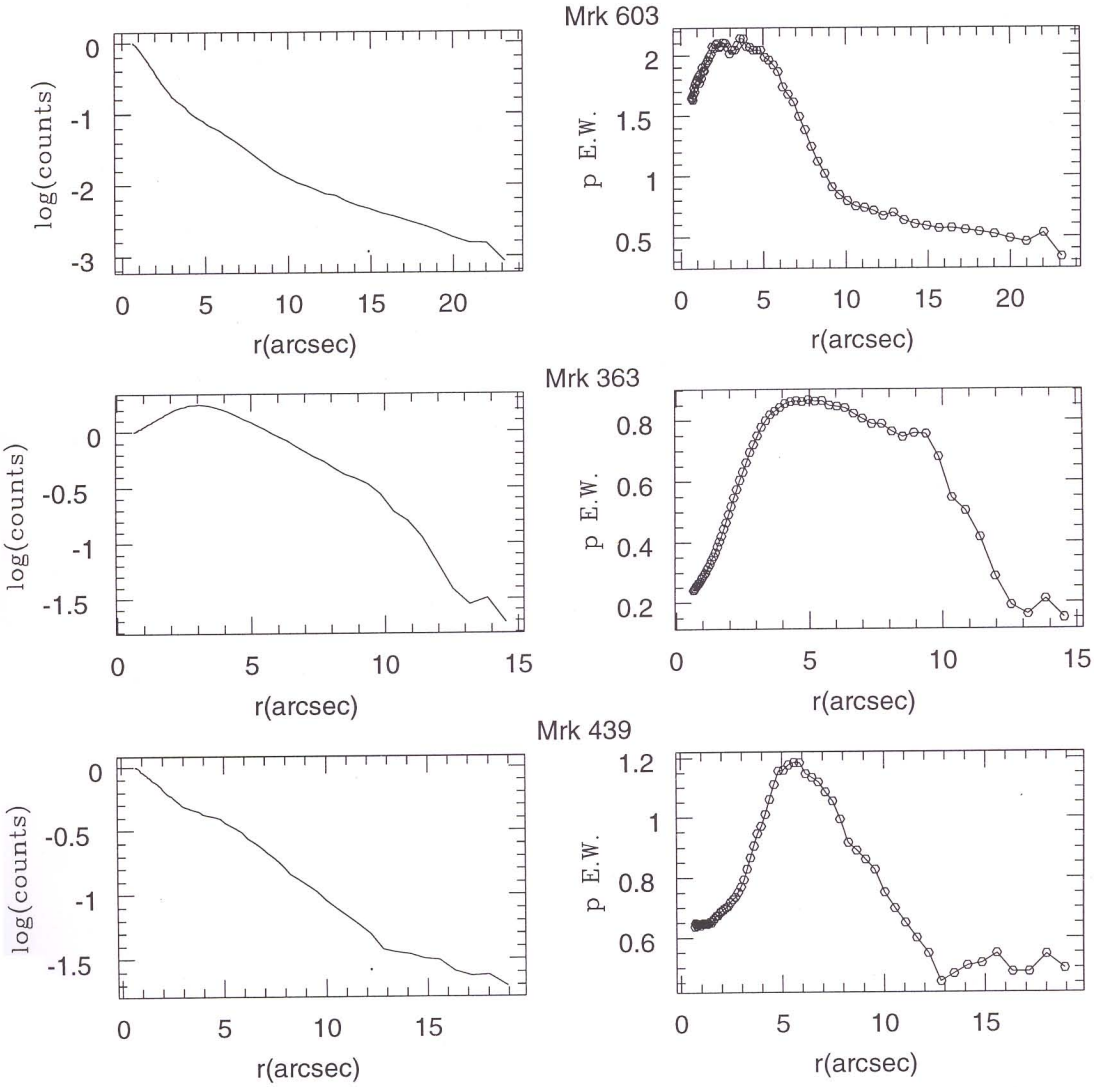

Figure 3.2 (contd.)

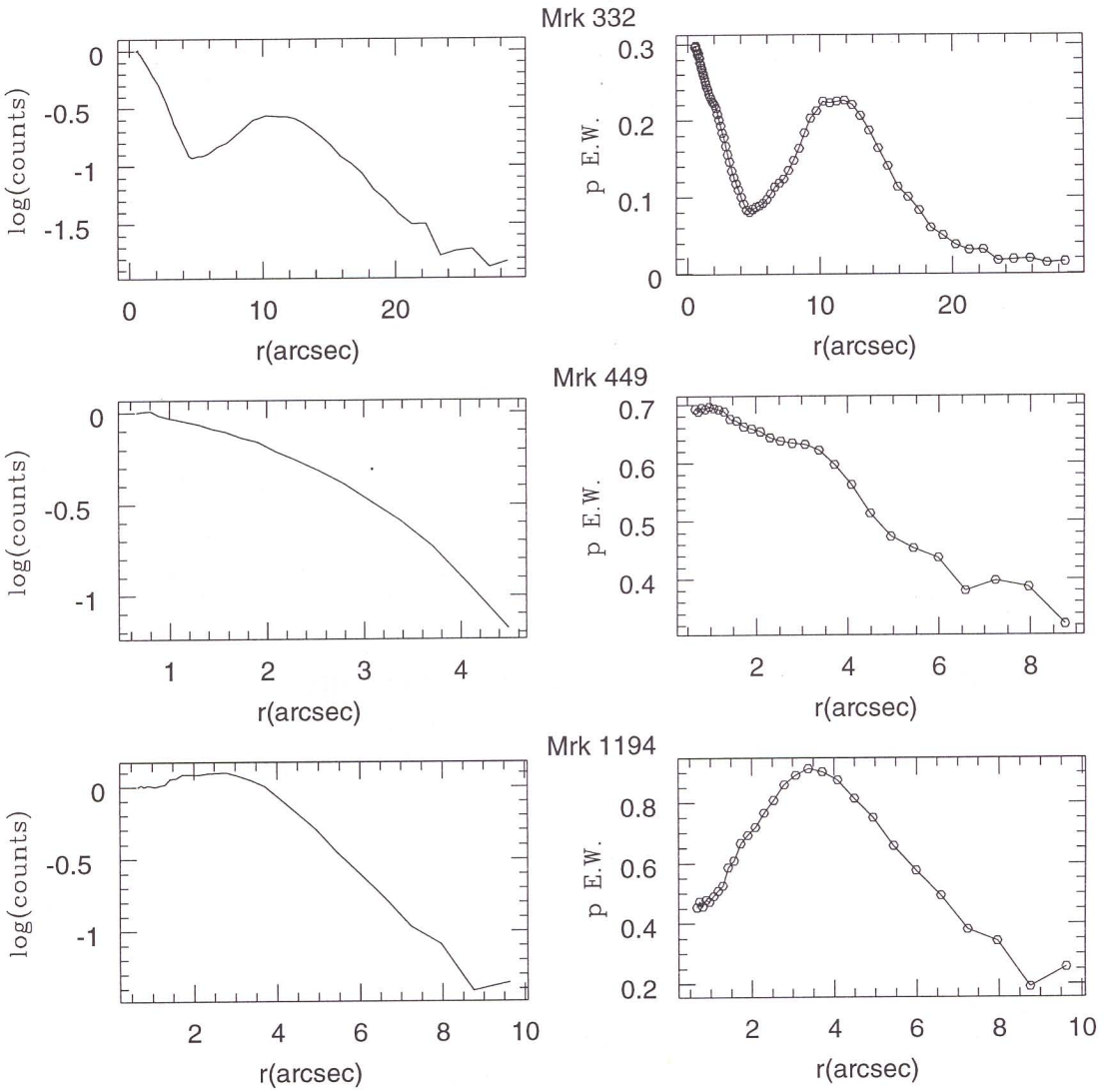

Figure 3.2 (contd.)

ongoing star formation in the host galaxy at a smaller rate as compared to that in the nucleus. We find that the contours are stretched out along the north-western side (Fig. 3.1c). The $(V - R)$ colour image shows a blue nucleus surrounded by a red clumpy region. The two companion galaxies also appear blue. This system shows global Hα emission, in the galaxy as well as in the companions, with the peak emission in the nuclear region of the galaxy. However, the pseudo E.W. is found to peak 4" away from the nucleus. It falls off steeply up to 10" and the fall is much smoother beyond 10".

- **Mrk 743 :**

  Mrk 743 is classified as a peculiar E0 galaxy in the Markarian catalogue. It forms a part of the sample of galaxies with double nuclei studied by Mazzarella & Boroson (1993). An inspection of the contour plots in the four bands reveals the presence of two nuclei surrounded by a common envelope (Fig. 3.1d). The envelope is asymmetric in the outer regions. Both the nuclei have comparable fluxes in the V band. The western nucleus appears brighter at longer wavelengths, while the eastern component becomes dominant at shorter wavelengths. Mrk 743 is one of the few HI sources among early type galaxies in which the HI distribution shows a central concentration, rather than the usual depression (Burstein et al. 1987). The HI distribution is in the form of a disk nearly as large as the galaxy diameter (van Driel & van Woerden 1991). Wrobel & Heeschen (1991) detect unresolved radio emission at 6 cm from this object. Hα shows an extended structure with its peak coinciding with the eastern nucleus. For deriving the variation of the line intensity and the pseudo E.W., the center was taken to be fixed on the eastern nucleus. The line intensity variation with radial distance follows a more or less exponential form, with its peak in the center.The pseudo E.W. remains constant in the central region up to a radius of 4" and then falls slowly outwards.

- **Mrk 1002 :**

  This galaxy is classified as S0 by Mazzarella & Balzano (1986) and as E1 in

the Markarian catalogue. The direct image appears smooth. On probing the contours we find that the central contours appear elliptical (Fig. 3.1e). At about 6″, they start deviating from perfect ellipses and seem to give a faint indication of spiral arms. Beyond 12″, they regain their elliptical nature. The colour maps show an interesting structure. We detect a S-shaped blue structure in the form of a spiral crossing the nucleus in the colour maps. Pogge & Eskridge (1993) have reported Hα emission in the nuclear as well as clumps of emission in the circumnuclear region in this galaxy. Our studies show that the line emission does not follow the structure seen in the colour maps but just shows extended emission in the central region. The Hα emission is peaked in the center and falls of smoothly. However, the radial distribution of pseudo E.W. shows a lot of structure. It peaks in the center and falls off till 2″ and then rises again to peak at 4″, before falling off smoothly outwards.

- **Mrk 1308 :**

  This is a small nearby galaxy of S0 type extending about half an arcminute. It has a small linear companion located at 30″ towards the west, which has been confirmed to be a physical neighbour (Doublier et al. 1997). The contours in the B and I filter bands appear smooth (Fig. 3.1f). Besides the blue nuclear region, there are no other features detectable in the colour maps. The $(B-V)$ colour for Mrk 1308 is 0.05 in the central regions and gets redder outwards, reaching a value of 0.7 near the periphery. The companion is a red object having a mean $(B-V)$ of 0.9. The colour and the Hα images show that the star formation activity is confined to the nuclear region. Radio imaging at 6 cm (Neff & Hutchings 1992) shows that the emission at 6 cm is in the form of a ring-like structure of diameter $\approx$ 3″. Our Hα image shows emission in the central region. The pseudo E.W. peaks 3″ away from the nuclear region.

3.4.2 *Spirals*

The sample contains 10 spirals. The isophotal contours and colour maps of these galaxies are given in Figs. 3.1g-p.

- **Mrk 87 :**

  Mrk 87 is a barred spiral with a prominent ring surrounding the bar as is clear from Fig. 3.1g. It is paired with the SBa galaxy KPG 160B. The ring appears more prominently in the B band and the $(B-I)$ colour map and starts merging with the underlying galaxy at longer wavelengths. Rings of stars and gas are often seen in barred spiral galaxies. They are believed to be formed by gas accumulation at the bar's Lindblad resonances. They are blue in colour and are the sites of enhanced star formation (Buta 1986). Arsenault (1989) has shown that the bar and ring features occur with a higher frequency in starburst galaxies as compared to normal galaxies. The Hα image shows emission only in the nuclear region and in the companion galaxy.

- **Mrk 213 :**

  This is a barred spiral galaxy. A faint arm is seen emerging from the south eastern end and curving around towards the north western side where it is attached to an almost stellar condensation (Fig. 3.1h). The contour plots of Mrk 213 in both B and I bands clearly show that the contours in the inner regions have a position angle different from that of the outer region. The contours in the central region appear elliptical. The $(B-I)$ colour map shows that this galaxy gets bluer outwards. The colour map also shows a dust lane starting from the nucleus, curving around it before proceeding towards the NW direction. Line emission is present in the nuclear region and at the ends of the primary bar. The isophotal contours in the Hα image show that the emission in the central region follows the contours seen in the direct images. The pseudo E.W. shows the same trend as the intensity profile.

- **Mrk 332 :**

The galaxy shows a bright nucleus and two spiral arms (Fig. 3.1i). A faint secondary arm-like structure starting from the eastern tip of the eastern spiral arm and going towards north is also seen. Though this feature is not apparent in the isophotal contours shown in the figure, it can be seen clearly in the direct images of Mrk 332. Inspection of the images shows that the spiral arms are embedded in a diffuse envelope. A number of knots are seen along the spiral arms especially in the U, B and Hα images. The R and I images appear much smoother than the U and B images. The U and B images do not show any indications of a bar but the isophotes at longer wavelengths show faint indications of a bar or a central oval distortion. This is discussed in detail in Chapter 4. The U and B band images show a number of knots tracing the inner boundary of the spiral arms and forming a ring. Towards the longer wavelengths, these images get smoother gradually and the I band isophote is devoid of any distinct knotty structure. The continuum subtracted Hα image also exhibits structure similar to that observed in the U and B bands confirming that these are knots of enhanced star forming regions, forming a ring at about 2.1 kpc from the nucleus and not a result of patchy extinction. Mrk 332 is a spiral galaxy with two spiral arms which show a number of clumpy star forming regions at shorter wavelengths. The nucleus appears highly reddened. The $(B-V), (B-I)$ maps shows a blue region associated with the nucleus, which is a little off-centered with respect to the nucleus, surrounded by a much redder region on the inner side of the ring. The diameter of this ring is deduced to be $\sim$ 4.2 kpc with a width of $\sim$ 600 pc; from the $(B-I)$ image. The nucleus is the highest surface brightness region in all the bands. The nuclear region shows a disturbed morphology in the emission-line image. The contours are not smooth and Hα is brightest in a region which is off-centered from the nucleus, similar to the structure seen in the $(B-I)$ image. In Hα, two of the brightest condensations seen along the spiral arms are comparable in brightness with the nucleus.

- **Mrk 449 :**

  Mrk 449 is the most inclined galaxy in our sample. We derive an inclination of 75° for this galaxy. In the direct image, this galaxy appears lenticular. The contour maps (Fig. 3.1j) show the presence of a central elongated nuclear region with another bright region lying towards the west separated by a constriction from the nuclear region. The constriction becomes shallower at longer wavelengths leading us to believe that it is probably caused by extinction due to dust. An inspection of the colour maps shows a reddened vertical band in this region. We infer that this is due to a dust lane. This dust lane lies neither along the major axis of the galaxy, nor along its minor axis, but is at an intermediate angle. Hawarden et al. (1981) observed such "skew" dust lanes in a small fraction of early type galaxies. They suggest that the properties of the galaxies with such "skew" dust lanes are best attributed to the accretion of cool material at a fairly recent epoch. The signature of this is also seen as a reddened region in the colour image. A cut across the dust lane taken at a position angle 97° is presented in Fig. 3.1j which clearly shows the extent and the reddening in $(B - R)$ due to the dust lane. $(B - R)$ changes from 0.8 in the nuclear region to 1.5 at the location of the dust lane. The Hα emission is confined to the central region and the distribution is elongated in the East-West direction.

- **Mrk 602 :**

  This is a galaxy with a strong bar. It has been classified as SBbc. The northern spiral arms is forked and a small companion galaxy is seen 52" to its north. The colour map shows a blue nucleus and blue regions at the ends of the bar. The Hα image shows intense emission from the nuclear region and some faint emission along the bar, in addition to two blobs of emission located at the ends of the bar.

- **Mrk 708 :**

  This galaxy has been classified as possibly being a barred spiral in the UGC

and the RC3 catalogues. The UGC catalogue describes it as a spiral with very broad ill-defined arms and with 3 or 4 stellar objects superimposed on it. The colour image (Fig. 3.1l) shows a reddened central region and the galaxy gets bluer outwards. The Hα image shows strong emission in the central region and a faint blob of emission on the north-eastern side. The central reddening in colour could be either due to dust obscuration or due to a dominant redder population. This will be discussed in Chapter 4.

- **Mrk 781 :**

  Mrk 781 is a barred, flocculent spiral. The contour map in the B band looks ragged while that in the R band appears much smoother (Fig. 3.1m). The colour map reveals the presence of a blue nuclear region ($(B-V) \approx 0.6$), surrounded by a much redder region with $(B-V) \approx 0.8$ in the bar region. The colours get bluer again at the spiral arms. The Hα image also shows strong emission in the nuclear region. The starburst activity is mainly confined to the nuclear region in Mrk 781.

- **Mrk 799 :**

  Mrk 799 is a barred spiral galaxy. The UGC catalogue describes the galaxy as having a very broad, slightly curved bar and three arms, one of which is off center. It contains an extremely luminous HII region showing very strong Wolf-Rayet emission features (Contini et al. 1997) at one end of its bar. In Fig. 3.1n, this region lies to the SE of the nucleus and is at a distance of 20" from it. It is clear from the colour image shown in Fig. 3.1n that this superassociation is the bluest region in the galaxy. Contini et al. (1997) also find that the nuclear region is dusty and they detect a circumnuclear ring of semi major axis length 3".5. The colour image shows a blue nuclear region surrounded by a reddened region. Curved dust lanes are also seen in the colour image. The Hα emission in the nuclear region shows a double structure. The strongest Hα emission is seen in the superassociation.

- **Mrk 1194 :**

  Mrk 1194 is an edge-on barred spiral. The contours in the inner regions are misaligned with the outer contours (Fig. 3.1o). The central region shows different structures in the B and the I bands. The I band shows a well defined nucleus while the nuclear region appears elliptical in the B band. The $(B-I)$ colour map shows two blue blobs along the NS direction and a dust lane curving around it. The colour map and the $H\alpha$ image shows that star formation is concentrated in a circumnuclear ring of diameter 4 kpc. Contini et al. (1995) have reported the detection of this ring.

- **Mrk 1379 :**

  Mrk 1379 is a VV object (Vorontsov-Velyaminov 1977), with nests of interacting objects (Fig. 3.1p). The nucleus is blue in colour with $(B-V) \approx 0.4$, surrounded by a redder region with $(B-V) \approx 0.8$. Strong Hα emission is seen in the nuclear region and diffuse emission is seen along the bar. Blobs of emission are seen at the ends of the bar and in the companion galaxies. The companion is the bluest with $(B-V)$ between 0.2 and 0.3. The $(B-I)$ image shows nuclear star formation in the form of a ring as well as extranuclear star formation. Knots of star formation are seen in the nuclear region as well as along the western periphery of the galaxy at the point where the spiral arms start. In addition to this, global star formation is detected in both the companions lying to the East.

3.4.3 *Irregulars and Peculiars*

Three galaxies namely Mrk 363, Mrk 439 and Mrk 1134 are classified under irregulars/peculiars. Refer to Fig. 3.1q-s for the isophotal contours and the colour maps of these three galaxies.

- **Mrk 363 :**

  This peculiar Sc type galaxy has been classified by Geller & Huchra (1983)

as belonging to a group made up of seven galaxies, based on their proximity in space and their radial velocities. A neutral hydrogen mapping by van Moorsel (1988) shows a central concentration of HI. Radio emission extended over the galaxy has been observed by Wrobel & Heeschen (1988). An inspection of the contours in the B and the I band (Fig. 3.1q) reveals that the morphologies are quite different in the two spectral windows. The blue continuum has an extended structure in the central region with no well defined nucleus while the I band image shows a well defined nucleus in the central region. The contours appear highly disturbed and asymmetric in both the bands, though they are more so in the B band. The contours in the B band are stretched out in the north more than those in the I band suggesting the presence of dust in the region at $\approx 9''$ from the nuclear region. The $(B-I)$ map (Fig. 3.1q) clearly shows a highly reddened region coinciding with this feature. This region has a mean $(B-V)$ of 0.7 while the nuclear region has a mean value of 0.3. The I band image shows a pointed structure starting from the nuclear region and extending upto $4''$ along the SE direction. There is another pointy structure starting at $6''$ and extending upto $12''$ along the southern direction. Hα emission is global but the morphology of the emission is quite disturbed and clumpy. The peak of Hα emission is off-centered by $3''$ with respect to the optical nucleus and lies on the NE side of the nucleus. The clumpy nature could be due to the presence of dust and this will be explored in detail in Chapter 4.

- **Mrk 439 :**

  This galaxy is classified as S0/Sa in the Markarian catalogue. The outer contours of the galaxy in the R band appears smooth and nearly circular. However, the inner region of the galaxy shows a very complex light distribution with clumps and drawn out plumes (Fig. 3.1r). The central region is elliptical and is elongated in the NS direction. Two distinct plumes are seen emerging - one along the NW direction and the other along the West. Faint indications of spiral arms in the NE direction are seen in the isophotal maps as well as

the colour image. The contour maps show indications of a bar-like feature along the NW-SE direction, the signature of which becomes progressively prominent at shorter wavelengths. Wiklind & Henkel (1989) report the detection of a molecular bar in the central region in this galaxy. The colour maps show a blue elongated bar-like feature corresponding to that seen in the isophote map. Many galaxies with weak stellar bars have been found to contain strongly bar-like gas distributions similar to the one found in Mrk 439 e.g. the center of the nearby Scd galaxy IC 342 harbors a bar-like molecular gas structure about 500 pc in extent and a modest nuclear starburst about 70 pc in extent. (Lo et al. 1984; Ishizuki et al. 1990; Turner & Hurt 1992) In addition, there is another blue clump present at the south-eastern end of the bar. The nucleus is the bluest region with a $(B-V)\approx 0.3$.

The continuum subtracted Hα image shows an elongated bar corresponding to the one seen faintly in the contour maps and the colour maps. Hα emission is seen along the bar in the form of clumps. Emission is most intense at the ends of the bar, though it is found to extend throughout the body of the galaxy. A comparison of the broad band images and the Hα emission-line image shows that the regions that are bright in the continuum are spatially separated from the regions that are bright in the emission-line image.

- **Mrk 1134 :**

  This galaxy has been classified as an I0 galaxy. It is a small object and is paired with the larger Sc galaxy NGC 7753. The western arm of the spiral is connected to this galaxy by a bridge. The contours show an off-centered nucleus (Fig. 3.1s) with its center lying towards the region where the bridge from the larger spiral touches this galaxy. The large Sc galaxy and the bridge are not seen in this figure as we have only displayed the region covered by Mrk 1134. An image of the interacting system is given in Fig. 2.2. The colour image shows the bluest region to be coincident with the nucleus in B. A reddened region is seen to the South of this blue nucleus. The emission line image shows global massive star formation in this galaxy, with the peak of

Hα emission coinciding with the optical nucleus. The contours in the central region are elliptical with a slight protrusion towards the southern side. Another blob of emission is seen towards the western end of the galaxy. There is no structure corresponding to this blob in either the colour image or the isophotal contours.

3.5 *Discussion and Conclusions*

Analysis of the galaxy images and their isophotes reveals that the sample of starburst galaxies can be split up into three major morphological types: the S0's and ellipticals; the spirals; and the irregulars and peculiars.

The S0's and ellipticals forming the first class of starburst galaxies generally show smooth outer isophotes. However, distortions are seen in the form of disturbed inner isophotal contours or outer isophotes being off-centered with respect to the nucleus. They are generally isolated and do not show the presence of companions except in a few cases like Mrk 603 which is a clearly interacting system. Only one other galaxy, Mrk 1308 shows the presence of a companion nearby which could be responsible for triggering the starburst in Mrk 1308 due to tidal interaction with it. On probing the inner regions, we find structures like faint spiral arms as in Mrk 1002 and Mrk 190 or double nuclei as in Mrk 743. The contours in the inner regions of many of these galaxies appear more disturbed than the outer regions. Star formation is seen only in the central region with an extent of a few arcsecs in all the S0's/E's except in the interacting galaxy, Mrk 603 where the star formation activity is present globally. The companion galaxies of Mrk 603 also show global enhancement in star formation. The pseudo E.W. peaks at the nucleus or within 3" of the nucleus.

The sample contains 10 spirals. Out of these 10 galaxies, 8 are barred spirals. Star formation enhancement is seen in the nuclear region and at the ends of bars in most cases. Mrk 332 and Mrk 449 are the two objects where there are no

clear indications of the presence of a bar. In case of Mrk 332, intense star forming activity is seen along a ring like structure tracing the spiral arms. The arms show a disturbed morphology are are embedded in a smooth outer envelope. Structural analysis of Mrk 332 (Chapter 4) shows faint indications of a bar. Mrk 1194 and Mrk 213 show indications of a nuclear bar misaligned with the primary bar. Only one spiral, Mrk 1379 is part of an interacting system. As in Mrk 603, star formation activity is enhanced globally in the companion galaxies.

We classify three galaxies viz. Mrk 363, Mrk 439 and Mrk 1134 under irregulars/peculiars because of their highly disturbed isophotal contours. Mrk 363 and Mrk 1134 exhibit a global starburst while the third galaxy, Mrk 439 though not a global starburst, nevertheless shows extended Hα emission. The Hα isophotal contours do not trace the optical contours and the peak of Hα emission also does not coincide with the optical nucleus in Mrk 363 and Mrk 439.

The colour maps show that star formation is generally concentrated in the central region in all galaxies. Some galaxies like the irregulars Mrk 363 and Mrk 1134 show global enhancement of blue colour. On the basis of the colour maps and the emission line images, it is evident that the star forming regions show a wide variety of morphologies and locations like spiral arms, ends of bars, along the bar, in the circumnuclear region in the form of clumps or rings. Cases discussed in the present study show that the star formation though predominantly found to occur in the central region, is not always confined to the inner few kpc. In general, the regions with intense Hα emission correspond to the bluest regions seen in the colour maps. However, it is found in certain cases like Mrk 439 that rather blue areas do not show Hα emission. This probably indicates that the HII region seating there in the relatively recent past was turned off.

Simulated concentric aperture photometry of the Hα images shows that the line emission peaks in the central region and falls off nearly exponentially outwards in almost all cases. However, the radial distribution of pseudo E.W. does not show a uniform behaviour. This seems to indicate that though the intensity

is maximum at the center, the relative star formation shows different trends. The nuclear pseudo E.W. is higher than the global pseudo E.W. in most of the galaxies. In a few cases like Mrk 363, Mrk 439 and Mrk 332 which show intense extranuclear star formation, the nuclear pseudo E.W. is lower than its global value. This suggests that the induced star formation relative to the underlying population is higher at locations other than the nucleus in these cases. In Mrk 1308, the pseudo E.W. peak is off-centered by 3". The pseudo E.W. traces the efficiency of star formation with respect to the underlying old population. In Mrk 1308, the efficiency is maximum at 3" from the center and is about 30% higher than that in the central region. This suggests that the physical conditions in this region are conducive to conversion of gas into stars. Radio observations of Mrk 1308 also reveal a molecular ring of the same size around the nucleus. Based on their study of isolated spiral galaxies, Hodge & Kennicutt (1983) concluded that the radial distribution of star formation in isolated spirals approximately follows the integrated light of the stellar disk. This would imply a more or less constant radial distribution of equivalent width, which is not consistent with the distribution of pseudo E.W.s found in the sample of starburst galaxies in the present study. A study of interacting galaxies by Bushouse (1986) also does not show a constant radial distribution of E.W.s and they conclude that the interaction induced star formation usually does not follow the same pattern of pre-interaction star formation, but occurs preferentially near the nuclear regions. In our sample, we find that the E.W. is generally maximum at the center or near the center.

Chapter 4

Structural properties

Summary

The structure of the galaxies in the sample has been studied using ellipse fitting techniques. Based on the radial variations of the luminosity, the ellipticity and the position angle, we discuss the various structural details of the starburst galaxies. The presence and the extent of features such as bars, isophotal twists etc. is studied. The colour profiles derived from the isophotal analysis have been examined to shed light on the radial distribution of the stellar population. We have also constructed smooth models from the isophotal analysis results to extract the underlying fine structure which provides useful information about the processes which could have triggered the starburst. Structural parameters such as half-light radii, disk scale lengths and central disk brightnesses have been derived.

4.1 *Luminosity profiles of galaxies*

One of the primary tools for studying the structure of galaxies is surface photometry i.e. the measurement of the two-dimensional brightness distribution. At visual and near-infrared wavelengths, most of the galaxy's light is produced by stars; thus the spatial distribution of light represents the spatial distribution of stars in the galaxy. The two-dimensional intensity map obtained by imaging can be exploited to give a lot of useful information like distribution of different stellar populations, gas and dust distributions, structures like bars, oval distortions, etc. in the galaxy. Photometric decomposition has long been used to describe the structural properties of galaxies like scale lengths, half-light radii and isophotal twists. Reynolds (1913) was the first to give a quantitative analysis of the photometric contributions when he studied the center of M81 and proposed a formula, subsequently applied to ellipticals by Hubble (1930). de Vaucouleurs (1953) introduced the $r^{1/4}$ law for spheroidal systems. Later, de Vaucouleurs (1959) noticed the exponential form of the disk luminosity profile. In the 1940's Baade (1944) introduced the concept of stellar populations. Population I consists of young stars (ages $\leq 10^9$ years) in general, associated with dust and clouds of ionized or molecular gas and are mainly found in the disk. On the other hand, Population II stars are redder, older, metal poor and usually associated with the bulge. These observations were further refined in the 1960's and the 1970's with the recognition of populations with various ages and dynamics in both the disk and the bulge. Hence, now stars are classified into the young, intermediate and old disk populations and the metal-rich and metal-poor spheroidal populations. Of these, the old disk population contains most of the mass and produces most of the light in late-type spirals. For instance, in the Galaxy the old disk population is found to contain more than 95% of the disk's luminous mass and produces 80% of the total light (Freeman 1987; Gilmore et al. 1990). For such studies, earlier researchers used an intensity profile, generally obtained by taking a cut along the major axis or the minor axis of a galaxy. With the advent of computers, it became possible to average the intensity along

isophotes and study the overall nature of the light distribution. The radial profiles of elliptical galaxies can be fit very well by the de Vaucouleur's $r^{1/4}$ law while the luminosity profiles of disk galaxies can be decomposed into a bulge following a de Vaucouleur's law and an exponential disk profile. The light distribution of disk galaxies can be represented by a sum of the following equations:

$$\mu(r) = \mu_{eff} - 8.327[\left(\frac{r}{r_e}\right)^{1/4} - 1] \quad (4.1)$$

$$\mu(r) = \mu_0 + 1.086\left(\frac{r}{h}\right). \quad (4.2)$$

where $\mu(r)$ represents the surface brightness at a distance r from the center, the effective radius r_e is the radius of the isophote enclosing half of the total luminosity, μ_{eff} is the surface brightness at r_e, μ_0 is the central disk surface brightness and h is the scale length. However, it was soon realized that less than half the spirals could be fit perfectly with this two component model alone (Boroson 1981). Indeed, the presence of components like bars, lenses, star forming regions, dust, etc. hamper a simple two component decomposition.

4.2 *Ellipse fitting*

In order to study the nature of the galaxy hosting the starburst and to provide a quantitative description of the morphological aspects of these objects, we explored the sample galaxies to look for structures known to be associated with or responsible for fueling the starburst. Our analysis is based on techniques previously utilized by other workers to study elliptical (Bender & Möllenhoff 1987; Bender et al. 1988) and spiral galaxies (Wozniak et al. 1995; Jungweirt et al. 1997) in more recent years. The procedure consists of fitting elliptical isophotes to the galaxy images and deriving one-dimensional, azimuthally averaged radial profiles for the surface brightness, ellipticity and the position angle of the galaxies. The ellipse fitting

technique is a powerful technique to probe the structural properties of the galaxies. The ELLIPSE task within the ISOPHOTE package in STSDAS[1] was used to derive the luminosity, position angle and ellipticity profiles for the sample galaxies in each filter. This method is based on Jedrzejewski's algorithm (1987a) and uses an iterative least squares fit to a Fourier expansion. The image is measured using the iterative method described by Jedrzejewski. Using the approximate values for the semi-major axis length, the X and Y axis center, th ellipticity and the position angle of the semi-major axis specified by the user, the image is sampled along a first-guess elliptical path, producing a 1-dimensional intensity distribution as a function of the ellipse eccentric anomaly E.

$$I = I_0 + \sum_{n=1}^{\infty}(A_n \sin(nE) + B_n \cos(nE)) \tag{4.3}$$

where I_0 is the mean intensity along the ellipse, E is the ellipse eccentric anomaly and $A_n, B_n (n = 1, 2, ...)$ are harmonic amplitudes. If the isophotes are ideal ellipses, the first four coefficients namely, A_1, B_1, A_2, B_2 are non-zero. All other higher coefficients are zero. A_3, B_3, A_4, B_4 determine the deviations of the isophotes from perfect ellipses. A positive value of the B_4 coefficient indicates the presence of a disk while a negative value of B_4 indicates boxiness. This method has widely been used in fitting the surface brightness profiles of elliptical galaxies. Jedrzejewski (1987b) has discussed isophotal shapes in detail. The contribution of the various terms in the Fourier series indicates the nature and the extent of the deviation of the isophote from ellipticity and helps in detecting the presence of bars, dust, star forming regions, spiral arms, disk components, etc. In recent years, Wozniak et al. (1995) have used this technique to study spiral galaxies and they have been successful in detecting hitherto undetected bars in some galaxies. Heraudeau et al. (1996) have also been successful in detecting bars in the central regions of galaxies from NIR surface photometry. We have applied this technique to our sample of starburst galaxies to study the properties of the underlying galaxy. The fitting procedure requires the following initial guess parameters : the center (x and y) of

[1]The Space Telescope Science Data Analysis System STSDAS is distributed by the Space Telescope Science Institute.

the guess ellipse, its position angle, ellipticity as input parameters. In our fitting procedure, the centers, position angles and the ellipticity of the ellipses were allowed to vary for all galaxies except Mrk 743 and Mrk 190. Mrk 743 shows the presence of two nuclei in the central region so ellipse fitting procedures would fail for this galaxy. Mrk 190 is a face-on galaxy. Hence its ellipticity is close to 0.0. In such a case, the ellipse fitting procedure does not give additional information. For these two galaxies, the luminosity profile was derived using concentric circular apertures. Details for individual galaxies are given in Section 4.5.1. We increased the semi-major axis length by 10% for successive ellipses. The top 10% intensity pixels were clipped off to avoid spurious values. Foreground stars were masked out with a circular mask before the fit was started. Also, in cases like Mrk 603 and Mrk 1379 which are a part of an interacting system of galaxies, we masked out the companion galaxies to avoid the light of the companions from contaminating the ellipse fitting procedure.

4.3 *Colour index profiles*

The radial distribution of the colour can be derived from the luminosity profiles. The colour index is a useful indicator of the spatial distribution of the stellar population in the galaxy, as has been discussed in detail in Chapter 3. Its distribution is a pointer to the location and extent of star forming regions, dust lanes, rings and other structures in the galaxy. Aperture photometric studies of Markarian starburst galaxies by Huchra (1977b) show that these galaxies get bluer towards their centers. For the present sample of starburst galaxies, we find that in most cases, they generally get bluer towards the center as found by Huchra (1977b), however, these profiles are modulated by the presence of other star forming regions and together with the luminosity, ellipticity and position angle profiles, they can be exploited to yield valuable information about the underlying structures as well as the photometric properties of the starburst regions.

4.4 *Detection of fine structure*

Fine structure such as shells, rings, dust lanes, etc. which are embedded in the galaxy may be hidden due to the much higher brightness of the galaxy. Mergers are believed to induce fine structure in galaxies. Schweizer & Seitzer (1988,1992) quantify such fine structure in E and S0 galaxies. The detection and the enhancement of these structures can give information about the dynamical processes undergone by the galaxy. We describe below the technique we used for extracting the underlying fine structure in our sample galaxies and some important results obtained. Faúndez-Abans & de Oliveira-Abans (1998) describe a number of techniques useful for extracting fine structure.

4.4.1 *Model construction and residual maps*

A smooth model of the galaxy was obtained by interpolation of the surface brightness, the ellipticity and position angle profiles of the fitted isophotes. As this is an averaged image, it would contain information about the axisymmetric structures only. This model image is subtracted from the original image and the residual image thus obtained was examined for clues to the non axisymmetric structures and other features like shells, ripples, vestiges of mergers, etc. The residual map contains a wealth of information which has been used by a number of workers to derive information about the underlying galaxy. Kenney et al. (1996) have reported the detection of banana-shaped isophotes , shell-like features and other structures generally associated with mergers and accretion events in the peculiar Virgo cluster galaxy NGC 4424. Based on a study conducted on the pair of interacting galaxies AM 0327-285, de Mello et al. (1995) have reported the detection of a rudimentary spiral pattern in one and shells in the other galaxy in the pair. Simulations by Hernquist (1992,1993) predict X-shaped structure with boxy isophotes for merger remnants. We have constructed residual images based on the results

of the isophotal analysis and have detected complex fine structure in the galaxies. In the barred spiral Mrk 213, we find indications for the presence of a central bar or oval distortion. This central structure is not aligned with the primary bar. The residual image of Mrk 1002 shows a X-shaped structure crossing the central region. A detailed discussion on the residual maps for each galaxy is given in Section 4.5.1. Residual maps for the galaxies showing interesting features are presented in Fig. 4.2. The residual images obtained using the R band images are shown for the galaxies : Mrk 213, Mrk 363, Mrk 439, Mrk 449, Mrk 1002, Mrk 1194, Mrk 1308 and Mrk 1379.

4.5 *Results of isophotal analysis*

The results of the isophotal analysis are displayed in Fig. 4.5 showing the averaged radial luminosity profiles in units of mag/sq.arcsec, the ellipticity (eps) and the position angle (P.A.) in degrees, of the major axis of the isophotes as a function of the semi-major axis length (a). The fitting was stopped at the point where the errors in the magnitude reached 0.2. Hence, the maximum errors on the surface brightness profiles are of this order. The figures are arranged in the increasing order of the Markarian number except for Mrk 743 and Mrk 190. Only the luminosity profiles are plotted for Mrk 190 and Mrk 743 since for these galaxies, the luminosity profiles were derived using concentric circular apertures. We derived the distribution in colour from the surface brightness profiles and Fig. 4.6 shows the radial behaviour of $(B-V), (B-R)$ and $(V-I)$ in the galaxy. The position angle is defined as the angle between the North and the major axis of the fitted ellipse, in an eastward sense. In Table 4.1, we list the position angles for each galaxy through each filter, calculated by averaging the values obtained from the three outermost elliptical isophote fits. The disk ellipticities of each galaxy through each filter are also presented by averaging in a similar manner. The inclination of the galaxy is derived from the ellipticity of the outermost isophotes using Tully's (1988) formula viz.

$$
\begin{aligned}
i &= \cos^{-1}\left\{\frac{(b/a)^2 - 0.2^2}{1 - 0.2^2}\right\}^{1/2} + 3^o \\
e &= 1 - \frac{b}{a}
\end{aligned}
\tag{4.4}
$$

assuming that edge-on systems would have $(b/a) = 0.2$. The correction constant 3^o is an empirical value (Aaronson et al. 1980). As discussed in the previous chapter, a red colour in the colour maps can be either due to reddening by dust in that region or due to a redder stellar population. It is possible to separate these two effects, at least in a qualitative manner by comparing the ellipticity profiles derived for images through different band passes (Prieto et al. 1992a,b). Dust would affect the shorter wavelengths to a greater extent and the isophotes at the shorter wavelengths would tend to be rounder. This would be accompanied by a reduction in the surface brightness in this region at shorter wavelengths. A reddening of colours accompanied by a decrease in surface brightness therefore, signals the presence of dust while a reddening of colours accompanied by an increase in the surface brightness indicates a redder stellar population in that region. In some cases, star forming regions at the ends of bars would contribute at shorter wavelengths and the isophotes would be more elliptical at shorter wavelengths, along with an increase in the surface brightness. Hence, from the trends observed in the surface brightness and the ellipticity profiles as we progress from shorter to longer wavelengths, it is possible to detect the presence of dust and redder stellar populations. Such a thing is not possible using colour maps or colour profiles alone.

4.5.1 *Individual galaxies*

The detailed study of each galaxy based on ellipse fitting was done. The behaviour of the luminosity, ellipticity and the position angle profiles and the results obtained are described below.

Table 4.1: The position angle (P.A.) in degrees, ellipticity (eps) in each filter and the inclination in degrees (i) of the galaxy to the line of sight.

Galaxy	P.A.				eps				i
Mrk	B	V	R	I	B	V	R	I	
14	3	21	7	32	0.17	0.17	0.17	0.18	38
87	60	62	60	62	0.40	0.53	0.51	0.50	64
190	-	-	-	-	-	-	-	-	-
213	148	142	141	133	0.60	0.59	0.55	0.51	69
332	67	78	84	81	0.11	0.11	0.14	0.12	32
363	168	164	177	178	0.30	0.27	0.15	0.19	43
439	99	121	18	21	0.03	0.06	0.05	0.11	23
449	83	82	82	82	0.69	0.71	0.70	0.64	78
602	31	39	30	34	0.27	0.22	0.21	0.19	43
603	160	147	150	170	0.43	0.38	0.38	0.36	56
708	73	75	75	80	0.68	0.63	0.64	0.62	75
743	-	-	-	-	-	-	-	-	-
781	18	28	29	161	0.14	0.16	0.18	0.16	37
799	163	180	180	182	0.33	0.41	0.41	0.40	57
1002	3	1	3	16	0.23	0.24	0.22	0.13	41
1134	96	95	94	95	0.52	0.50	0.52	0.46	65
1194	78	84	85	89	0.37	0.32	0.35	0.38	54
1308	19	20	25	15	0.13	0.09	0.08	0.09	29
1379	60	57	53	57	0.51	0.45	0.45	0.34	60

S0's and ellipticals

Ellipticals were believed to be old systems devoid of gas and dust and supported by the velocity dispersion of the stars in them. However, the detection of features like dust lanes, shells, ripples in some ellipticals gave indications that these were not uninteresting oblate or prolate spheroids but had a wealth of information hidden in them. Liller (1960,1966) noticed isophotal twisting in some ellipticals. Isophotal twisting was rediscovered by Barbon et al. (1976); King (1978) and Williams & Schwarzchild (1979). Isophotal twists are a signature of non-circular motions of gas, increasing the rate of collision as well as the radial transport of gas towards the galactic center. Kormendy (1982) argues tht some of the twists may be tidal in origin. Scoville & Hersh (1979) suggest that this mechanism could be responsible for enhancing the gas density in the nucleus and triggering star formation there. A number of features discovered subsequently like faint shells (Malin 1979), kinematically decoupled cores (Franx & Illingworth 1988), anomalous blue

cores (Zepf et al. 1991), counter rotating dust lanes and gaseous disks (Bertola et al. 1985), all point to a history of cannibalism and merging for these present day ellipticals. Binney & Petrou (1985) propose that boxy isophotes are created by the slow cannibalism and orbital decay of a low luminosity galaxy into a host bulge or elliptical. The high orbital angular momentum of the stars initially associated with the cannibalized galaxy causes them to overpopulate the box orbits in the host giving rise to boxy isophotes. de Vaucouleurs & Capaccioli (1979) noticed the existence of faint systematic deviations (ripples) in the light profile of the classic elliptical NGC 3379. They suggested that these deviations could be the photometric signature of a faint underlying structure which was later identified as a weak disk. Isophotal shape analysis is a powerful method for studying such weak fine structure in galaxies. A large number of ellipticals have been studied and the fine structure interpreted to give valuable information about the structure and hence the dynamical and evolutionary history of those ellipticals.

Our sample contains 6 early type systems that have been classified differently in different catalogues as SO/E. A detailed description of each galaxy is presented below.

- **Mrk 14 :**

  The luminosity profile (Fig. 4.5) is made up of two components. An inner part steeply rising towards the center and an outer exponential part. Ellipticity is highest in the central region in all the filters, with a maximum of ($\sim$0.35) in the B filter. It drops to a value of 0.1 at 9" . Beyond 9", the ellipticity rises again, showing a number of peaks before reaching a value of 0.2 in the outermost region. The isophotes show a continuous twist (40^o) from the central to the outer regions. The contours in the inner 8" show a boxy nature while beyond 10", they become pointy, indicative of a disk; as is seen from the negative and the positive values respectively of the coefficient B_4 of the cos(4E) term in Fig. 4.1. A strong isophotal twist and boxiness of the isophotes are indicative of possible interaction in the past. Similar inferences have been

drawn by Nieto & Bender (1989) and Bender & Möllenhoff (1987) for other early type systems. This is the most likely cause for triggering the central starburst in Mrk 14. The colour profile (Fig. 4.6) shows a very blue ($B - V$ = 0.2) nuclear region, with the colour getting redder outwards. The residual image constructed with the model light distribution subtracted from the direct image fails to reveal any other structure besides a bright nuclear region.

- **Mrk 190 :**

  This S0 galaxy is nearly face-on and the ellipticity remains more or less constant near 0. In this case, the luminosity profile was extracted using concentric circular apertures and we do not derive any information about the variation of the position angle. The luminosity profile shows an inner steep part and an outer exponential form. The colours for this object also get redder outwards, however, the bluest region is seen to be off-centered from the optical nucleus by about 3″. We do not detect any structures in this galaxy except that the residual image shows a double structure in the central region.

- **Mrk 603 :**

  Mrk 603 forms a part of an interacting system of galaxies. The two companion galaxies were first masked out before starting the fitting to avoid contamination of the results by the luminosity of these galaxies. The luminosity profile is made up of two components similar to that seen for Mrk 14 and Mrk 190. The ellipticity gradually increases as we move outwards from the center. The ellipses are boxy in the inner 13″ as shown by the negative value of B_4 in Fig. 4.1. The position angle shows a steep change of 30° between 6″ and 9″. The colours get bluer outwards for Mrk 603. The residual image in R shows clumpy structure in the inner 6″ lying along the major axis of the fitted ellipses. Towards shorter wavelengths, these clumps start reducing in intensity.

- **Mrk 743 :**

  This galaxy is made up of two nuclei surrounded by a common envelope,

so we have not used ellipse fitting techniques for this object. The luminosity profiles were derived in a manner similar to that used for Mrk 190. In this case, since the relative intensity of the nuclei was wavelength dependent as discussed in Chapter 3, we kept the center fixed at a point midway between the two nuclei. This was maintained for all filters. The luminosity profile shows a two component nature. The central region is the bluest and the galaxy gets red outwards till about 10" and beyond that there is a mild trend towards the bluer side. Since Mrk 743 shows such a peculiar morphology, we cannot comment on the nature of the underlying galaxy. However, the presence of double nuclei with star formation enhanced in only one and the presence of an asymmetric outer envelope seem to indicate that this galaxy is a result of the merger of two galaxies which may be responsible for the burst of star formation.

- **Mrk 1002 :**

  The surface brightness profile shows, more or less, a smooth nature. The position angle jumps abruptly by 70^o between 3 and 10". This is accompanied by a sudden sharp increase in ellipticity from less then 0.1 in the central region to 0.3 at 10". This jump can be attributed to the spiral arm like features seen in the isophotal contours and the colour maps in Fig. 3.1e. Between 5 and 10", there is a twisting of isophotes, accompanied by boxiness of the isophotes in this region, as seen from the negative values of the B_4 coefficient in Fig. 4.1. The colour profiles show that the bluest region in this galaxy is off-centered from the nucleus by about 3". The residual image (Fig. 4.2) also shows a X-shaped structure crossing the nuclear region. The isophotal twisting, boxiness and the X-shaped residuals indicate that the enhancement in star formation in this galaxy is result of a past merger.

- **Mrk 1308 :**

  Mrk 1308 exhibits two component surface brightness profiles, similar to those discussed above. We detect a very strong systematic twisting of isophotes

in this galaxy. Though the ellipticity shows a small variation of less than 0.1 beyond the inner 3″, there is a continuous variation in the position angle. Within the inner 10″ , the position angle changes by nearly 180°. Mrk 1308 exhibits strong isophotal twisting between 5″ - 10″, and non-concentric isophotes in the outer regions. The B_4 coefficient (Fig. 4.1) oscillates around zero and shows no clear trends.The residual image (Fig. 4.2) shows faint indications of tiny spiral arms in the central region. The isophotal twisting and the faint signature of spirals in the residual image could be due to gravitational interaction of this galaxy with its companion.

Spirals

In recent years, the techniques of ellipse fitting have been utilized for studying not only ellipticals, but also spirals. Studies by Wozniak et al. (1995) and Jungwiert et al. (1997) on samples of spiral galaxies using this technique have been useful in detecting underlying structures like bars which were hitherto undetected, oval distortions, shells and rings. This technique can be used to study the underlying structure of starburst galaxies in a similar manner. Barth et al. (1995) have used these techniques to study a sample of emission line southern starburst galaxies. Individual cases are discussed below.

- **Mrk 87 :**

  The luminosity profiles in this strongly barred spiral are composed of three distinct components. In addition to the two components seen in the above early type galaxy, a plateau is seen between the inner and the outer components. This is due to the bar in Mrk 87. Isophotal twisting is seen in the inner region. The ellipticity gradually increases outwards. Beyond 5″, the behaviour of the ellipticity and position angles is similar in all filters. The ellipticity profile shows a slight discontinuity at 8″ . Between 5″ and 10″ , the position angle is nearly constant at 75° and then slowly changes by 15°

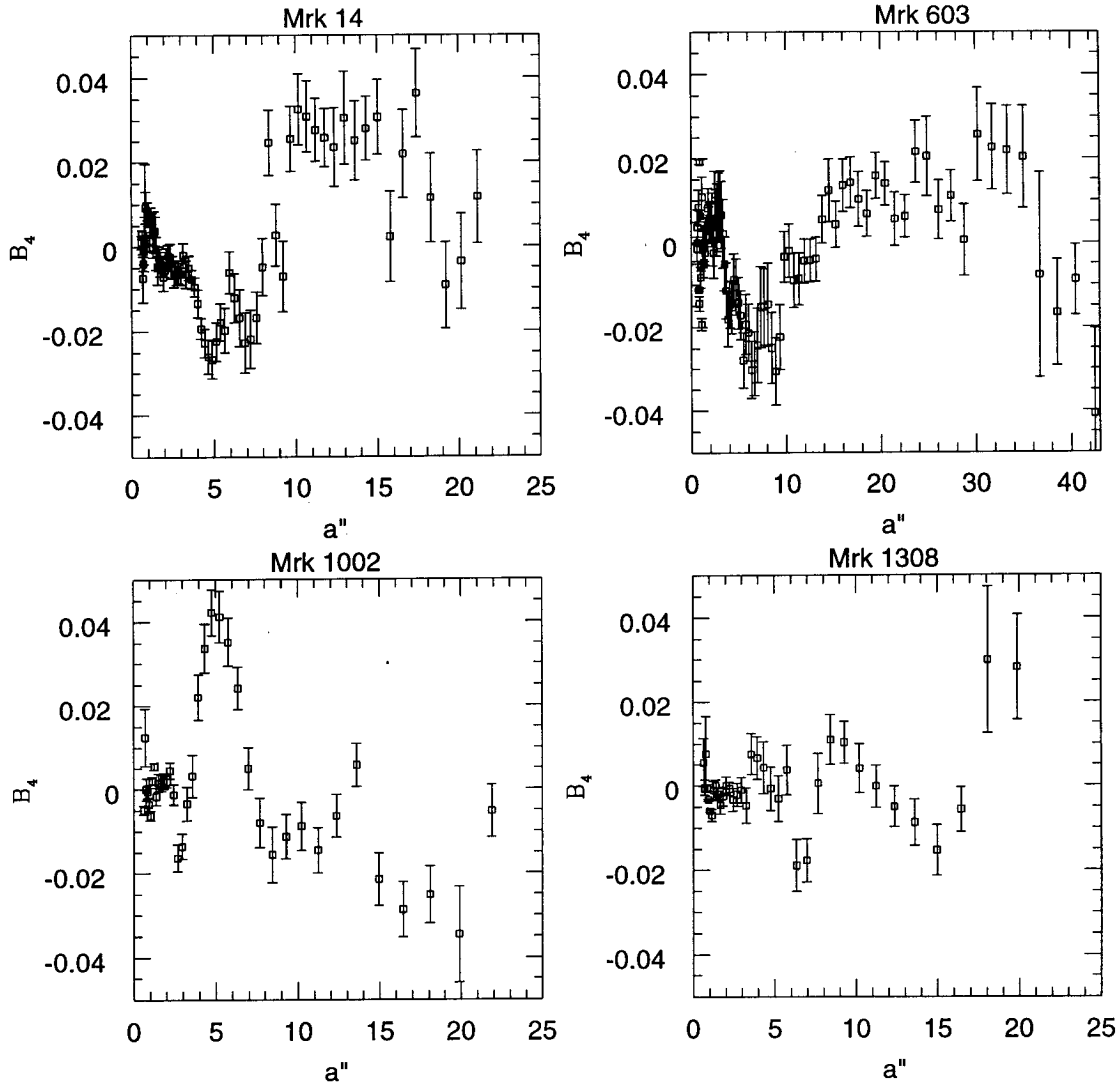

Figure 4.1: The variation of the B_4 coefficient as a function of the radial distance. Mrk 14 and Mrk 603 show inner boxiness and Mrk 1002 shows boxiness in the outer regions. For Mrk 1308 the B_4 coefficient fluctuates about 0.0

before reaching the final value of 60^o . The presence of the blue ring is clearly seen in the colour profiles in Fig. 4.6. The signatures of the bar are seen very clearly in the ellipticity and position angle profiles. The strong bar in Mrk 87 may be responsible for triggering the starburst in this galaxy.

- **Mrk 213 :**

  The surface brightness distribution is multi-component: a central steep part, a plateau corresponding to the bar and an outer disk. The ellipticity profile in the inner region shows a peak at 4″ and then falls to a value of 0.3 at 8″. Beyond 8″, the ellipticity rises again to the disk ellipticity of 0.6. The position angle curves show a constant value $\sim 130^0$ in the inner 8″ . We attribute these features to the presence of a nuclear bar or an oval distortion of length 16″. Beyond 8″, the P.A. rises and stays at nearly a constant value beyond 10″. This shows the presence of the primary bar. This indicates that the inner bar is misaligned with the primary bar by 20^o and corresponds to the feature seen in the central region in the isophotal contours. These bars are believed to be an efficient mechanism for driving gas into the nuclear region and fueling the starburst. The position angle changes by 25^o between 8″ and 10″. The residual map (Fig. 4.2) shows the signature of the central bar-like structure in the form of a linear feature in the inner region. This galaxy is a peculiar case of a bar within bar.

- **Mrk 332 :**

  The surface brightness profiles of this spiral galaxy show a sharp rise in intensity in the inner region. Between 6″ and 10″, the luminosity profiles show a strong wavelength dependence. This is seen as a rise in the intensity, which is most prominent in the B band and disappears in the I band luminosity distribution. The ellipticity shows a corresponding rise in this region. The ellipticity also shows a strong wavelength dependence with the peak ellipticity maximum at 0.75 in B and falling to a value of 0.4 in the I band. The increase in intensity at 10″ in the B band accompanied by a highly elliptical

region indicate the presence of a star forming region at this location. The colour profiles also show the bluest region to be situated at 10″ from the center, which confirms that the maximum in ellipticity is due to the star forming region present at this location in the galaxy. One interesting feature seen is that the change in position angle in the inner region upto 10″ reduces at longer wavelengths. This is an isolated galaxy which does not show any kind of interaction. The ellipticity and position angle at longer wavelengths, especially in the I band are indicative of the possible presence of a bar, which may be responsible for triggering the starburst. Imaging at near infrared wavelengths would be useful in checking for the presence of a bar in this galaxy. Beyond 10″, the position angle changes abruptly signaling the region where the ellipse fitting program has hit the spiral arms.

- **Mrk 449 :**

  The surface brightness profile is made up of two components. The most prominent feature in the surface brightness profile is the dip at 10″, which becomes shallower at longer wavelengths. This dip is a consequence of the depression in the intensity in this region due to the presence of the dust lane seen clearly in the $(B - I)$ image in Fig. 3.1j. The position angle remains constant throughout except for a small dip in the central region. The very high inclination of this system makes it difficult to interpret the results of the ellipse fitting uniquely. The residual image (Fig. 4.2) shows that an excess luminosity is present in the nucleus as well as in the region to the east of the dust lane. However, no structure is seen in the region to the west of the nucleus.

- **Mrk 602 :**

  The most prominent feature in the surface brightness profile is the plateau, a signature of the presence of a bar. The plateau region shows a small increase in brightness between 8″ and 10″ in the B band. The ellipticity rises to its maximum value at ~16″. Beyond this, the ellipticity falls to a value between

0.2-0.3 which is filter dependent. The P.A.is nearly constant between 4" and 16". From the ellipticity and position angle profiles, we estimate the total length of the bar to be 32", which corresponds to a linear scale of 5.8 kpc. The ellipticity peak is wavelength dependent showing a higher ellipticity at shorter wavelengths, indicating the contribution of star forming regions situated at the end of the bar. This is supported by the colour profiles too as a local minima at the end of the bar.

- **Mrk 708 :**

  The luminosity profile appears to be made up of three components similar to that seen in Mrk 87. There appears to be a break in the luminosity profile at 15". The P.A. changes gradually from the central region upto 15" and then jumps abruptly between 15" and 20". This change is largest in the B band. Beyond 20", the position angle reamins nearly constant. The ellipticity profiles show a gradual increase in ellipticity from the center outwards. A number of peaks are seen in the ellipticity profiles. The most prominent peak which is seen in all bands is at 15". The ellipticity in this region is filter dependent with the ellipses being rounder at longer wavelengths. The colours are highly reddened in the inner region of this galaxy and they get bluer outwards. However, Hα emission is found in the central region of this galaxy. The isophotal analysis fails to detect the presence of dust in the inner region. Therefore we infer that the older, redder population dominates the colours in the inner regions of this galaxy.

- **Mrk 781 :**

  The surface brightness falls sharply upto 10" and then remains steady up to 30". The ellipticity rises gradually and reaches a maximum of 0.7 in B and 0.6 in I at 30". Beyond 30", it shows a sharp decrease in all the bands. The position angle remains nearly constant within a radial distance of 30" except for the large fluctuations seen in the inner 4". The luminosity, nature of the ellipticity and position angle all show the presence of a bar. We estimate

the total extent of the bar to be 60″ which corresponds to 11 kpc. However, there is a systematic shift in the peak ellipticity from B to I with the shorter wavelength peak showing a larger ellipticity. This is due to the star forming regions at the end of the bar, in the spiral arms. Faint signatures of the ring detected in the colour maps are also seen in the ellipticity and the colour profiles. However, imaging at a higher resolution is required to study the details in the ring.

- **Mrk 799 :**

  The luminosity profile of Mrk 799 is made up of three distinct components. In the innermost 5″, it shows an exponential behaviour, between 5″ and 15″ the profile shows a plateau with the luminosity remaining more or less constant and in the outer region beyond 15″, it falls gradually. Correspondingly, the the ellipticity falls sharply from the center up to 5″, accompanied by a large change in the position angle. Between 5″ and 22″, the ellipticity increases sharply and reaches a maximum value of 0.55 showing a broad peak. This is accompanied by a nearly constant position angle between 10″ and 25″. From the profiles, we infer the presence of a bar and we estimate the extent of the bar to be 50″ which translates to a linear scale of 9.1 kpc.

- **Mrk 1194 :**

  The luminosity profile is complex in nature and appears to be made up of at least three distinct components. The ellipticity profile shows a sharp decrease in the inner 4″, then a gradual rise reaching a maximum near 20″ in all the bands. Another small peak is seen near 6″ in V, R and I bands. The position angle shows a small plateau between 3″-7″ which becomes clearer at longer wavelengths and then jumps abruptly and again shows a constant value between 10″-25″. These features along with the nature of the isophotal contours are indicative of the presence of a bar or an oval distortion in the inner region. Moreover, this distortion is not aligned with the primary bar of the galaxy. The position angle of these two differs by 50°. We estimate

the inner bar to be about 12″ (3.67 kpc) long and the primary bar to have an extent of 44″ (13.46 kpc). The colour profiles in Fig. 4.6 get redder outwards. The bluest region in the colour profiles has a diameter of about 6″ (1.83 kpc) and corresponds to the ring seen in the Hα image. The residual image (Fig. 4.2) shows two lobes lying along the primary bar and another short bar-like feature in the inner regions.

- **Mrk 1379 :**

  Mrk 1379 forms a part of a system of interacting galaxies. The irregular galaxy lying towards the eastern edge of Mrk 1379 was first masked out to prevent the results of the ellipse fitting to be influenced by its luminosity. The luminosity profile appears to be made up of two distinct components with small superimposed features at 16″ and 22″. The position angle increases to 75^o between 5″ and 8″, accompanied by a kink in the ellipticity profile between these points. We detect two peaks in the ellipticity profiles, the ellipticities of which are wavelength dependent. The first peak corresponds to the blue structure seen in the colour image (Fig. 3.1p) lying at 13″ to the west of the nucleus. Also, the local minima at 19″ between the two maxima becomes more prominent at longer wavelengths. There is no appreciable variation in the position angle in these two regions. However, the surface brightness profiles have a small kink at this position in all the filters, the most prominent being in the *B* band. In the inner 10″, the blue isophotes are rounder as compared to the red ones. The colour profiles in Fig. 4.6 show a sudden reddening between 2″ and 8″. Hence we infer that the reddening of colours seen in the inner 10″ is due to the presence of dust in this region. Between 10″ and 15″, the ellipticity profiles do not show any wavelength dependence. Beyond 15″ the trend reverses and the *I* band isophotes are rounder. Beyond 30″, the contribution to the blue light is predominantly from the spiral arms while the light distribution at longer wavelengths is smoother and in the form of a common envelope, which accounts for the wavelength dependent behaviour

of the ellipticity profiles in this region. The residual maps vary in their appearance in the B and the I bands. Enhancements in luminosity are seen in the nuclear region, in the blue knot to the west and along a curved spiral arm which appears to start from the nucleus. Spiral arms with two bright blobs connected to this linear structure are also seen.

Irregulars and Peculiars

- **Mrk 363 :**

  In case of Mrk 363, the luminosity profile seems to be made up of a single exponential part. A small kink is seen in all bands, but it is more prominent in the R band. The ellipticity in the central region is close to 0.2 for V, R and I. Close to the nucleus, the ellipticity profile shows a small kink in these three bands. It rises to a value of 0.4 at 10″. The P.A. in the B band remains nearly constant at 145° in the inner 6″ and then gradually increases reaching a value of 175° at 11″. The P.A. shows strong wavelength dependence. In V, R and I, the P.A. value slowly decreases in the inner 5″ and then gradually rises to reach a value of $\sim$ 175° as in the B band. Beyond 12″, the position angles in different filters show different behaviours. Twisting of isophotes is seen in this galaxy. The ellipticity profiles do not show any clear trends. This galaxy shows global star formation and the colours do not show an appreciable change. The residual image obtained by subtracting the smoothed image from the direct image revealed complex fine structure (Fig. 4.2). A bright nucleus, with spiral arms lying along the NS direction and extending right upto the nucleus are seen. Another small arm is seen emerging from the nucleus from its western side. As this galaxy belongs to a group of seven galaxies, tidal interactions with the other galaxies of the group are a likely cause of the enhancement in star formation activity in this galaxy.

- **Mrk 439 :**

  Fitting isophotes to the images reveals changing ellipticity and position angle

throughout the body of the galaxy. The luminosity profile is smooth except for small features at 5″ and 10″. The ellipticity profile shows a double peaked structure in the inner region. The ellipticity of the first peak is wavelength dependent, the isophotes at shorter wavelengths being rounder. The colour map also shows a redder region at this location. We infer the presence of dust in the inner 4″ of this galaxy. The other peak occurs at 5″ which corresponds to the brightest region seen in Hα. Beyond 5″, eps drops to a low value ($\sim$0.1) at 15″ and remains at a low value beyond that in all filters. The position angle is nearly constant in the inner 10″. The contours are boxy in the inner 6″. Beyond 6″, the galaxy contours show the presence of a disk structure which is nearly aligned with the major axis. The residual image (Fig. 4.2) shows the presence of the bar that is seen clearly in Hα as discussed in Chapter 3. It also shows a number of shell like features.

- **Mrk 1134 :**

  The luminosity profile in this irregular galaxy shows a behaviour similar to that seen in Mrk 363. A small kink is seen at 5″ in the luminosity profile in the B band and it flattens out at longer wavelengths. The ellipticity in the inner region upto 5″ shows a peculiar bahaviour. Upto 5″, the ellipses are rounder in B as compared to V and R, indicating the presence of dust in the inner region s. The P.A. profiles show a peculiar behaviour in the inner region upto 10″. The change in P.A. in the B band is in an opposite sense as compared to that in the other three bands. This means that the spatial distribution of young stars is oriented differently as compared to the older stars. Beyond 10″, the ellipticity remains nearly constant throughout the body of the galaxy. However, the isophotes twist by nearly 20 ^{o} from 10″ to the outer regions. The colour profiles (Fig. 4.6) are bluest at the center and generally get redder outwards though they show a multiple peaked behaviour in $(B-V)$ and $(B-R)$.

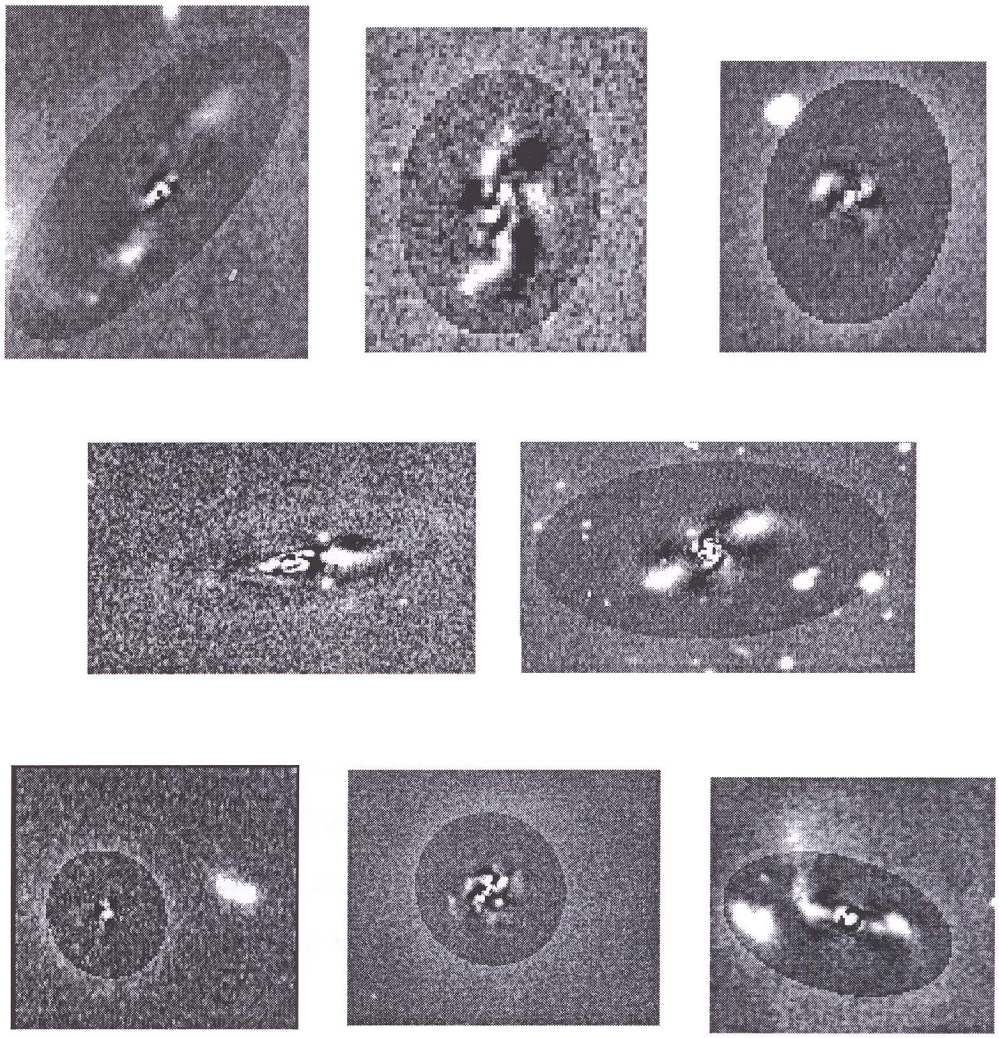

Figure 4.2: Residuals of the images in the R band. From left to right in the top row : Mrk 213, Mrk 363, Mrk 1308; middle row: Mrk 449, Mrk 1194; bottom row: Mrk 1002, Mrk 439, Mrk 1379. North is at the top and East to the left.

4.5.2 *Discussion*

Based on the reslts of the isophotal analysis discussed in Section 4.5.1, we find the following. The central starburst dominates the profiles in the inner regions and all the luminosity profiles exhibit a steeply rising part towards the central region. The colour profiles show the same general trend, blue in the central region and getting redder outwards. The presence of star forming regions and dust affect the profiles and they get duly modulated. A typical example is Mrk 449 where the dust lane shows up as a depression in the luminosity profile, as discussed in Section 4.5.1. However, inspite of the differences in the colours in the inner regions, the outer regions of the colour profiles show similar colour indices in most of the galaxies; typical of a G or F type stellar population (Bessell 1990). Since the ages of this stellar population are of the order of 10^9 years, it indicates that the starburst galaxies are not young systems but have an underlying older population in addition to the burst which has taken place at a later stage in its evolution.

All the galaxies grouped under S0/E show luminosity profiles made up of two components : the inner steep part where the burst dominates and the outer exponential part which is the underlying disk. Star formation is confined to the inner region in these galaxies. The colours get redder outwards. The only exception is Mrk 603 which is a part of an interacting system and shows global star formation. Strong isophotal twisting is observed in most of these galaxies. A few show boxiness in the inner regions.

The spirals in our sample are predominantly barred. The luminosity profile is made up of three components : The steep innermost part, an intermediate plateau indicating the presence and extent of the bar and an outer exponential disk. In addition to the nuclear region, star formation is also found at various other locations like the ends of bars (Mrk 213, Mrk 799), along rings (Mrk 1194, Mrk 1379)and in spiral arms (Mrk 332). The colour profiles are modulated by the presence of the star forming regions as well as by dust. Many of these galaxies show a double

peaked ellipticity profile. One of the peaks is generally wavelength dependent and can be attributed to the presence of dust or star forming regions according to the trend seen from shorter to longer wavelengths. In one case namely Mrk 213, we detect the presence of an inner bar or oval distortion misaligned with the primary bar. Mrk 1194 also shows the presence of such an inner feature misaligned with the primary bar. The irregular/peculiar galaxies show a smooth luminosity profile.

We note that although the colour index profiles generally do get bluer inwards for all the sample objects, the bluest regions are not always the nuclear regions. Most profiles reach their bluest colours at about 2" outside the central region. Besides the general trend discussed above, the colour profiles also show signatures of dust lanes, star forming regions, etc. and can be used to study the stellar populations in those regions. For Mrk 363 which shows global star formation, the colours do not change much throughout the galaxy. Mrk 603 and Mrk 708 show the opposite trend and get bluer outwards. In a study conducted by Barth et al. (1995) on a sample of emission-line MBG starbursts, they find that the MBG starbursts get bluer outwards which they attribute to contamination by the prominent bulge in these early-type systems. In the Markarian sample also, more than half the starburst nuclei are early-type (Balzano 1983). However, barring a few exceptions, the Markarian starburst galaxies get redder outwards. The burst dominates the luminosity in the central region in these galaxies. We detect the presence of dust in certain regions in Mrk 439, Mrk 1134, Mrk 1379 and a dust lane in Mrk 449.

4.6 Structural parameters

The decomposition of a galaxy profile into a bulge and a disk component requires the profile to be fitted by the sum of two empirical laws. As illustrated in the above sections, the luminosity profiles show a variety of types. The presence of

structures like bars, dust lanes, lenses and rings render such a straightforward two component fit very difficult. The luminosity profiles of the program galaxies are complex in nature. The burst of star formation in the central region manifests itself as a sharp rise in intensity in this region. The burst luminosity completely dominates the light output in this region and the estimation of the bulge component becomes nearly impossible. To characterize the light distribution of the sample in a homogeneous manner, standard parameters are necessary. In order to allow inter comparison of the sample galaxies and for uniformity, we derive the half-light radius, the disk scale lengths and the central disk surface brightness. This approach has been used by Kent (1984) and is especially useful in characterizing galaxies which belie a simple two component decomposition.

4.6.1 *Half-light Radius*

The half-light radius a_e is the radius within which half of the total light of the galaxy is contained.

$$m_{\rm hl} = m_{\rm total} + 0.752 \tag{4.5}$$

a_e is generally derived from the growth curve. However, if the image suffers from a poor signal-to-noise ratio in the outer regions, it could lead to an underestimation of the total light and hence an underestimate in the half-light radius. To minimize the errors, we derived the total light of the galaxy in each band by fitting an exponential disk to the outer part of the galaxy and extrapolated this disk to infinity. The light contained in the extrapolated profile is added to the apparent magnitude derived to get the total magnitude of the galaxy in each band. Since the fitting procedure is done over a range of radii, errors in calculating the total magnitude are reduced. The results are tabulated in Table 4.2. Fig. 4.3 shows the relation between the half light radius in B and that in R. It is seen that the S0's/E's have smaller half-light radii in B (a_{eb}) as compared to that in R (a_{er}). This suggests that the blue light distribution is more concentrated towards the central region as compared to the redder bands for the early type galaxies in our sample. The only exception is

Mrk 603 for which the a_{eb} is marginally greater than a_{er}. However, this is the only early type galaxy which shows a global starburst. Hence, the contribution to the blue light from the extranuclear regions is evident. The spirals in the sample have $a_{eb}>a_{er}$ in general, as many of these objects show strong extranuclear star formation which contributes to the total blue light in the galaxy. Mrk 781 and Mrk 1194 deviate from this behaviour. They have $a_{eb}<a_{er}$. This is expected since the starburst in seen in the inner regions of these galaxies and the outer spiral arms do not show any substantial star formation. The three peculiar galaxies (Mrk 363, Mrk 439 and Mrk 1134) show a behaviour similar to the early type galaxies.

4.6.2 *Disk scale lengths and central disk brightnesses*

In the Markarian starburst galaxies, the luminosity profiles are complex in nature showing two or in some cases three different components. In the inner region, the profile falls steeply upto about 10", where the light is completely dominated by the burst component. The outer parts of the luminosity profile can be well described by an exponential scaling law described in Eqn. 4.2,

$$\mu(r) = \mu_0 + 1.086\left(\frac{r}{h}\right)$$

The outer exponential nature is also seen in case of dwarf ellipticals dwarf irregulars and HII galaxies, (Telles 1995). This outer part is likely to represent the old underlying population of the parent galaxy. Structural properties like scale lengths and central disk surface brightnesses can be derived from these profiles. We fit an exponential law to the outer part of the profile down to where the signal falls to 3σ of the background noise level. Figs. 4.7 depict the fits to the outer regions. The results of exponential fits to each filter are tabulated in Table 4.2. A plot of the scale length in B (h_b) versus the scale length in R (h_r) (Fig. 4.4) indicates that the blue scale lengths are comparable to the red scale lengths in most cases. The scale lengths were derived using the outer exponential part of the luminosity profiles. Hence, galaxies in which enhanced star formation is present in the outer regions on the disk would tend to show a contribution from these star forming regions to

Table 4.2: Distribution of half-light radii (a_e), scale lengths (h) and the central disk surface brightnesses (μ_0). The subscripts b, v, r, i denote the filters for which the values are presented. The half-light radii and scale lengths are in kpc and the surface brightness in mag/sq.arcsec. The first row gives the derived values and the second row gives the errors on the corresponding quantities

Mrk	a_{eb}	a_{ev}	a_{er}	a_{ei}	h_b	h_v	h_r	h_i	μ_{ob}	μ_{ov}	μ_{or}	μ_{oi}
14	0.99	1.34	1.47	1.47	1.13	1.37	1.29	1.27	20.76	20.39	19.68	19.10
					0.04	0.02	0.03	0.04	0.08	0.03	0.04	0.07
87	2.8	2.4	2.1	2.5	7.66	5.89	4.87	4.10	21.92	21.04	20.22	19.39
					1.23	1.22	0.42	0.22	0.07	0.14	0.07	0.05
190	0.39	0.45	0.57	0.55	0.44	0.46	0.68	0.59	19.85	19.28	18.90	18.25
					0.003	0.004	0.014	0.008	0.01	0.01	0.02	0.02
213	3.38	2.75	2.28	3.03	2.77	2.75	2.60	2.74	20.09	19.61	19.01	18.54
					0.46	0.35	0.42	0.32	0.19	0.15	0.19	0.15
332	2.25	2.14	2.14	2.36	1.68	1.83	1.81	2.14	19.91	19.55	19.01	18.82
					0.06	0.11	0.09	0.10	0.07	0.09	0.08	0.06
363	1.59	1.71	1.84	1.71	0.92	0.99	0.93	0.85	19.20	18.77	18.21	17.83
					0.01	0.01	0.01	0.01	0.04	0.03	0.03	0.02
439	0.51	0.59	0.66	0.62	0.97	0.86	0.84	0.71	21.01	19.92	19.46	18.54
					0.14	0.03	0.02	0.03	0.21	0.06	0.06	0.08
449	1.33	1.33	1.21	1.46	0.71	0.73	0.69	0.66	19.18	18.49	17.89	17.19
					0.03	0.02	0.02	0.02	0.08	0.06	0.05	0.07
602	3.3	2.99	2.99	2.78	2.79	2.28	2.19	2.09	21.07	19.94	19.27	18.55
					0.18	0.10	0.10	0.06	0.05	0.04	0.03	0.03
603	1.56	1.42	1.42	1.35	1.40	1.39	1.24	1.12	19.99	19.35	18.52	18.26
					0.03	0.01	0.02	0.01	0.02	0.01	0.02	0.02
708	5.90	5.12	4.88	4.23	5.70	4.01	3.74	3.47	22.12	21.13	20.69	20.06
					0.96	0.31	0.27	0.17	0.08	0.07	0.06	0.05
743	0.35	0.49	0.40	0.54	0.47	0.45	0.48	0.57	21.10	20.02	19.60	19.25
					0.02	0.01	0.01	0.01	0.07	0.06	0.04	0.03
781	5.30	6.00	5.83	5.85	3.14	3.07	2.96	2.47	21.44	20.71	20.11	19.32
					0.54	0.21	0.18	.14	0.04	0.03	0.03	0.03
799	4.31	4.10	4.10	4.10	1.73	2.51	2.96	2.62	19.23	19.41	19.08	17.69
					0.32	0.13	0.14	0.16	0.30	0.10	0.14	0.16
1002	2.28	2.28	2.51	2.51	1.79	1.78	1.85	1.79	20.06	19.39	18.86	18.38
					0.04	0.14	0.10	0.09	0.16	0.11	0.10	0.11
1134	2.44	2.50	2.50	2.63	1.81	1.99	2.11	3.49	19.89	19.47	18.95	18.87
					0.14	0.13	0.13	0.22	0.22	0.17	0.15	0.10
1194	2.09	2.36	2.47	2.14	2.70	2.76	3.96	3.74	19.89	19.44	19.63	19.31
					0.80	0.31	0.69	0.52	0.43	0.44	0.43	0.33
1308	0.38	0.53	0.56	0.65	0.36	0.39	0.40	0.43	20.02	19.44	18.95	18.45
					0.01	0.01	0.01	0.01	0.04	0.03	0.04	0.03
1379	2.32	2.63	2.39	2.83	1.94	1.81	1.72	1.66	20.17	19.37	18.72	17.96
					0.07	0.05	0.05	0.05	0.05	0.04	0.05	0.04

the scale lengths. From Fig. 4.4 it is seen that three galaxies, namely Mrk 602, Mrk 708 and Mrk 87 deviate substantially from the h_b=h_r line. Mrk 602 and Mrk 708 are two galaxies in the sample which get bluer outwards. Mrk 87 has a blue ring in the outer regions. Hence, for these three objects we derive the blue scale lengths to be greater than the red scale lengths.

4.6.3 Comparison with other samples

The plot of the blue scale length versus the corrected central disk brightness shows that Markarian starburst galaxies in our sample have scale lengths less than about 2 kpc in the B band. The parameters viz. the scale lengths and the central disk surface brightnesses derived in the present study were compared with those derived by de Jong (1996) for spirals. These are shorter compared to those derived by de Jong for normal spirals using a bulge-disk decomposition. The central disk surface brightness in our study is also brighter then that observed in normal spirals by other workers. Bothun et al. (1989) report a mean value of 2 kpc for the scale lengths derived using "marking the disk" method based on the study of the Wasilewski sample of emission-line galaxies in the Gunn R band. They also find the mean central surface brightness to be about $1^m.5$ brighter than that for normal spirals in Gunn R. However, Courteau (1996) cautions against the comparison of scale lengths derived by different workers due to the subjective nature of the measurements. He argues that "marking the disk" approach would lead to smaller scale lengths over those obtained from bulge-disk (B/D) decomposition fits. In the (B/D) decompositions, the inclusion of the bulge reduces the amount of light contributed by the inner disk and thus leads to a shallower slope for the disk profiles. Knapen & van der Kruit (1991) find discrepancies up to a factor of two in the scale lengths measured by various workers.

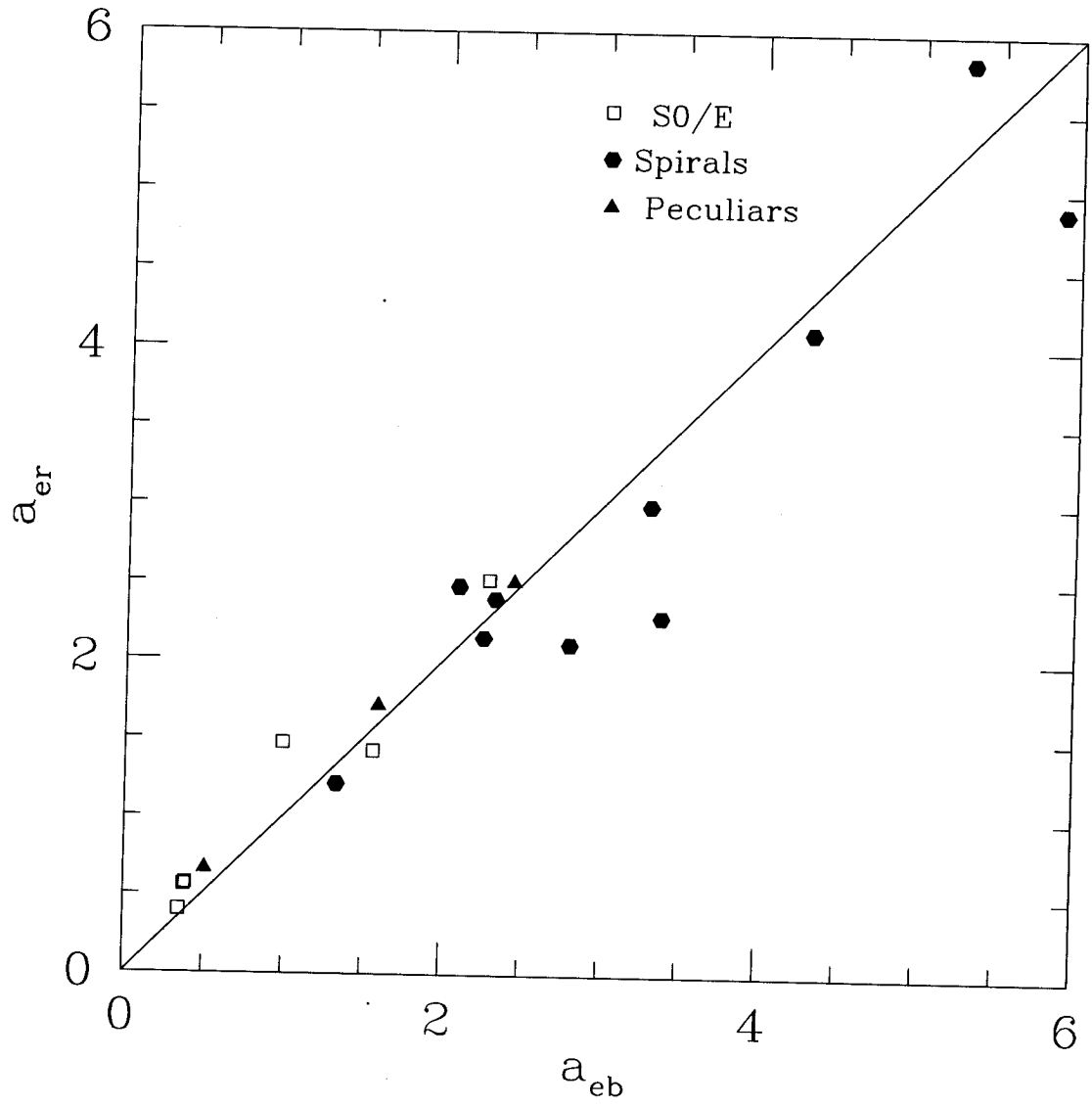

Figure 4.3: Comparison of the half-light radius in B (a_{eb}) and in R (a_{er}). Both the axes are in units of kpc. The points denote the derived values and the solid line is the locus of a_{eb}=a_{er}.

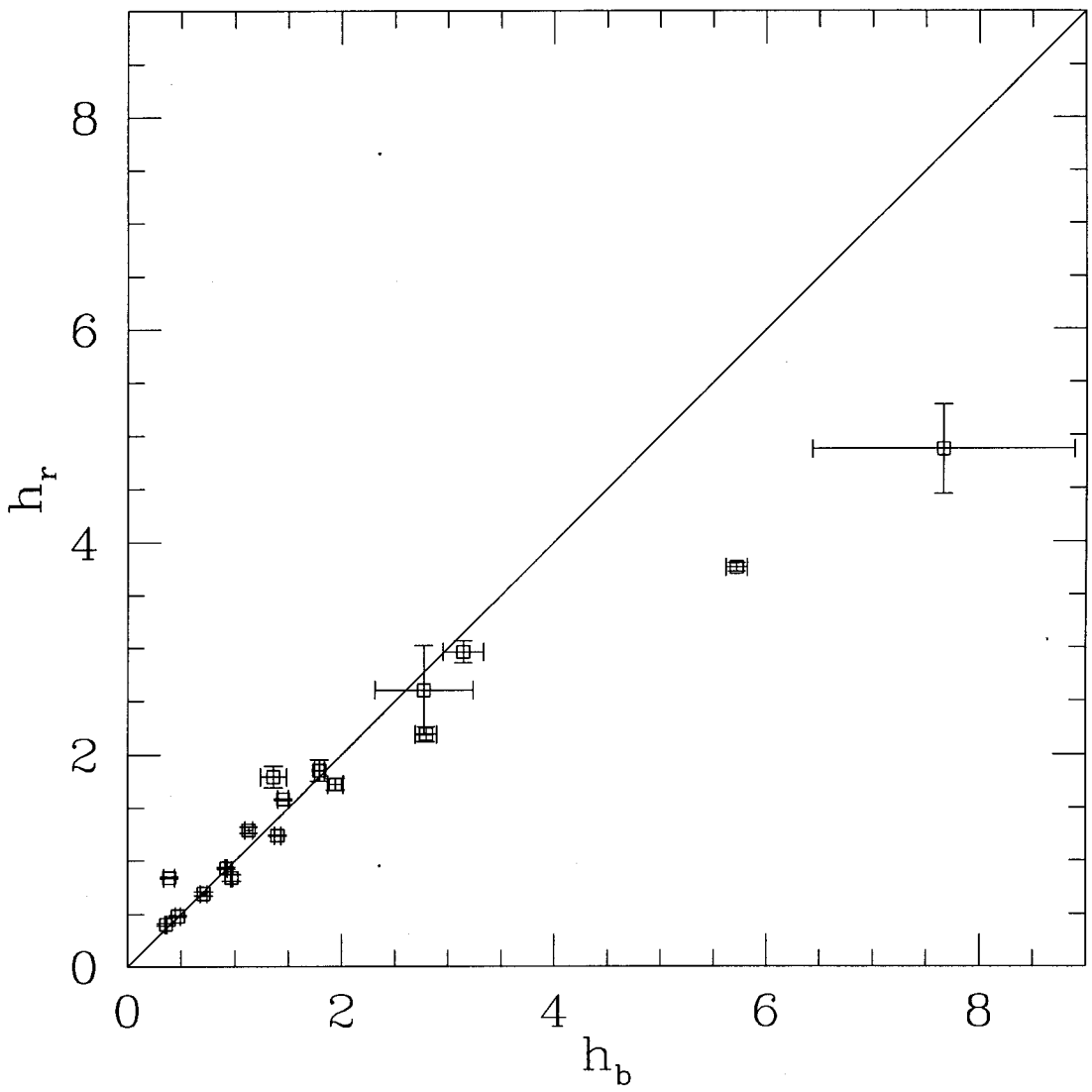

Figure 4.4: Comparison of the scale lengths in B (h_b) and R in (h_r). Units of kpc are used for both axes. The points are the derived values and the solid line is the locus of h_b=h_r.

4.7 Global properties

The magnitudes of the sample galaxies were derived by summing up the light within the elliptical annuli. The total light within the isophote at 24 mag/arcsec^2 in the B band was computed and has been given in Table 4.3. The exponential disk was fit and extrapolated to derive the total magnitudes of the galaxies in all the filter bands. The total magnitudes are presented along with the magnitudes within the 24, 23, 23, 22 mag/arcsec^2 in the B, V, R, I bands respectively. The errors on the magnitudes listed by RC3 are typically $0.^m2$ to $0.^m4$. The values for the total magnitudes derived by us agree very well with the values listed in RC3 within the error bars in most of the cases. In case of Mrk 439 and Mrk 602, we find slight deviations from the values in RC3. Our values for the total magnitudes are derived by extrapolating the exponential fitted to the outer regions in the galaxy while the values in RC3 are derived from the curve of growth. Telles (1995) discusses the discrepancies arising in the values obtained using these two different approaches. He finds differences upto $0.^m5$ between the values derived using these two approaches.

4.8 Conclusions

A detailed study of the structural properties of a sample of starburst galaxies shows the following properties: The luminosity profile is dominated by the burst in the central region and has a central part sharply rising towards the nuclear region. In the outer part, all the galaxies show an exponential behaviour. The colours generally get redder outwards. However, the bluest regions are often off-centered with respect to the optical nucleus. Hence, the star formation is circumnuclear in many cases. The scale lengths in B and R are comparable.

In the S0's/E's in the sample, the luminosity profiles are made up of two components : the inner part sharply rising towards the nucleus and the outer exponential part. We find strong isophotal twisting in almost all the galaxies. This

Table 4.3: Total magnitudes and colour indices uncorrected for galactic absorption and inclination effects. column 1 : Galaxy number; column 2: the B magnitude obtained by summing over the pixels within the elliptical isophote at 24 mag/arcsec^2; columns 3,4,5 : colours determined from the apparent magnitudes as described above; columns 6,7,8,9 : The total magnitudes determined by extrapolating the fitted disk to infinity; columns 10,11 : the total magnitudes from the RC3.

Mrk	m_B	$B-V$	$V-R$	$R-I$	B_T	V_T	R_T	I_T	B_T(R)	V_T(R)
14	14.74	0.52	0.51	0.47	14.67	14.11	13.54	13.09	14.9	14.49
87	14.12	0.84	0.67	0.71	13.87	12.77	12.04	11.49	13.8	12.85
190	13.51	0.66	0.57	0.67	13.38	12.56	11.72	11.26	13.22	12.55
213	13.39	0.60	0.54	0.59	13.18	12.68	12.06	11.44	13.10	12.50
332	13.00	0.53	0.53	0.49	12.84	12.27	11.76	11.13	12.97	12.37
363	14.31	0.53	0.56	0.59	14.28	13.69	13.14	12.87	14.28	13.72
439	12.96	0.59	0.37	0.41	12.65	11.96	11.58	11.19	12.33	11.67
449	13.69	0.66	0.53	0.63	13.45	12.87	12.39	11.69	13.50	12.85
602	14.40	0.90	0.68	0.64	13.50	13.21	12.22	11.64	13.87	13.12
603	13.26	0.57	0.56	0.00	13.24	12.67	12.12	12.13	13.10	12.50
708	13.09	0.61	0.23	0.44	12.53	12.11	11.89	11.47	—	—
743	13.57	0.36	0.47	0.63	13.19	13.04	12.67	12.06	—	—
781	13.40	0.64	0.53	0.59	13.07	12.42	11.92	11.44	13.19	—
799	12.91	1.06	0.74	0.83	12.90	11.81	11.09	10.12	—	—
1002	13.72	0.57	0.55	0.60	13.60	13.05	12.47	12.09	—	—
1134	14.79	0.57	0.65	0.66	14.75	14.07	13.43	12.68	15.0	14.34
1194	13.26	0.77	0.53	0.75	13.23	12.46	11.84	11.15	13.24	—
1308	14.24	0.50	0.47	0.52	14.04	13.45	12.99	12.39	—	—
1379	13.43	0.63	0.58	0.77	13.29	12.59	12.04	11.31	13.00	12.34

is accompanied by boxiness in a few cases. Isophotal twisting and boxiness support a scenario of strong interaction or merger experienced by these galaxies. The half-light radii are shorter in the blue band as compared to the half-light radii in the red band. This suggests that the blue light is more centrally concentrated in the S0's/E's in our sample. In Mrk 603, the starburst is global and a_{eb} is marginally greater than a_{er}.

The spirals in our sample are mostly barred. The luminosity profiles are made up of multiple components. Mrk 213 and Mrk 1194 show indication of the presence of a nuclear bar-like distortion misaligned with the primary bar of the galaxy. These galaxies show the half-light radii in the red to be smaller than the half-light radii in the blue indicating that there is a large contribution to the total blue light from the extra nuclear star forming regions located away from the center.

The irregulars/peculiars in our sample show a smooth luminosity profile. The half-light radii in blue are smaller similar to that observed for the early type galaxies in our sample.

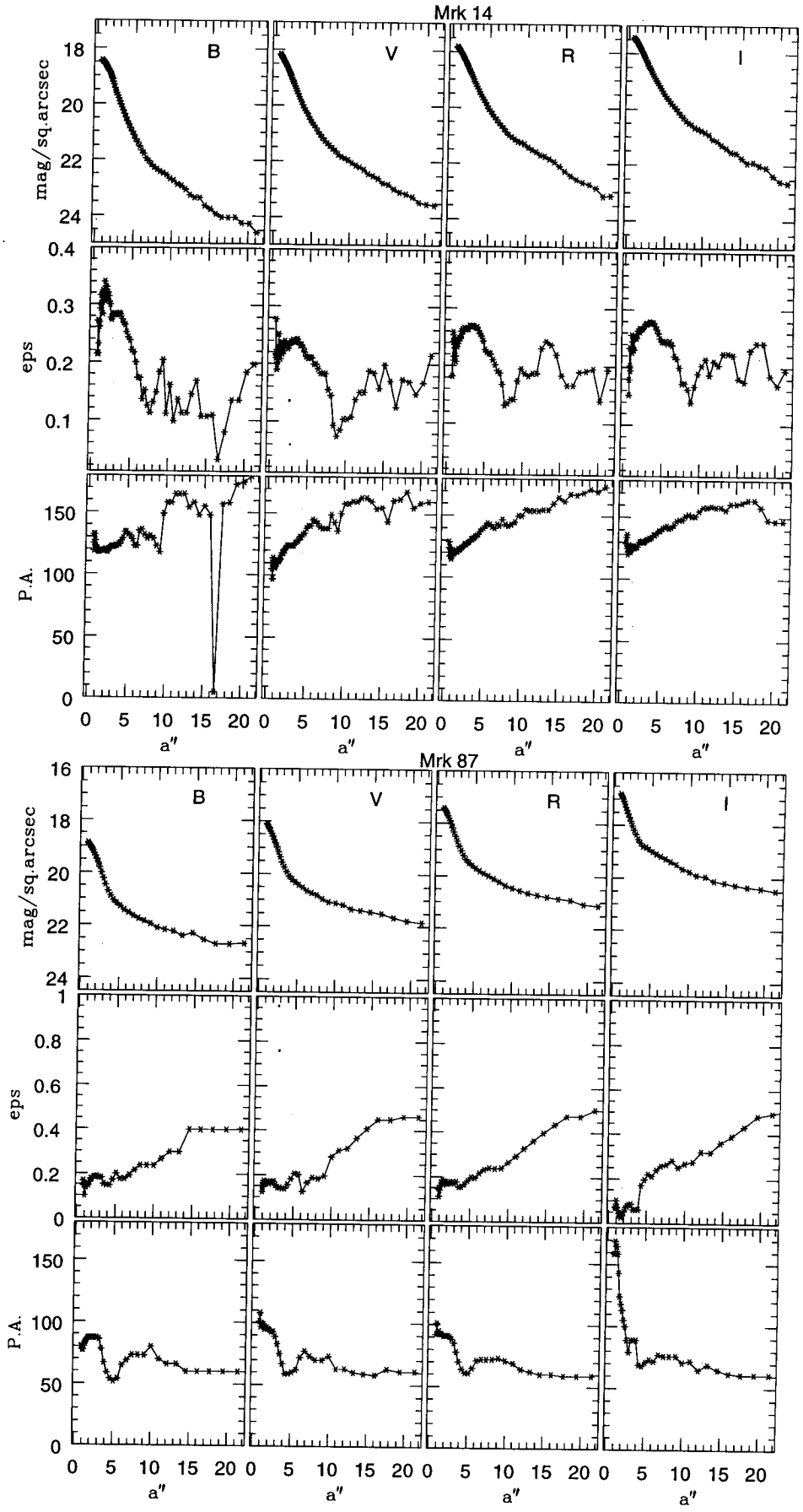

Figure 4.5: Variation of surface brightness, ellipticity and position angle

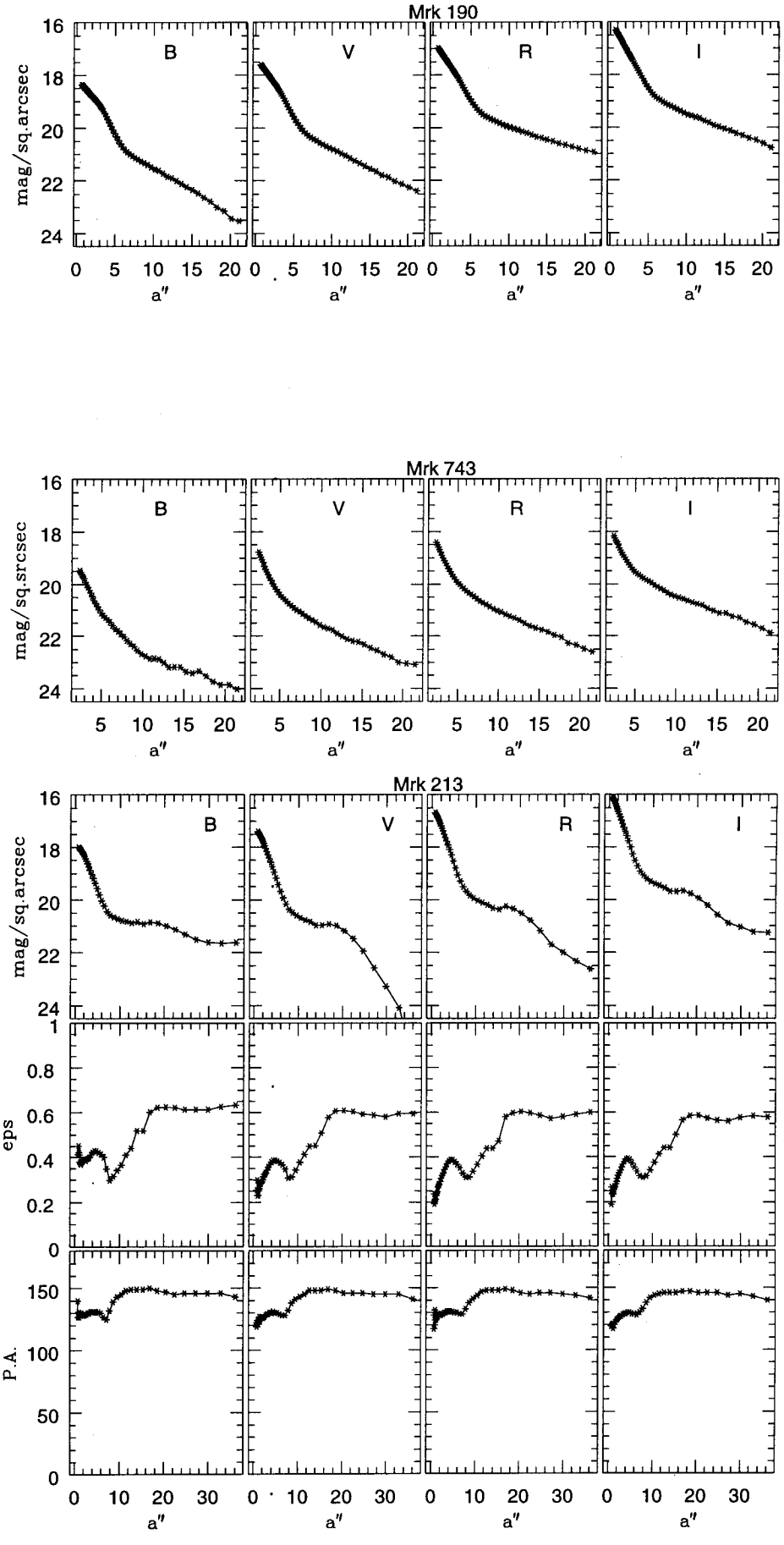
Mrk 190
B
V
R
I
mag/sq.arcsec
a″
Mrk 743
mag/sq.srcsec
Mrk 213
eps
P.A.

Fig 4.5 (contd)

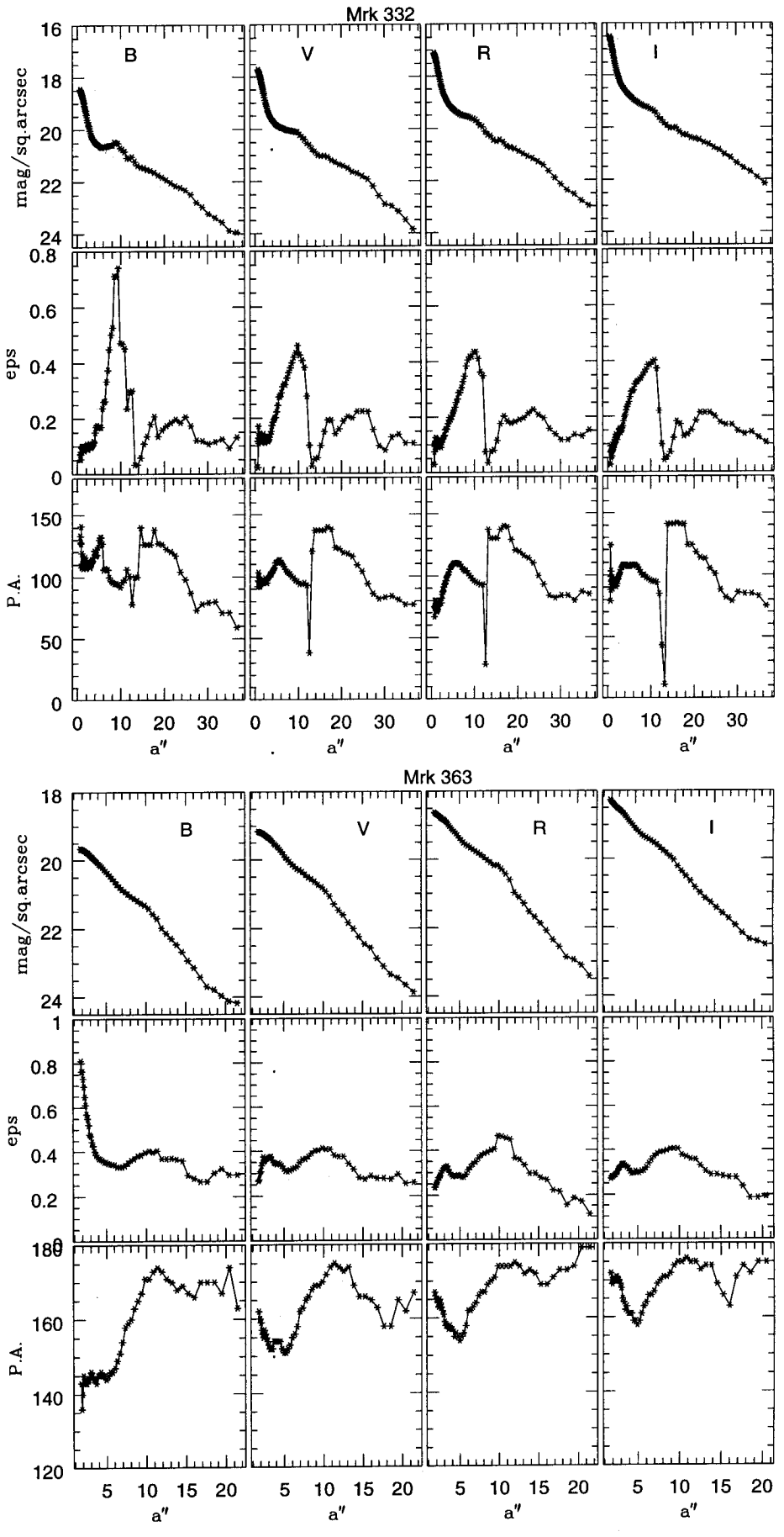
Mrk 332
B
V
R
I
mag/sq.arcsec
eps
P.A.
a″
Mrk 363
B
V
R
I
mag/sq.arcsec
eps
P.A.
a″

Fig 4.5 (contd)

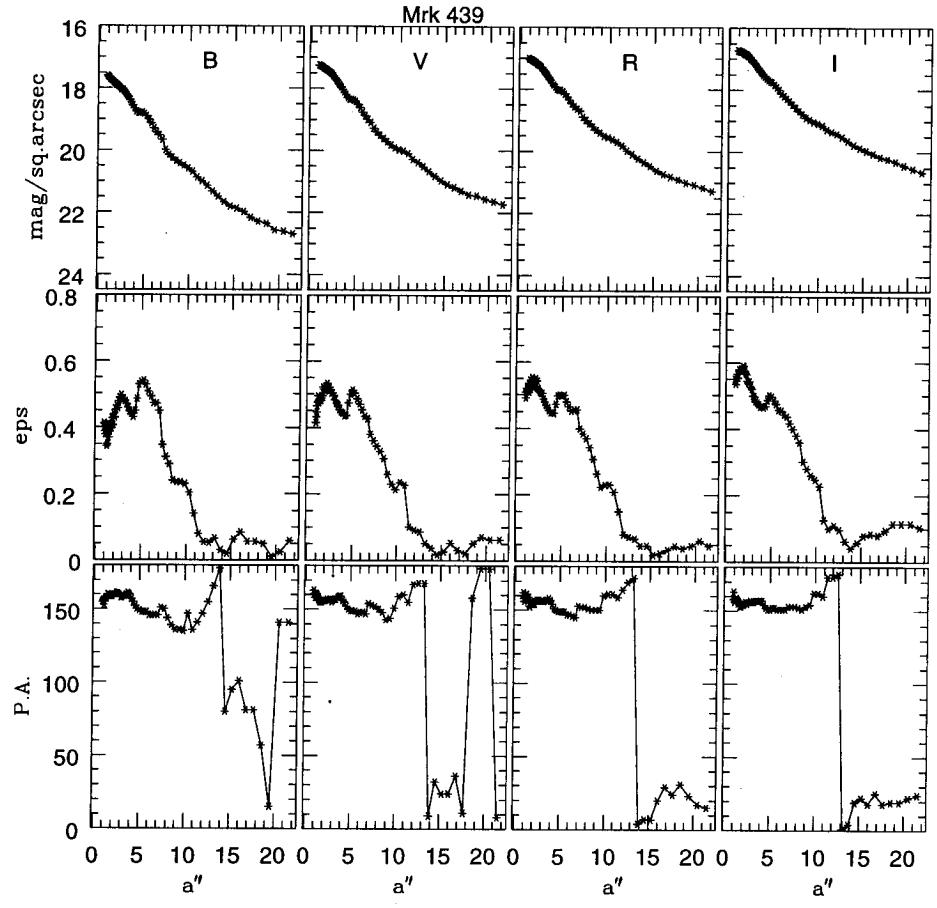
Mrk 439
B
V
R
I
mag/sq.arcsec
eps
P.A.
a″

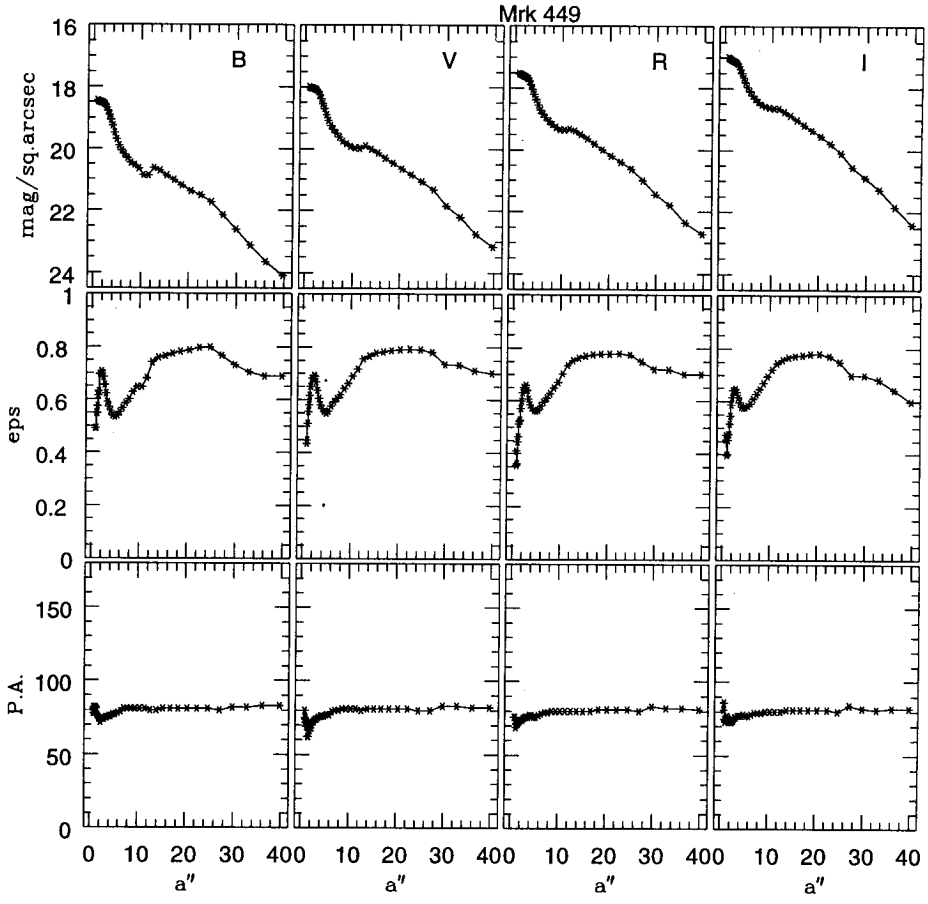
Mrk 449
B
V
R
I
mag/sq.arcsec
eps
P.A.
a″

Fig 4.5 (contd)

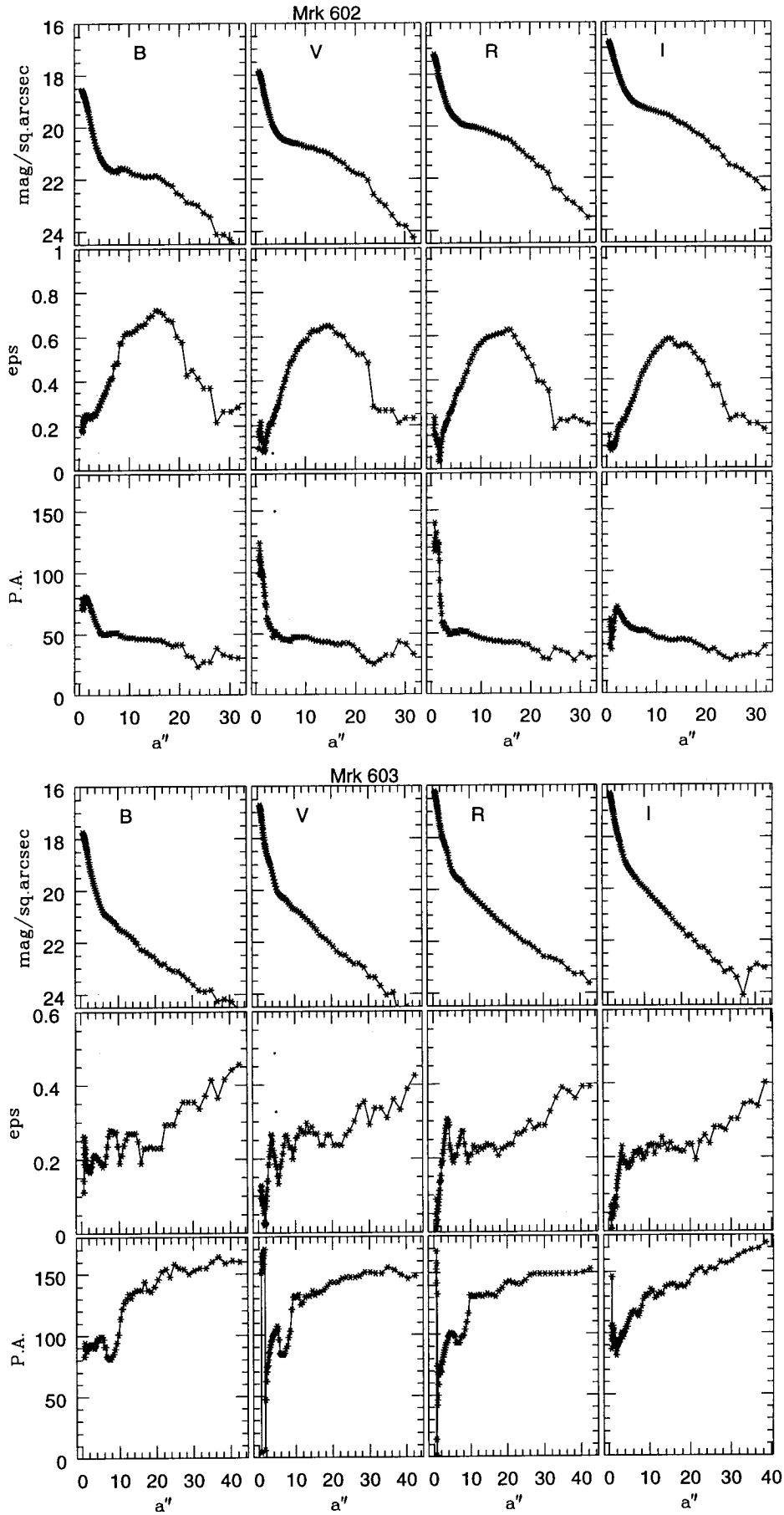
Mrk 602
B
V
R
I
mag/sq.arcsec
eps
P.A.
a″
Mrk 603
B
V
R
I
mag/sq.arcsec
eps
P.A.
a″

Fig 4.5 (contd)

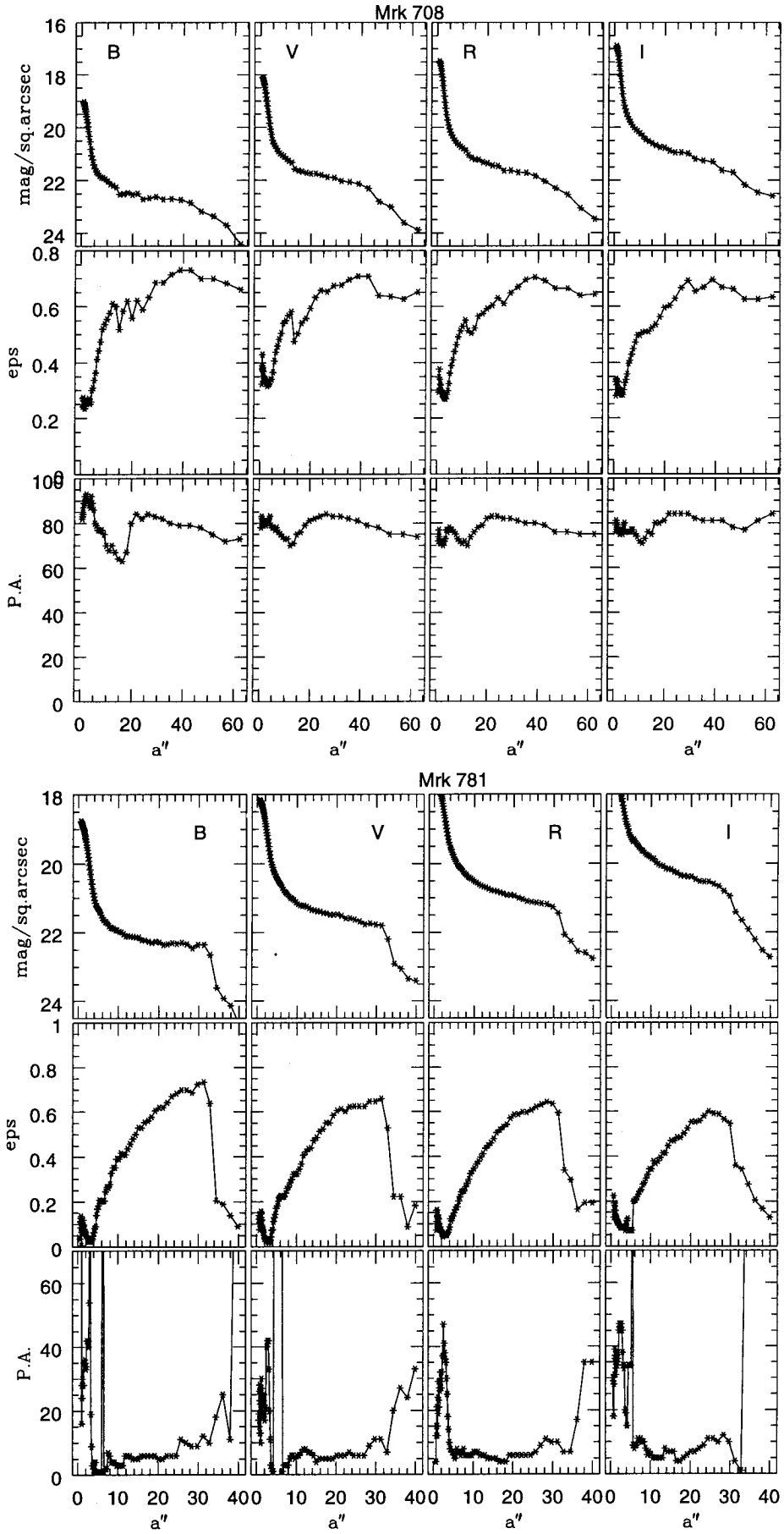
Mrk 708
B
V
R
I
mag/sq.arcsec
eps
P.A.
a″
Mrk 781
B
V
R
I
mag/sq.arcsec
eps
P.A.
a″

Fig 4.5 (contd)

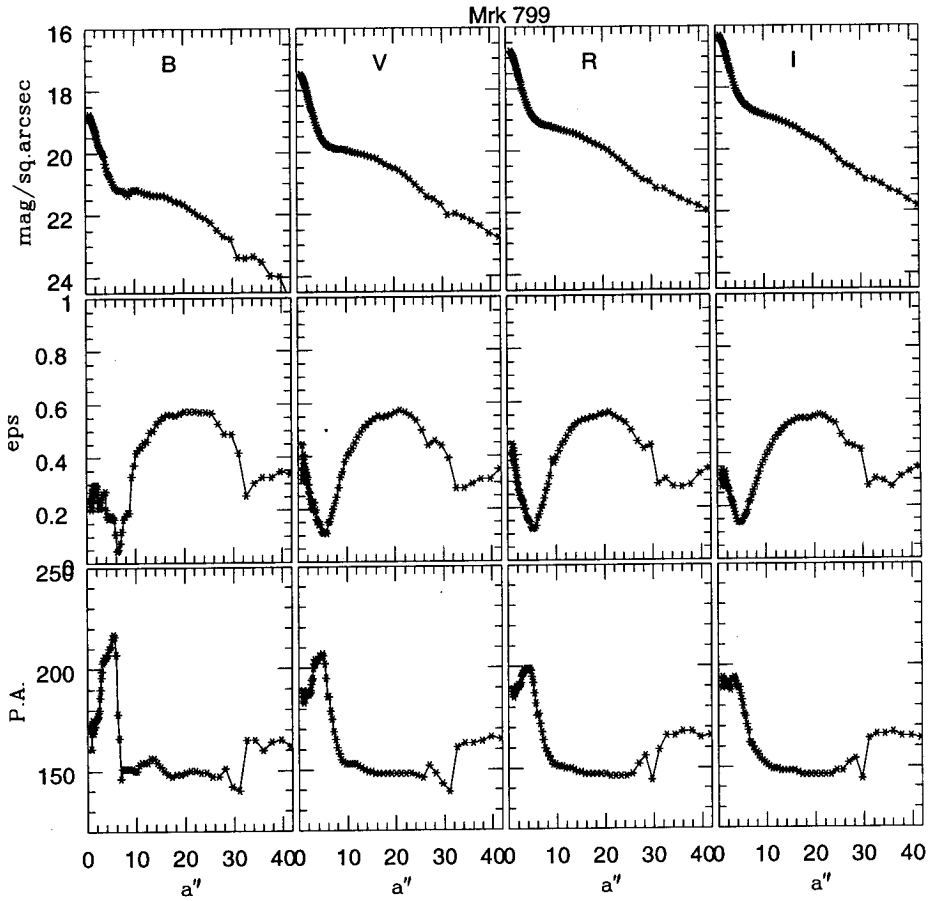
Mrk 799
B
V
R
I
mag/sq.arcsec
eps
P.A.
a″

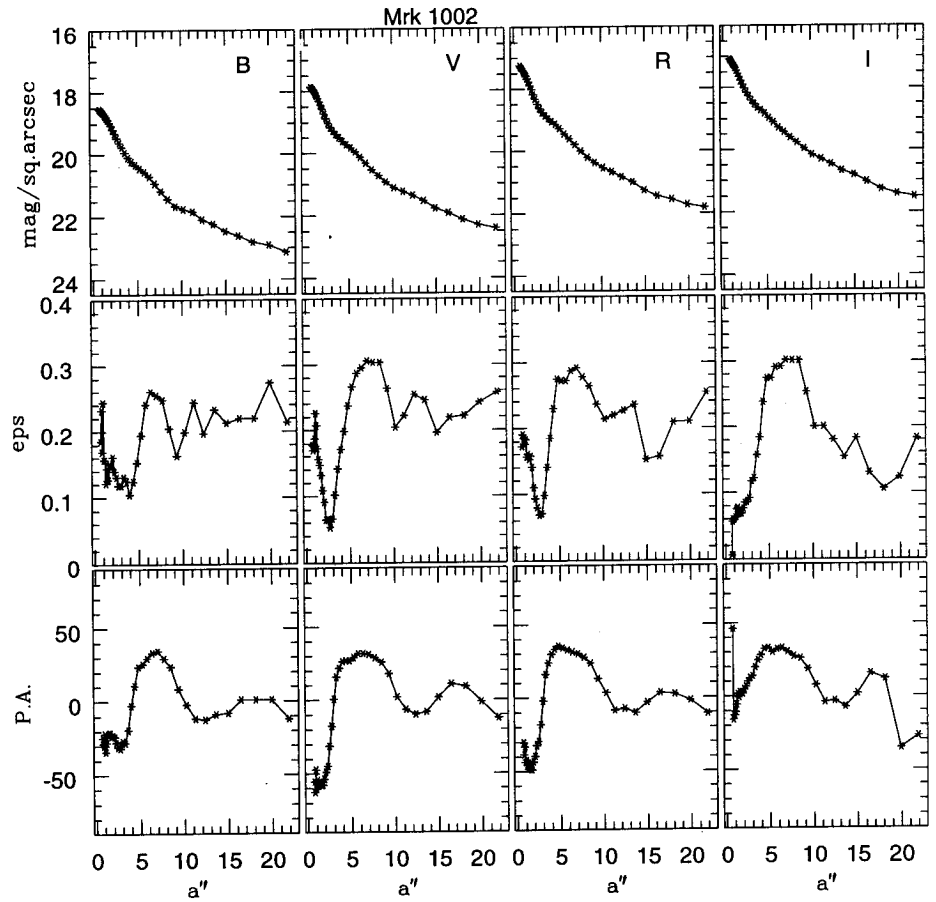
Mrk 1002
B
V
R
I
mag/sq.arcsec
eps
P.A.
a″

Fig 4.5 (contd)

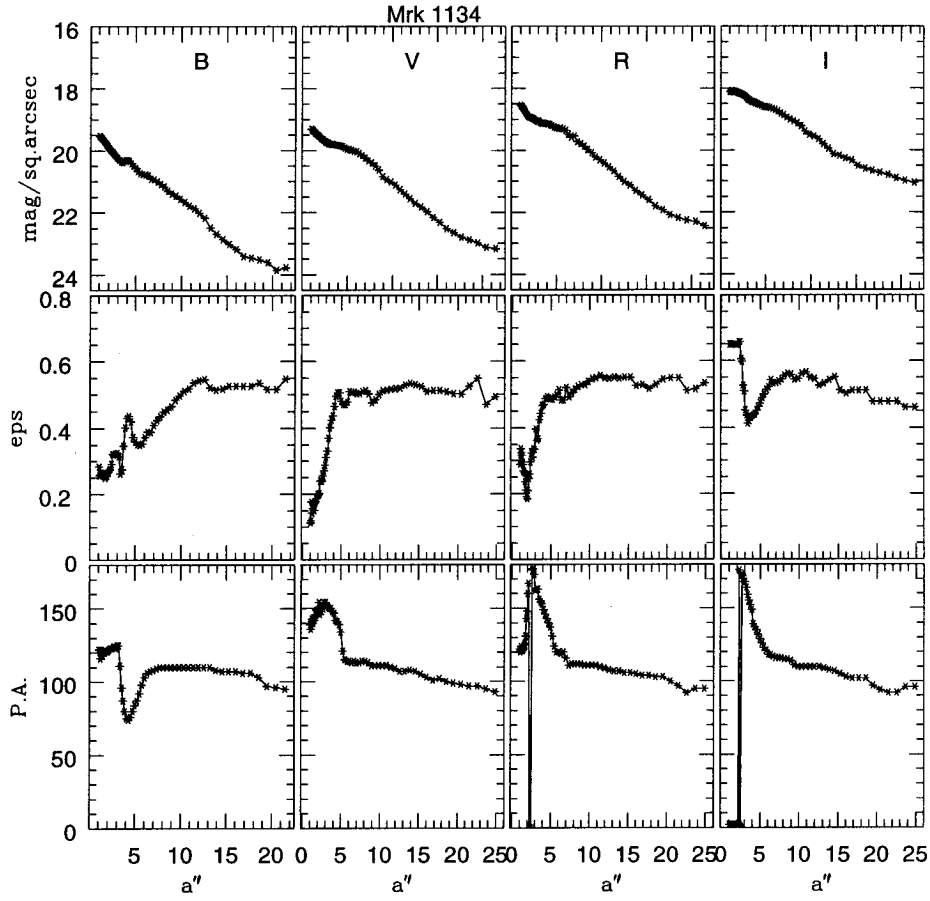
Mrk 1134
B
V
R
I
mag/sq.arcsec
eps
P.A.
a″

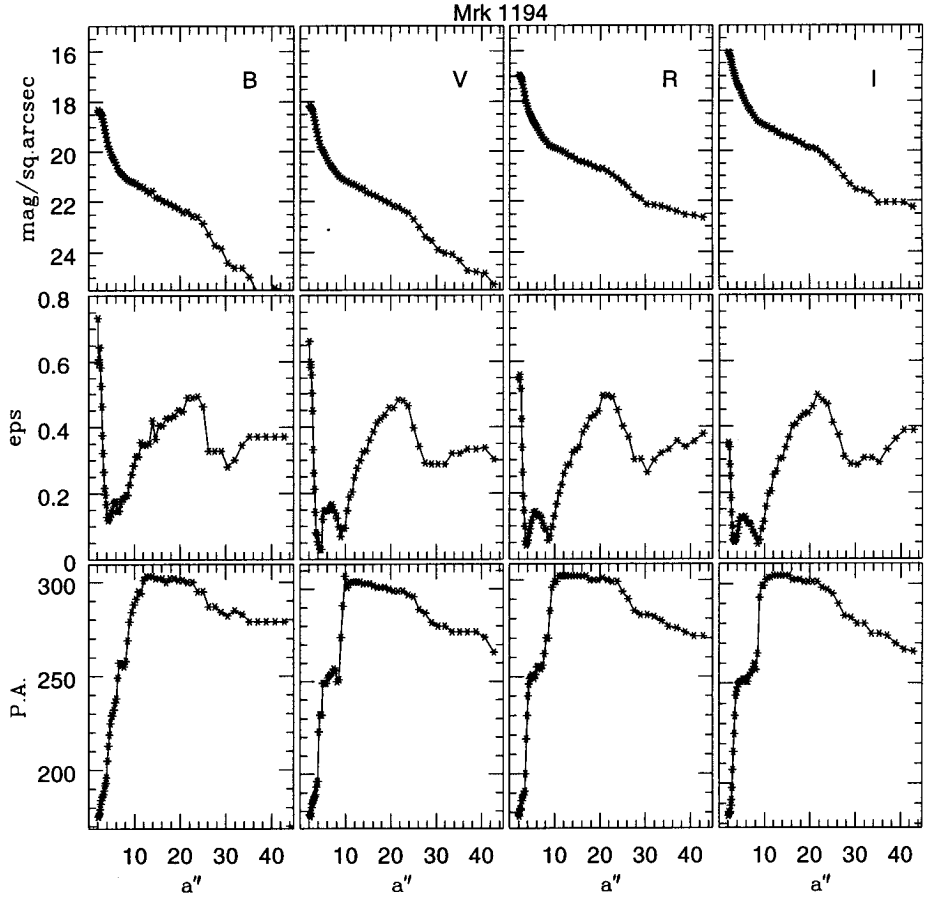
Mrk 1194
B
V
R
I
mag/sq.arcsec
eps
P.A.
a″

Fig 4.5 (contd)

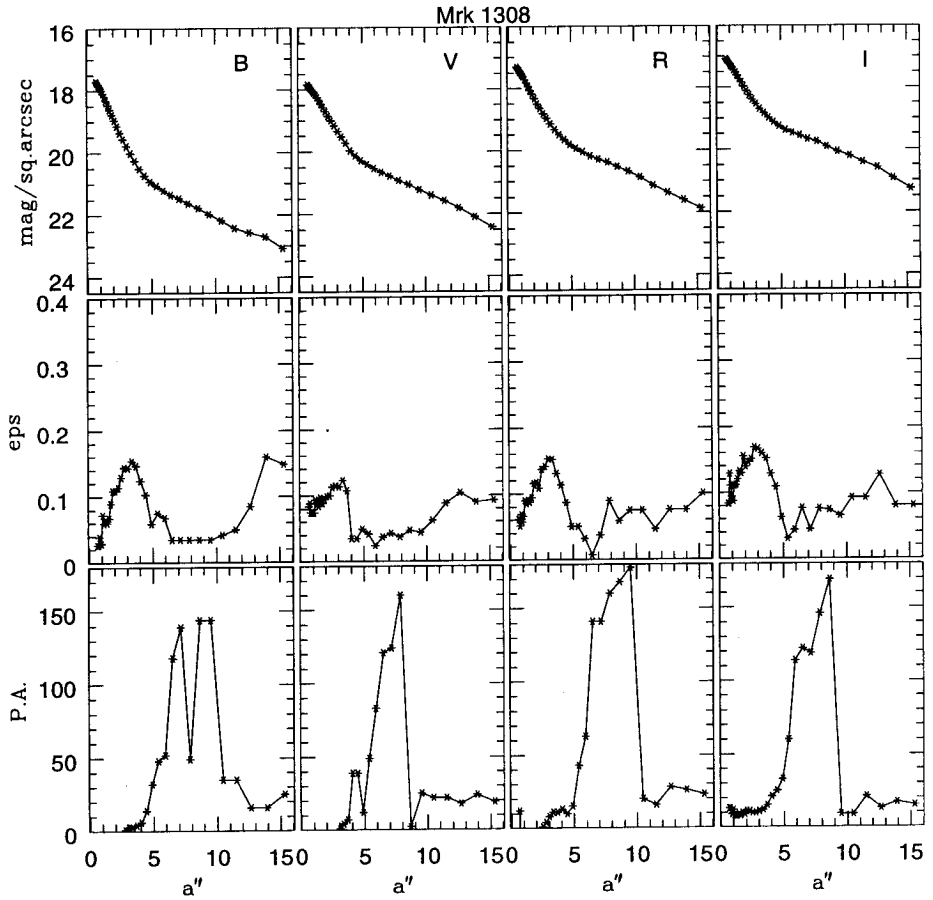
Mrk 1308
B
V
R
I
mag/sq.arcsec
eps
P.A.
a″

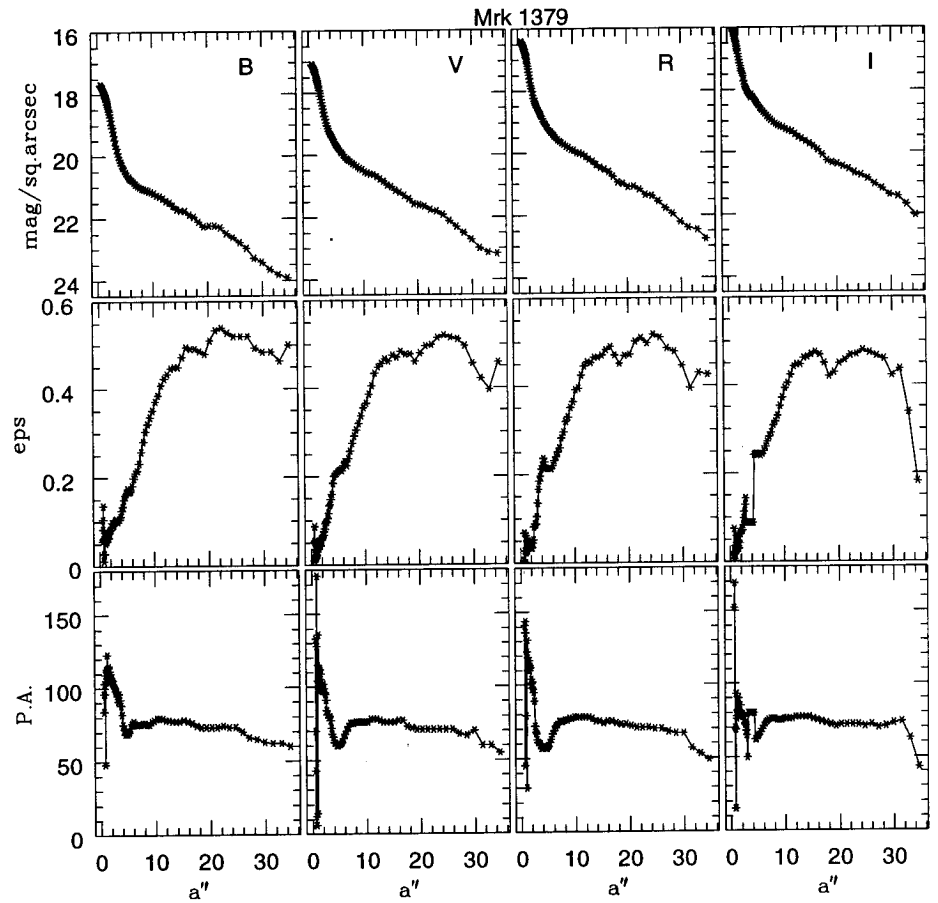
Mrk 1379
B
V
R
I
mag/sq.arcsec
eps
P.A.
a″

Fig 4.5 (contd)

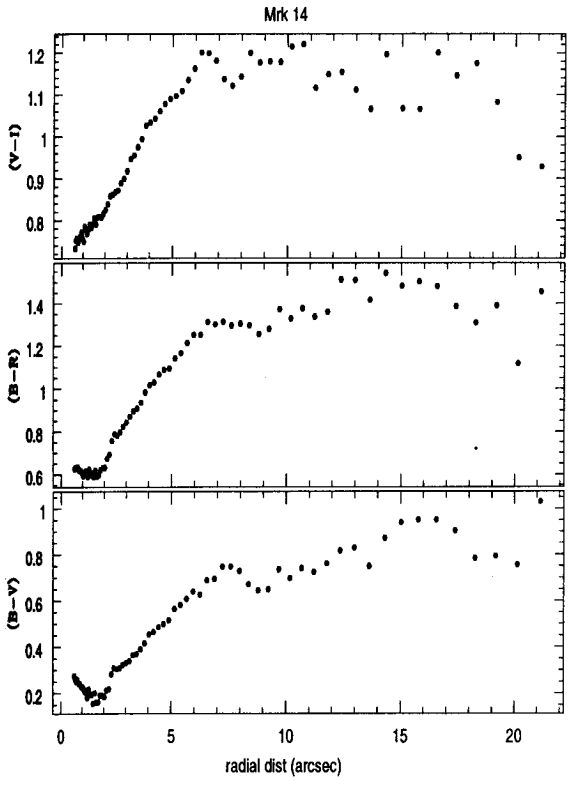

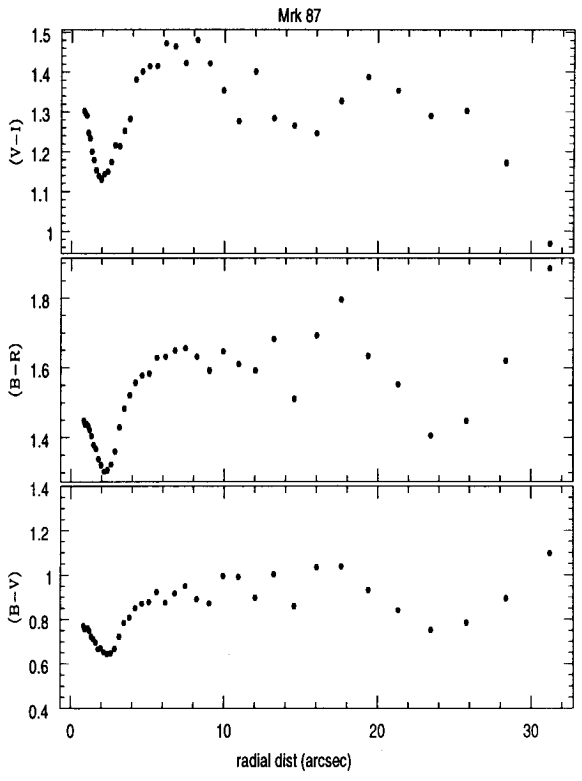

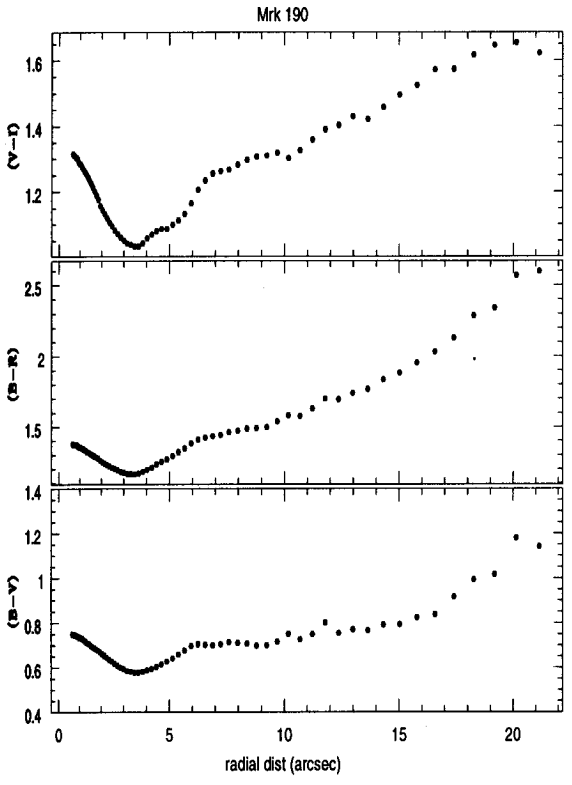

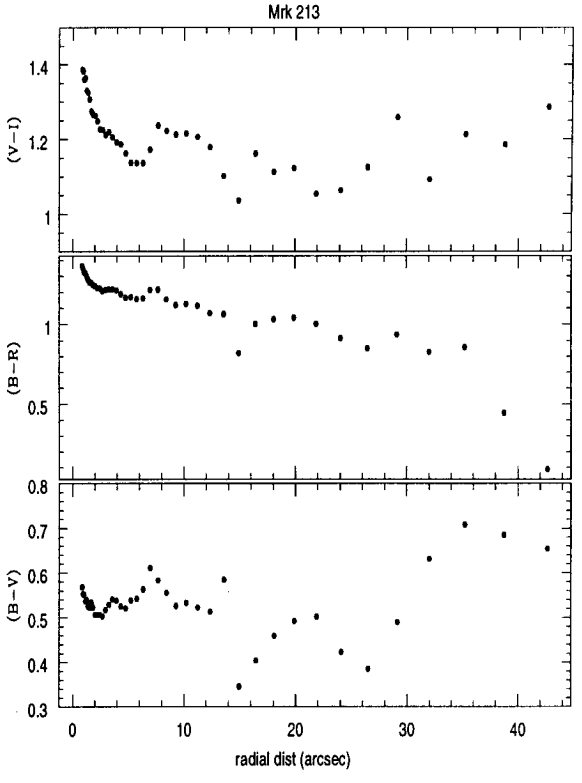

Figure 4.6: Distribution of (V-I), (B-R) and (B-V) with radial distance

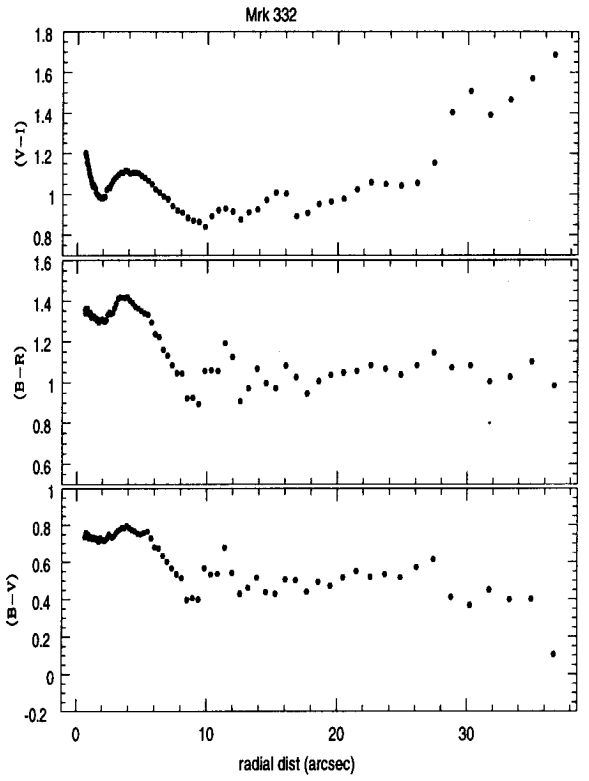
Mrk 332
(V−I)
(B−R)
(B−V)
radial dist (arcsec)

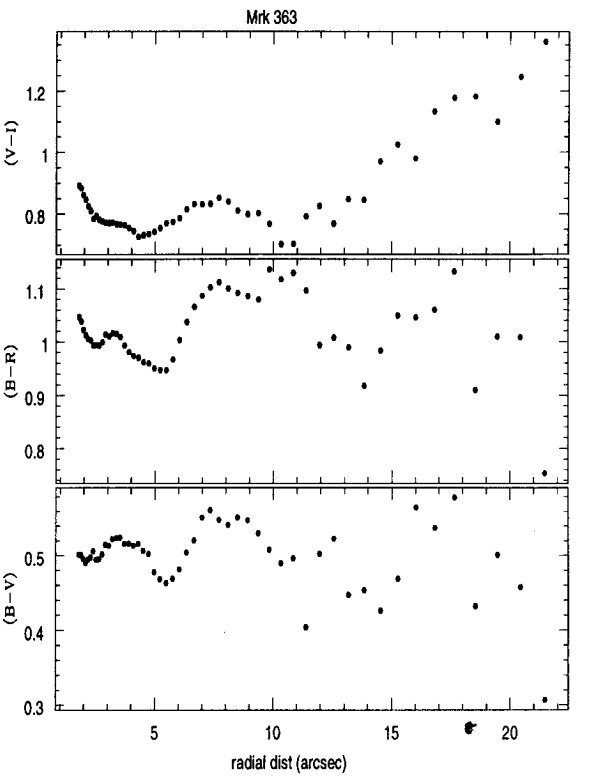
Mrk 363
(V−I)
(B−R)
(B−V)
radial dist (arcsec)

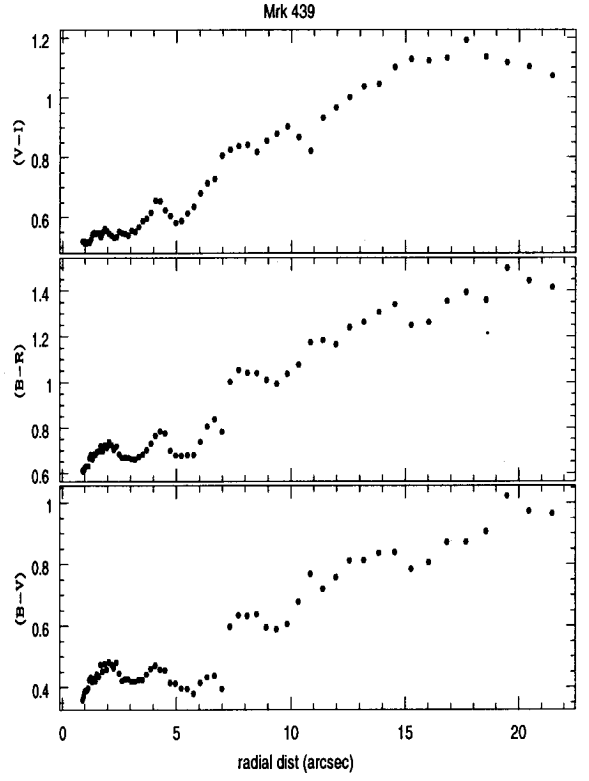
Mrk 439
(V−I)
(B−R)
(B−V)
radial dist (arcsec)

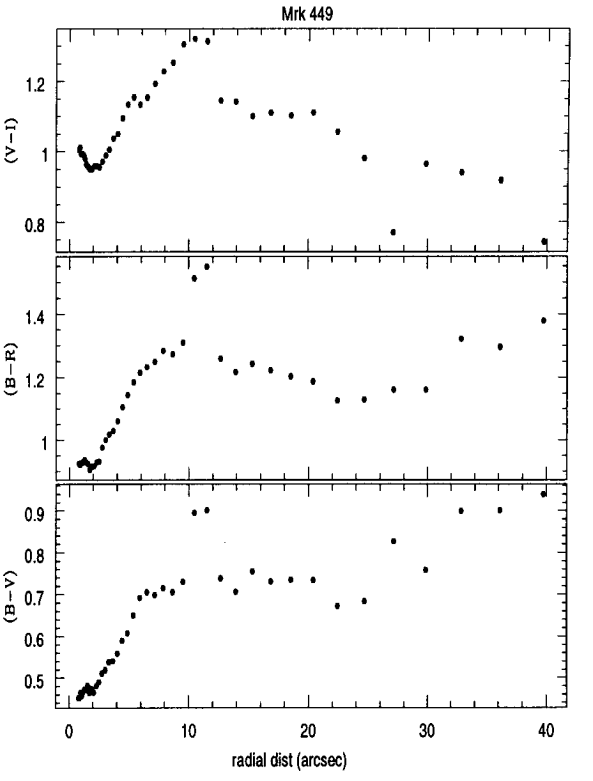
Mrk 449
(V−I)
(B−R)
(B−V)
radial dist (arcsec)

Fig 4.6 (contd)

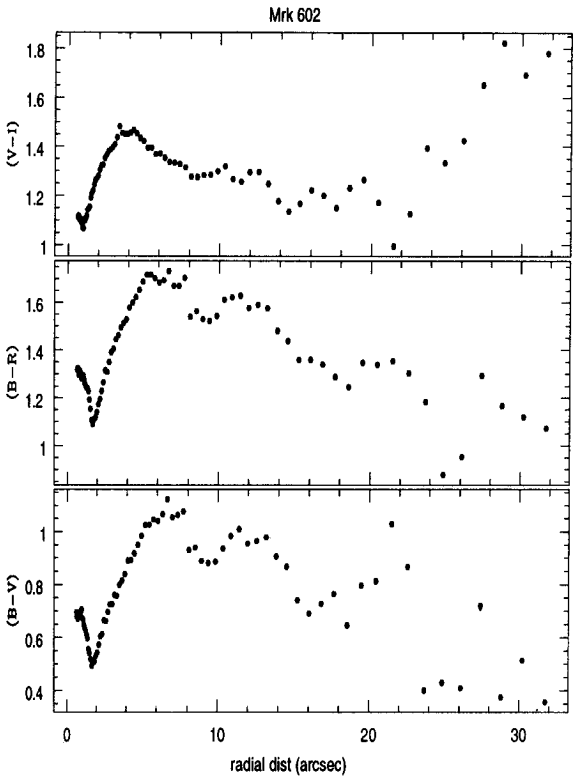
Mrk 602
(V−I)
(B−R)
(B−V)
radial dist (arcsec)

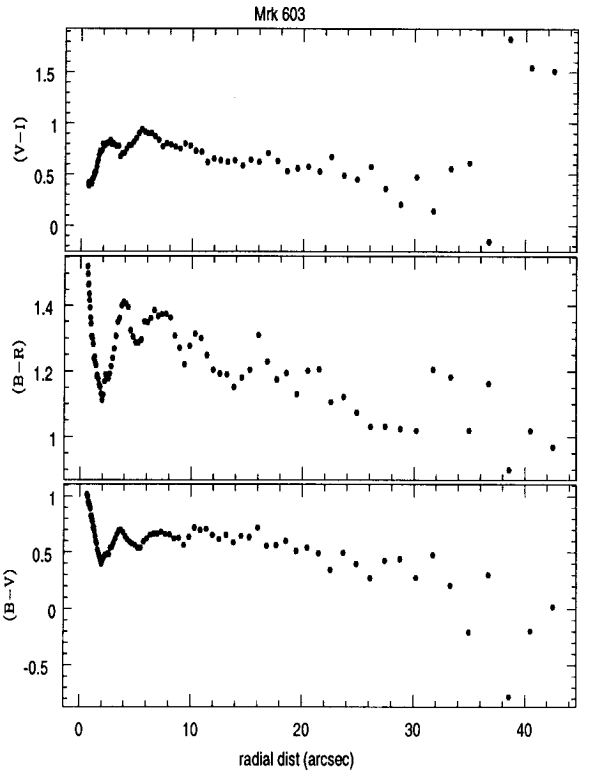
Mrk 603
(V−I)
(B−R)
(B−V)
radial dist (arcsec)

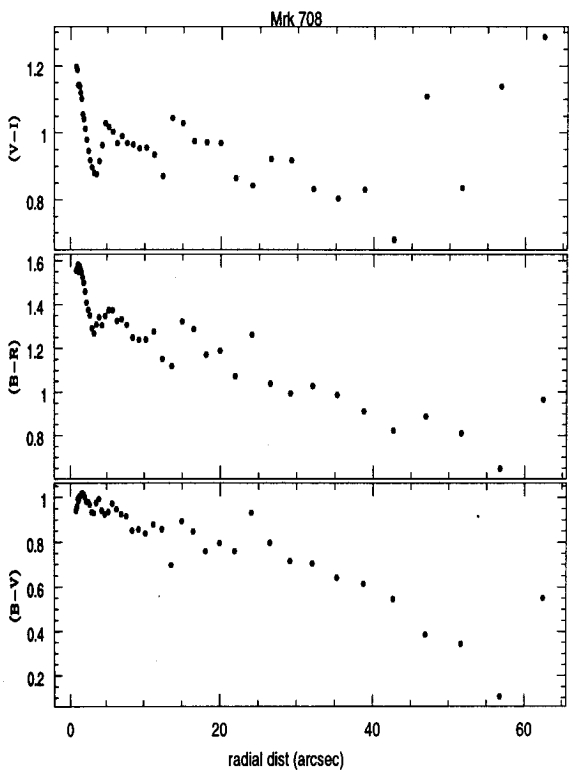
Mrk 708
(V−I)
(B−R)
(B−V)
radial dist (arcsec)

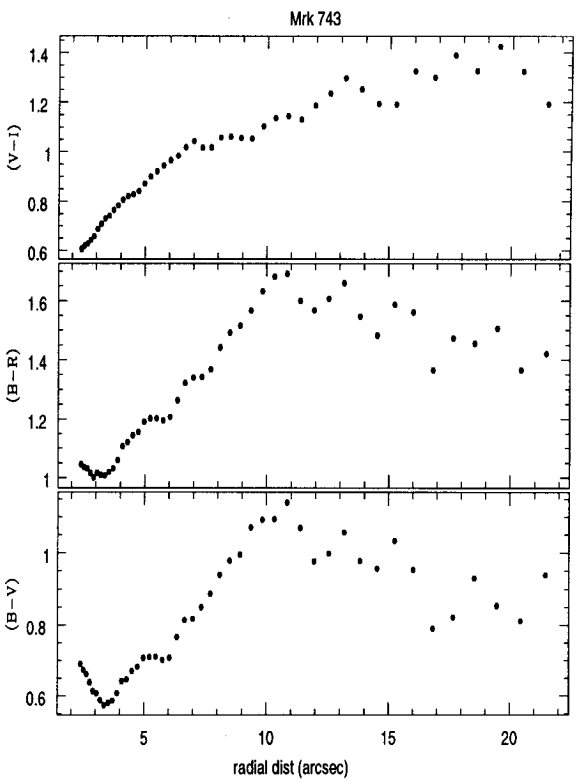
Mrk 743
(V−I)
(B−R)
(B−V)
radial dist (arcsec)

Fig 4.6 (contd)

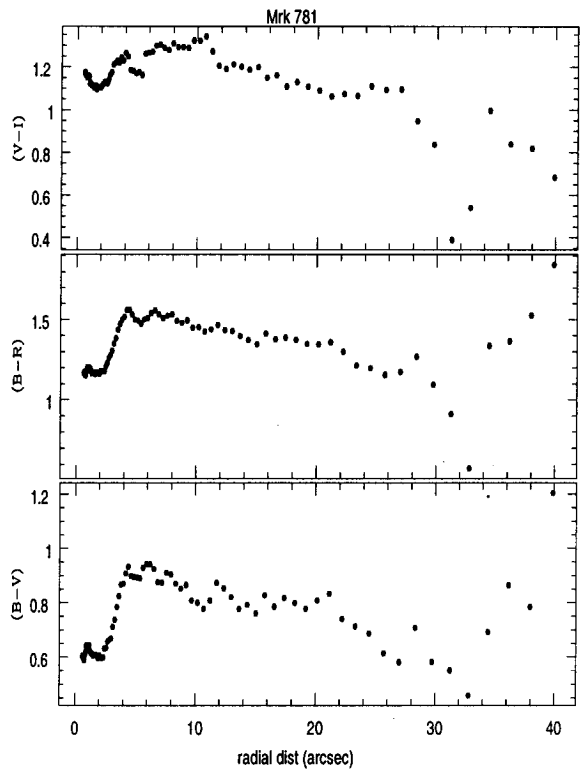
Mrk 781
(V−I)
(B−R)
(B−V)
radial dist (arcsec)

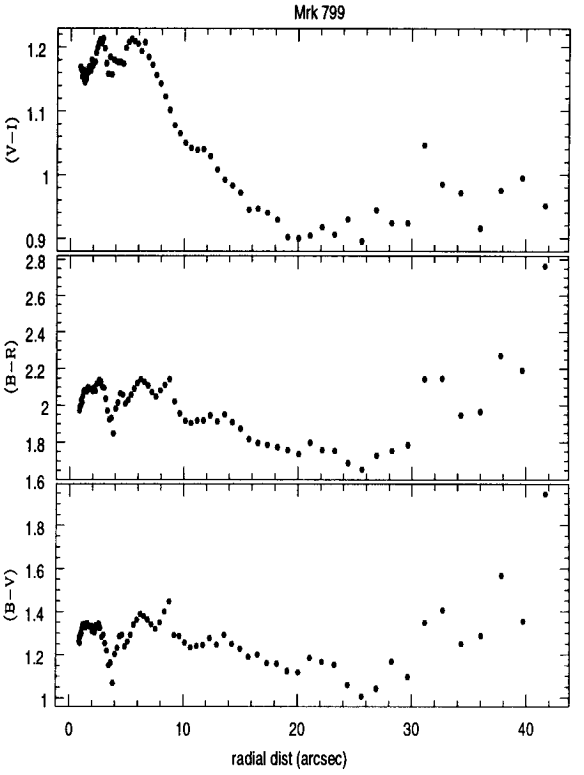
Mrk 799
(V−I)
(B−R)
(B−V)
radial dist (arcsec)

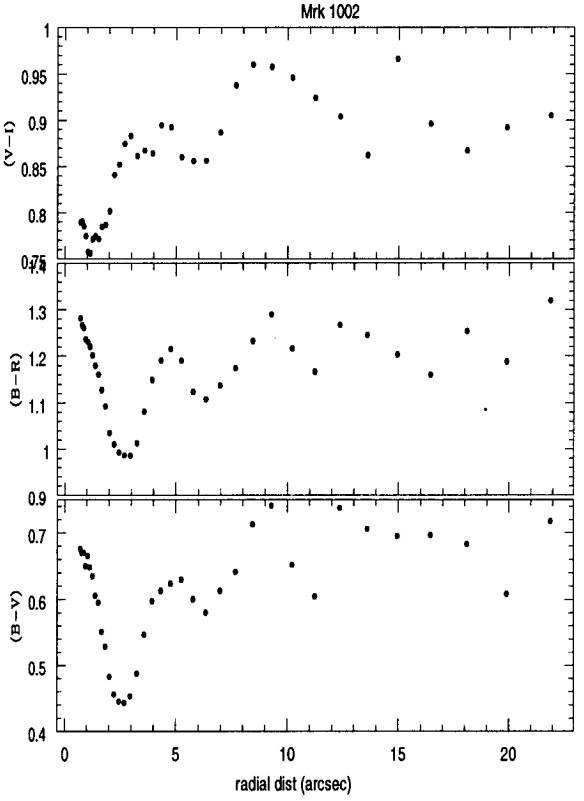
Mrk 1002
(V−I)
(B−R)
(B−V)
radial dist (arcsec)

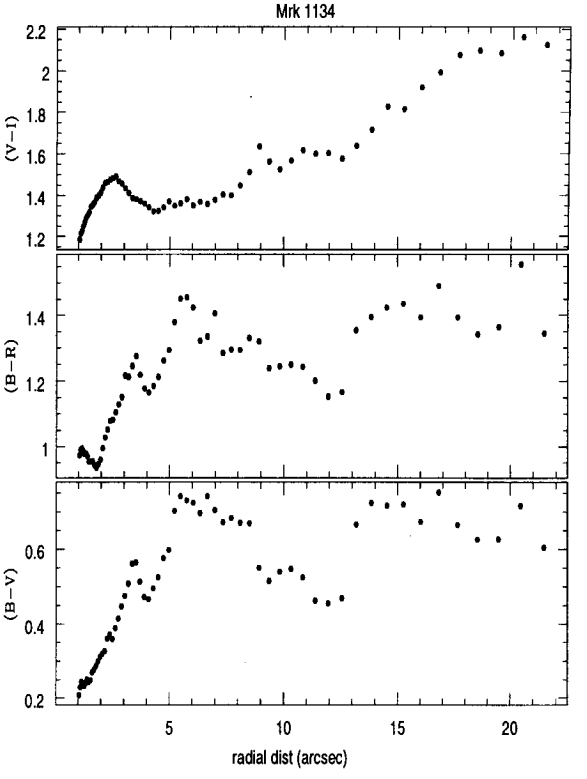
Mrk 1134
(V−I)
(B−R)
(B−V)
radial dist (arcsec)

Fig 4.6 (contd)

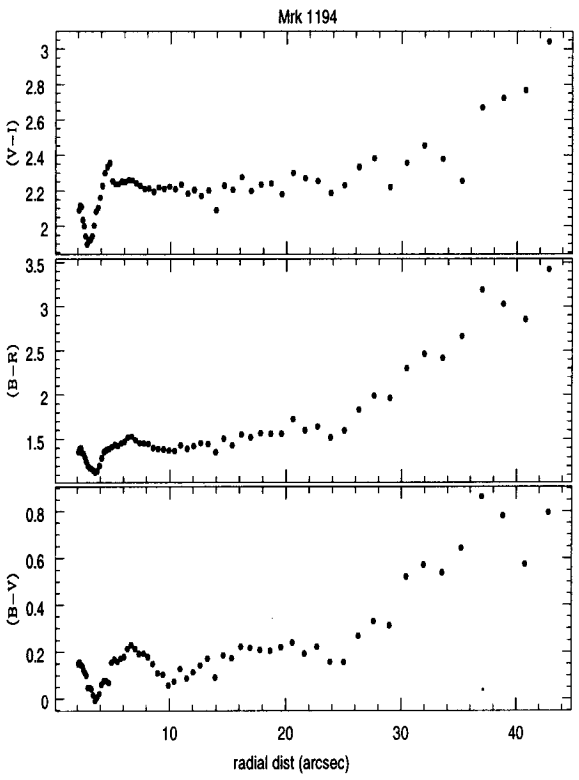
Mrk 1194
(V−I)
(B−R)
(B−V)
radial dist (arcsec)

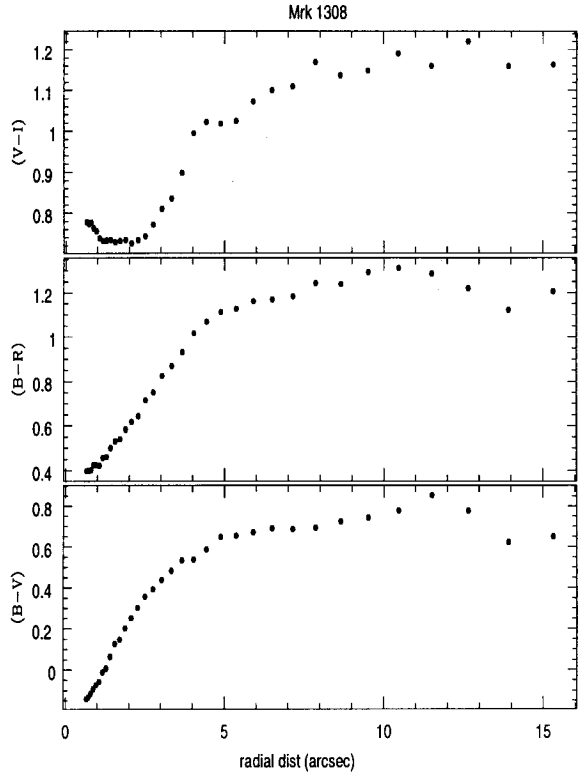
Mrk 1308
(V−I)
(B−R)
(B−V)
radial dist (arcsec)

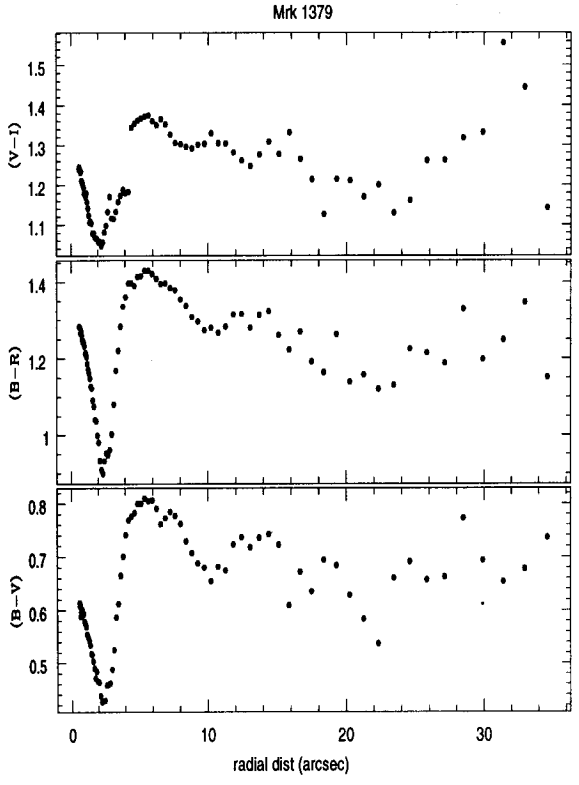
Mrk 1379
(V−I)
(B−R)
(B−V)
radial dist (arcsec)

Fig 4.6 (contd)

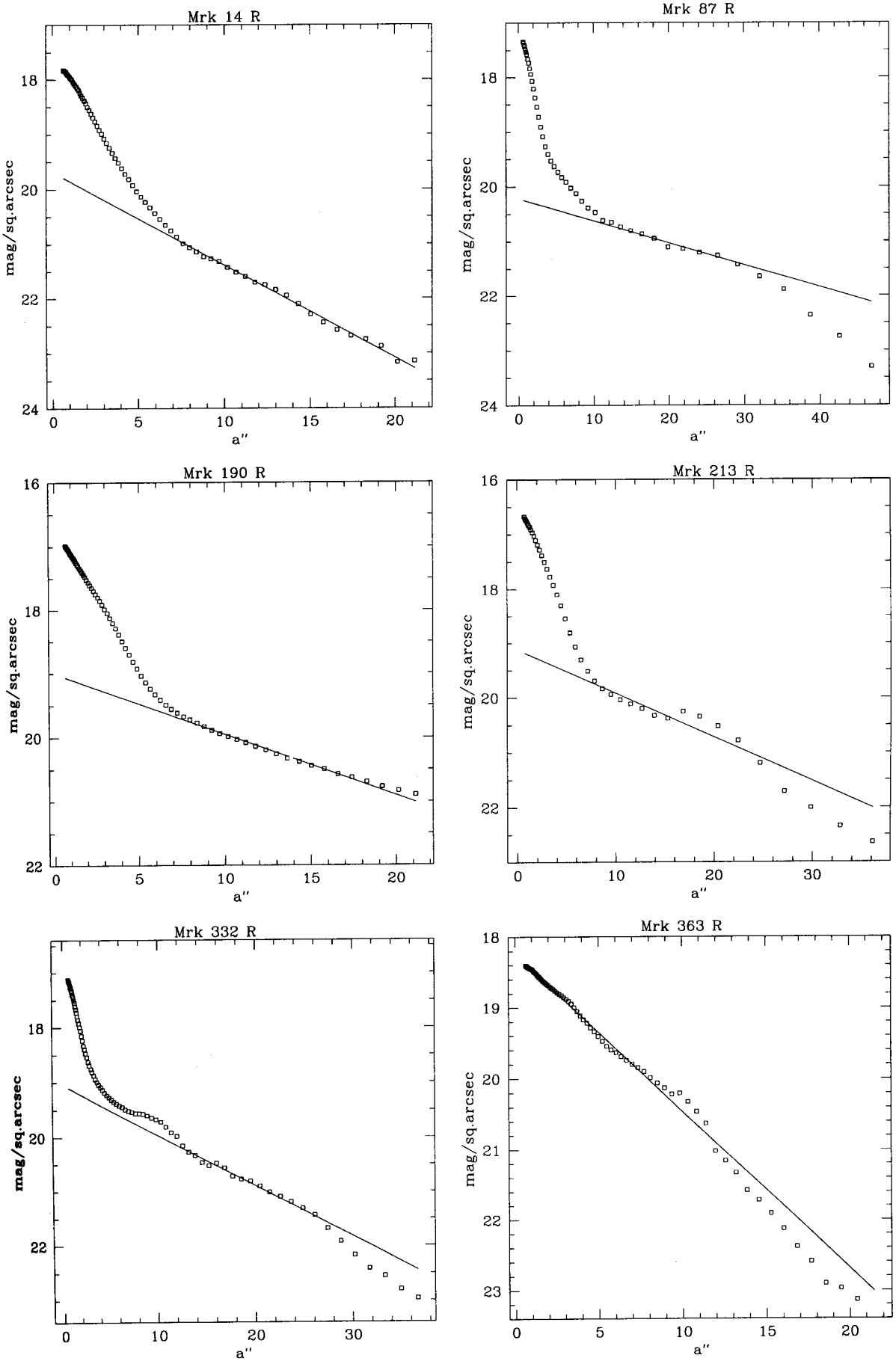

Fig 4.7 : Exponential fits to the R band image

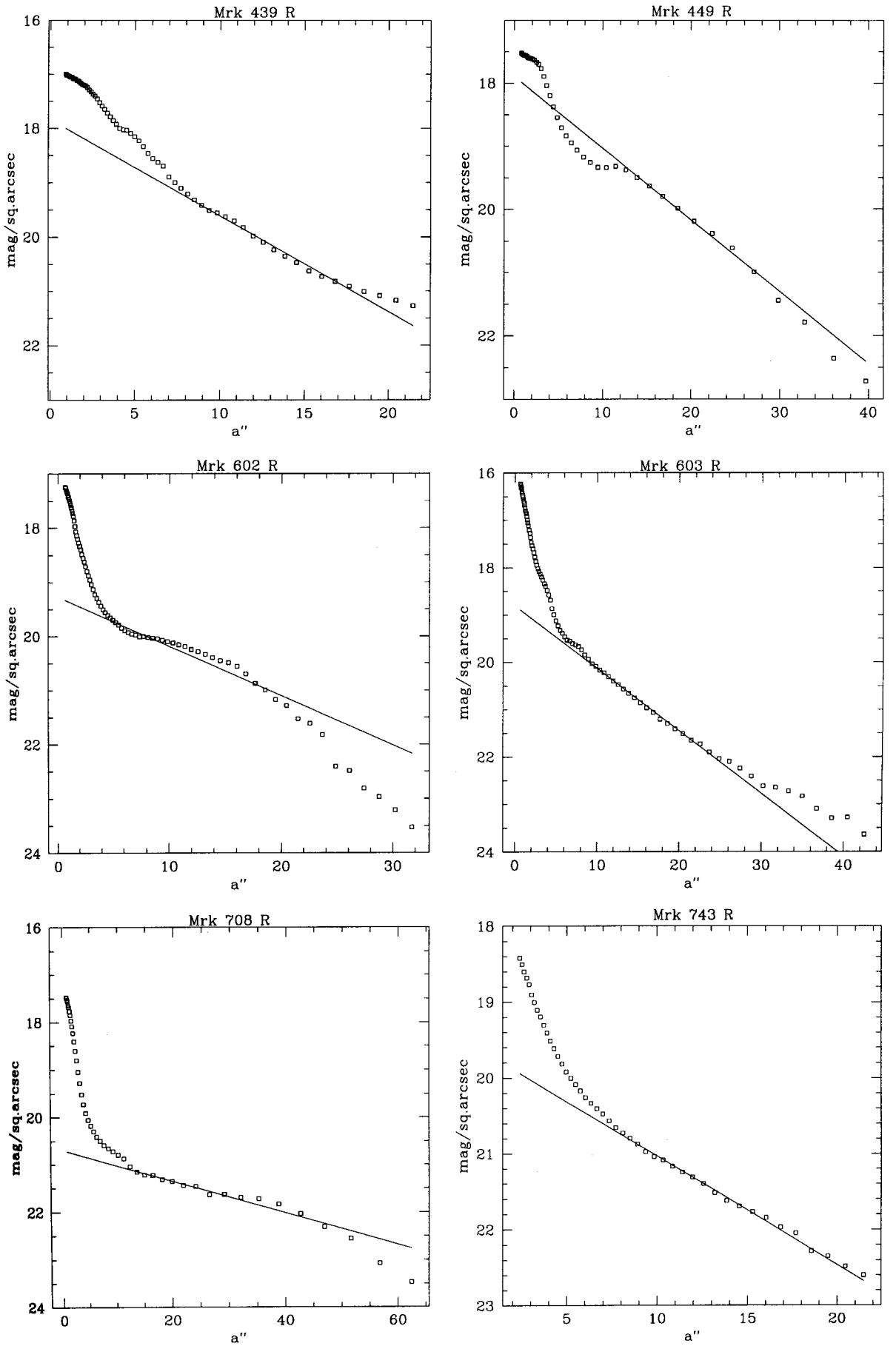

Fig 4.7 : Exponential fits to the R band image

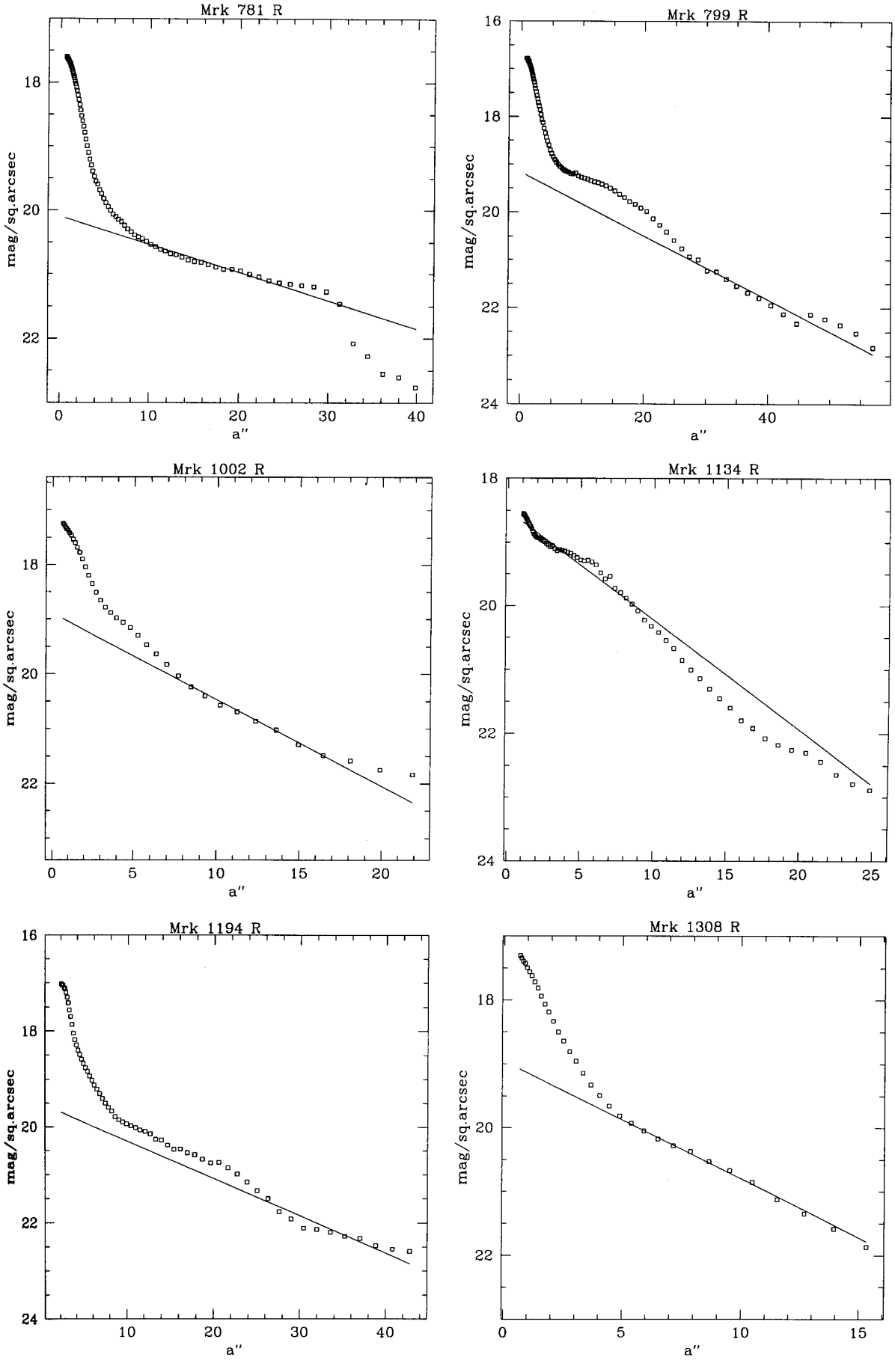

Fig 4.7 : Exponential fits to the R band image

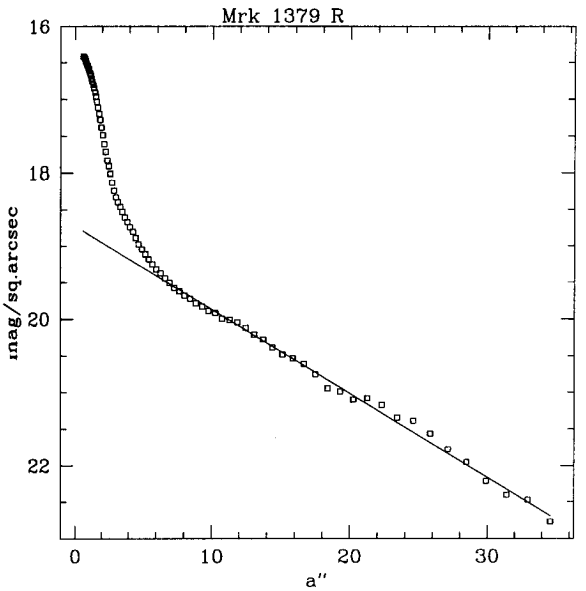

Fig 4.7 : Exponential fits to the R band image

Chapter 5

Models of starburst galaxies

Summary

We have attempted to estimate the age and the mass fraction involved in the burst episode for the sample galaxies. The present day stellar population of these galaxies is assumed to be made up of an old population and a younger burst population. An instantaneous burst is assumed. Both actively and passively evolving underlying populations have been considered. Ages between 10^6 and 10^7 are obtained for most of the galaxies.

5.1 *Overview*

Star formation seems to proceed in starburst galaxies as a series of short-lived but intense pulses followed by long quiescent periods (Searle et. al. 1973). These starbursts can completely dominate the output radiation almost at all observable wavelengths. As the stars of different masses evolve, the relative contribution of radiation at different wavelengths varies which gets reflected in the spectroscopic and the photometric properties of the starburst galaxy. While the stellar populations of only very few nearby galaxies can be resolved into individual stars, one has to depend on the integrated spectra and colours to derive information about the stellar population in distant galaxies. Larson & Tinsley (1978) modeled the colours of blue galaxies by superimposing a young starburst on an old galaxy population.

A star cluster is a population of coeval stars with a specified mass distribution and a galaxy is a superposition of such clusters weighted according to the rate of star formation at the epoch of cluster formation. Theoretically, all stellar populations may be broadly divided into two categories : the passive and active populations, the first supposed to have formed instantaneously and lacking any subsequent star formation and the second characterized by continuous ongoing star formation. Bica et al. (1990) simulate the occurrence of star formation events superimposed on old population by combining integrated spectra of star clusters of different ages with those of a red nucleus and derive $BVRI$ magnitudes. They consider two types of the underlying populations. Their E1 population represents ellipticals and S0s while the E3 population model is assumed for red nuclei in early type galaxies. Mas-Hesse & Kunth (1991) also present a set of evolutionary synthesis models to study the properties of the star formation episodes taking place in starburst regions.

Massive stars evolve off the main sequence in a only a few million years. Since their lifetimes are very small as compared to the age of the galaxy, it is reasonable to assume that they have all formed coevally in an instantaneous burst of

star formation. Charlot (1996) has reviewed various existing models of young/ star forming galaxies. In this chapter, we discuss the construction of starburst models using the spectra of different ages. These models are subsequently applied to the observed data.

5.2 *Model Construction*

We have attempted to estimate the ages and the mass involved in the burst component for our sample of starburst galaxies. For generating the models, we have used synthetic spectra provided by Guiderdoni. The details of the generation of the spectra for different ages is explained in Guiderdoni & Rocca-Volmerange (1987). The synthetic spectra have been generated using the Scalo (1986) piece-wise IMF which is of the form :

$$\begin{aligned} \phi(m) \propto m^{-x} \quad \text{with} \quad & x = 0.25 \quad 0.1M_{\odot} < m < 1.0M_{\odot} \\ & x = 1.35 \quad 1.0M_{\odot} < m < 2.0M_{\odot} \\ & x = 1.70 \quad 2.0M_{\odot} < m < 120M_{\odot} \end{aligned} \tag{5.1}$$

Stellar tracks from the Geneva group were used. The tracks include four evolutionary stages viz. Main Sequence, Giant Branch, "red" Horizontal Branch and Asymptotic Giant Branch. The output spectra has been generated for the ages 0,1,2...9 Myr, 10,20,...90 Myr, 100,200,...900 Myr, 1G,1.1G,1.2G,....20G. The spectra covers the wavelength range from 0.009 μm to 140 μm. The fluxes have been computed at intervals of 0.01μm and the fluxes are given in units of erg $s^{-1}\mu m^{-1}{M_{\odot}}^{-1}$. We used the spectra corresponding to solar metallicity since the mean metallicity of stars rapidly approaches the solar value. Guiderdoni & Rocca-Volmerange (1987) adopt a stellar library of observed stellar spectra computed from far UV to IR by using the IUE spectral atlases given by Wu et al. (1983) and Heck et al. (1984) and the visible atlas given by Gunn & Stryker (1983).

5.2.1 *Pure burst models*

The colours of the passive evolution of a pure burst of star formation were computed by convolving the synthetic spectra for the various ages mentioned above with the filter response curves and the resultant magnitudes in U, B, V, R and I bands were derived.

$$M = -2.5\log\left\{\int F_\lambda S_\lambda d\lambda\right\} \tag{5.2}$$

where M is the magnitude, F_λ and S_λ are the flux and the filter response at a wavelength λ. These were then converted to the colours $(U-B), (B-V), (V-R)$ and $(R-I)$. The colours corresponding to the passive evolution of an instantaneous burst population are presented in Fig.5.1. Leitherer & Heckman (1995) have reviewed the colour and the luminosity evolution of an instantaneous starburst. The colour evolution of an instantaneous burst shows the following three distinct phases.

1. During 0-3$\times 10^6$ years, there is very little colour evolution as the optical colours of hot stars are quite insensitive to temperature changes. The synthetic colours are similar to individual O and early B stars with an added nebular contribution.

2. After a few million years, massive stars of mass $\approx 50 M_\odot$ reach the red supergiant phase. This leads to a distinct reddening during the red supergiant phase. This leads to a distinct reddening of colours in all passbands at around 10^7 years.

3. After about 20 Myr, the O stars have either disappeared in case of an instantaneous burst and the colours redden gradually.

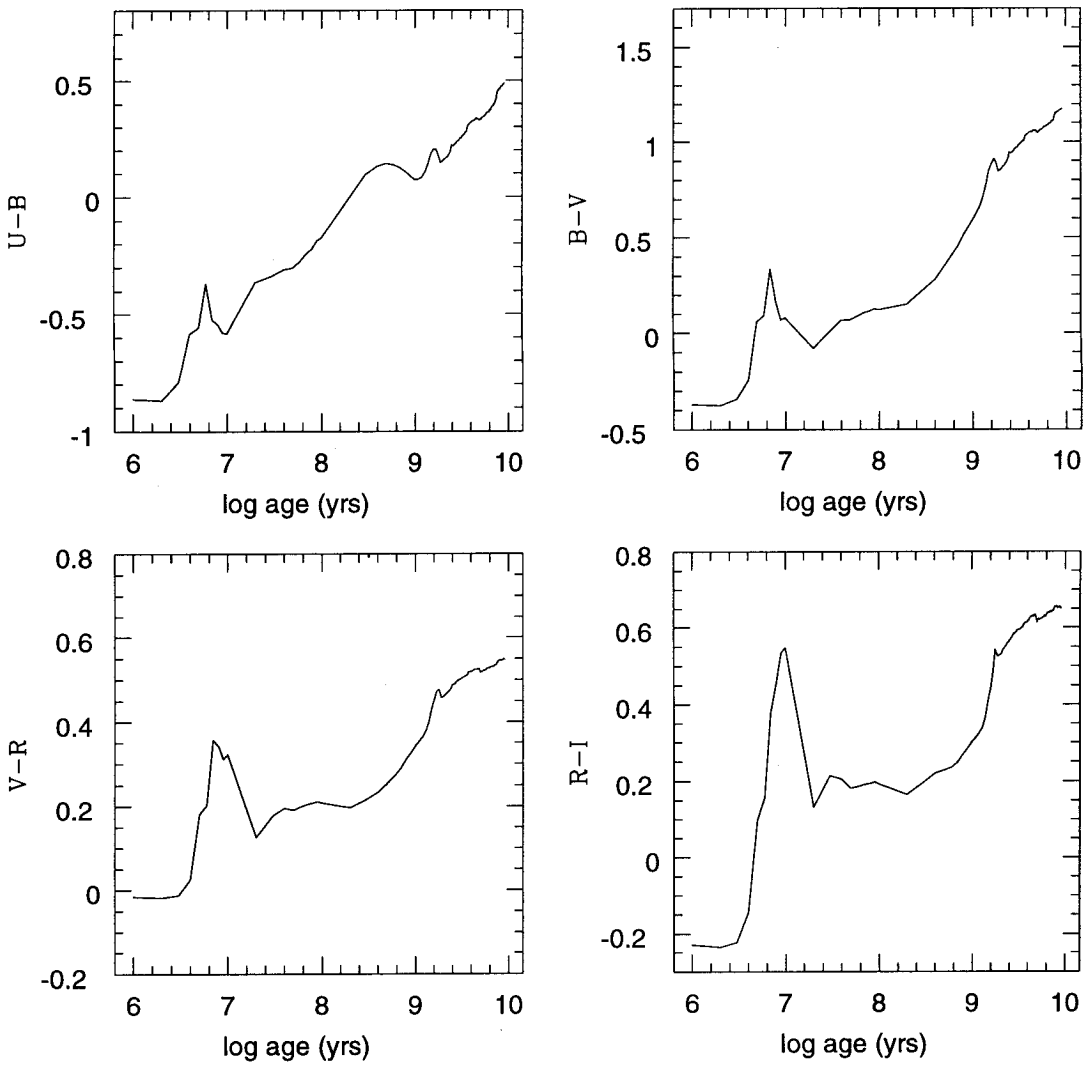

Figure 5.1: Colours of the passive evolution of an instantaneous burst population

5.2.2 *Composite populations*

We have constructed composite models to derive the ages and the mass contribution of the starburst component from the observed broad band colours. This basically involved adding a burst component to an old galaxy population and tracing its evolution in colour with time. An instantaneous burst was taken in both the cases. We tried to model the colours using two approaches. In one case, the underlying population was considered to be a single age population and in the second case, the underlying population was considered to be actively evolving. These two approaches are described below.

5.2.3 *Model A : Passively evolving population*

O'Connell (1996) suggests that the simplest approach would be to use a pure, single generation model. The first approach assumed the underlying galaxy to be made up of a coeval population of stars and an instantaneous burst was superimposed on this population and the resulting evolution studied. We call this Model A. The synthetic spectra for the various ages were first split to include only the optical wavelengths. The filter response curves were interpolated with the same resolution as that of the spectra. The fluxes at 13 Gyr were taken to be representative of the old underlying population of stars. The burst component was added to this spectrum. We varied the burst ages from 1 Myr to 9 Gyr. The burst strength 'b' as the ratio of the mass of the newly formed stars to the total mass of the galaxy. Larson & Tinsley (1978) put an upper limit of 5% on the fractional mass of the stars formed in the burst since this is approximately the gas content of a typical spiral galaxy. We varied the mass contribution from 1% to 5%. The total flux at each wavelength was computed by summing over the contribution from the old population and the young burst at that wavelength using the scaling factor of mass taking part in the burst. These fluxes were then convolved with the filter response curves and the resultant magnitudes and colours determined. The resultant evo-

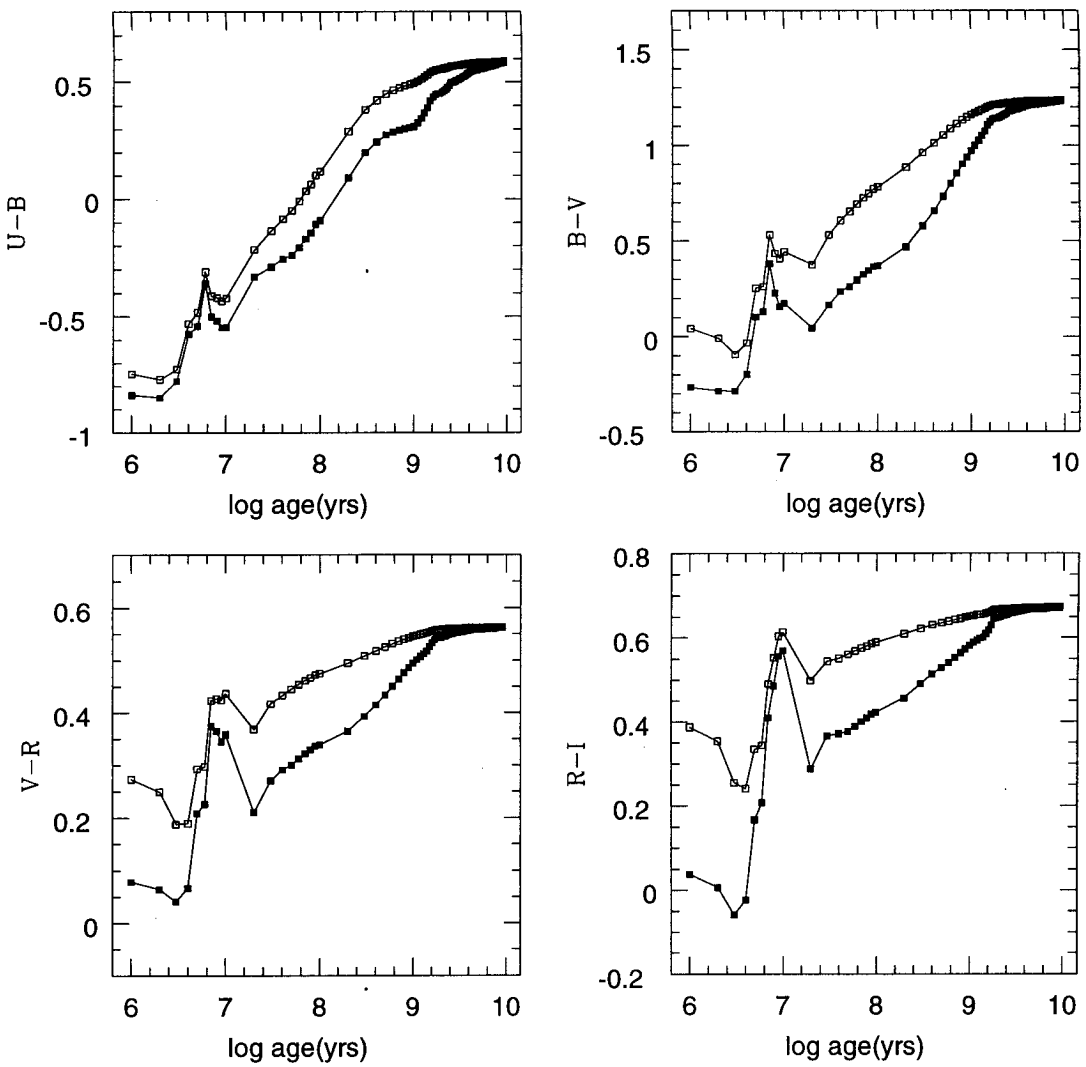

Figure 5.2: Colour evolution of a composite population comprising of an old population (13 Gyr) and an instantaneous burst. The X-axis represents the age of the burst and the Y-axis the colour of the composite population. The curves with the filled squares and the open squares correspond respectively to a mass fraction of 1% and 5%.

lution of the colours of a starburst galaxy in which the burst comprises of a mass fraction of 1% and 5% are shown in Fig. 5.2. It is seen that $(R-I)$ is most sensitive to age for ages between 10^6 and 10^7 years. After about 10^9 years, the mass fraction does not influence the colour of the galaxy to a great extent.

5.2.4 *Model B : Actively evolving population*

The Hubble sequence is described as a sequence of changing star formation histories (Kennicutt 1998 and references therein). The stellar birthrate changes with the galaxy type. The star formation history for a normal galaxy is usually parameterized as an exponential function of time (Huchra 1977b). We parameterized the star formation law by an exponential of the form :

$$\psi(t) = \exp(-t/\tau) \tag{5.3}$$

In this case, the underlying population will contain contributions from all ages scaled by the above equation. We used values of τ ranging from 0,1,2,2.5,3,5...15,∞. The spectra were scaled using this law, added together and the resultant colours computed for each value of τ. These colours were compared with the disk colours from the colour profiles given in Fig. 4.6. We found that most of the disk colours are consistent with the colours obtained using τ = 2.5. Donas et al. (1987), based on uv flux measurements also find the median value of the gas consumption time scale in star formation to be 2.5 Gyr. Using this as the underlying galaxy template, a burst was superimposed on this template. Following the same procedure explained in the case of Model A, the colour evolution of this system was derived. Fig. 5.3 shows the evolution in colours for a model comprising of an actively evolving underlying galaxy and a superimposed instantaneous burst. It is seen that for young systems, the two models would predict similar results. For systems having ages greater than about 3×10^7 years, the two models show a large difference in their behaviour. This is because the burst population starts reddening gradually

while the young stars in the underlying galaxy start contributing at shorter wavelengths. The asymptotic values reached by the colours in Model B are bluer than those predicted by Model A.

5.3 *Comparison with observed colours.*

The colours obtained for the galaxies were corrected for galactic and inclination extinction and compared with the colours derived by Model A. We present the results in Table 5.1. From a comparison of the observed colours and the model values in Table 5.1 we see that Model A is able to reproduce most of the observed colours. The predicted values fit the observed values quite well especially for early type systems. A comparison of the observed values and predicted values is shown in Fig. 5.4 for three galaxies, one from each class : S0/E0(Mrk 1308), spiral (Mrk 332) and irregular/peculiar (Mrk 363). The observed values and the model calculations match quite well.

The galaxies in our sample belong to different Hubble types and hence the star formation histories of the underlying galaxies will be different. In other words, the value of τ will depend on the Hubble type of the galaxy. Each galaxy in the sample has to be studied separately in Model B. Additional spectrophotometric data as well as data in the IR, radio and UV will help in correctly estimating the reddening as well as give information about characteristic lines which will help in understanding these galaxies in more depth. Such multiwavelength information will help to derive burst ages and strengths with greater accuracy.

5.4 *Conclusions*

We have constructed composite models to estimate the age and strength of the burst in the sample galaxies. We find that a model constructed by superimposing a young burst on a single generation old population is able to produce the colours

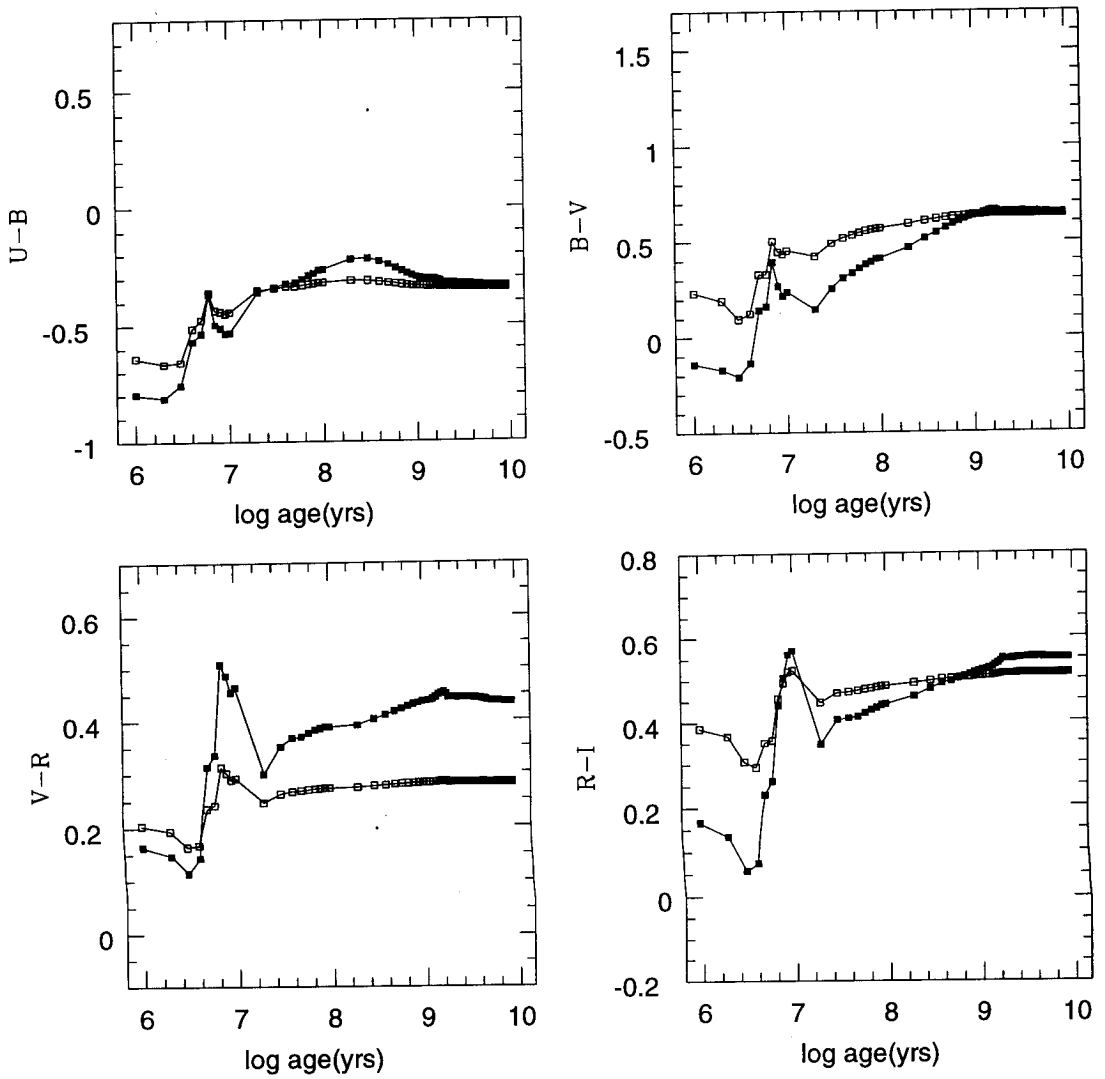

Figure 5.3: Colour evolution of a composite population comprising of an actively evolving population and an instantaneous burst. The X-axis represents the age of the burst and the Y-axis the colour of the composite population. The curves wit h the filled squares and the open squares correspond respectively to a mass fraction of 1% and 5%.

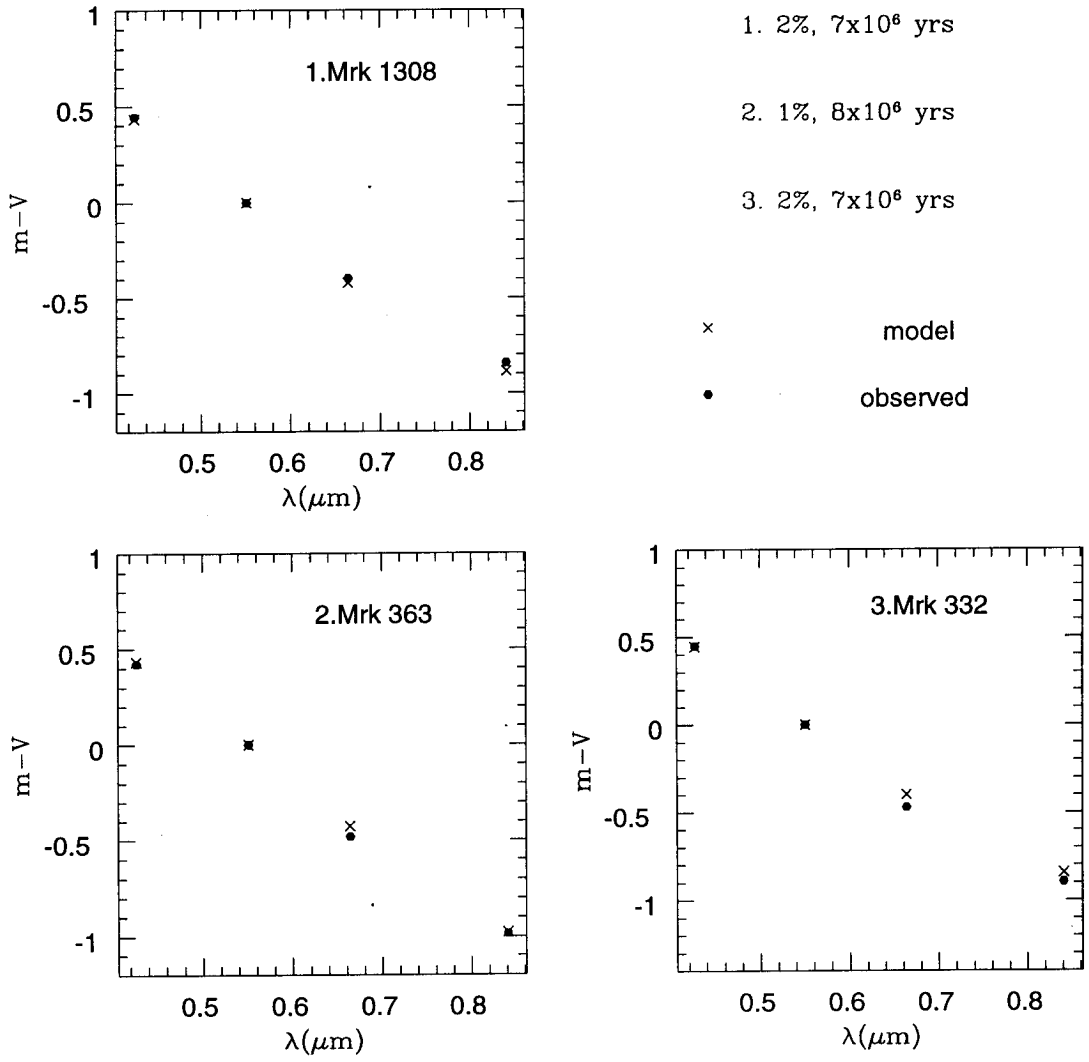

Figure 5.4: Comparison of the observed and model colours

Table 5.1: Comparison of the observed colours with the model predictions for Model A along with the mass fraction (b) and the ages of the burst predicted by Model A.

Galaxy	Observed			Model A				
	$(B-V)$	$(V-R)$	$(R-I)$	$(B-V)$	$(V-R)$	$(R-I)$	b	age(10^6)
14	0.41	0.43	0.38	0.39	0.38	0.41	4	7
87	0.73	0.59	0.62	0.77	0.47	0.58	1	90
190	0.61	0.53	0.63	0.65	0.44	0.56	1	50
213	0.51	0.47	0.51	0.53	0.42	0.49	1	7
332	0.45	0.47	0.42	0.44	0.40	0.45	2	7
363	0.42	0.48	0.50	0.43	0.43	0.55	1	8
439	0.54	0.33	0.37	0.47	0.36	0.45	5	200
449	0.49	0.41	0.49	0.49	0.39	0.50	2	60
602	0.83	0.63	0.58	0.88	0.49	0.61	1	100
603	0.50	0.51	-	0.38	0.37	0.41	5	7
708	0.44	0.10	0.30	0.26	0.29	0.34	1	6
743	0.31	0.43	0.59	0.44	0.43	0.61	2	10
781	0.58	0.48	0.54	0.60	0.43	0.55	1	40
799	0.97	0.67	0.76	1.012	0.517	0.63	1	400
1002	0.50	0.49	0.55	0.53	0.41	0.54	1	30
1134	0.47	0.58	0.58	0.44	0.44	0.61	1	1
1194	0.59	0.40	0.61	0.60	0.43	0.55	1	40
1308	0.43	0.42	0.46	0.44	0.40	0.45	2	7
1379	0.51	0.49	0.67	0.44	0.44	0.61	1	10

observed. In most cases, we find that the model values compare very well with the observed values and we derive ages ranging from 10^6 to 10^7 years for these cases. In a few cases like Mrk 799 and Mrk 439, we get older systems. For a detailed study of each object, spectral information and additional data at other wavelengths can help constrain the models better.

Chapter 6

Conclusions and scope for future work

This thesis has concentrated on describing the spatial distribution and the properties of the star forming regions and the structure of the underlying galaxy hosting the starburst. The conclusions have been given in detail at the end of each chapter. A brief summary is given below.

- Optical Morphology

  The morphology of the galaxies was studied through various broad bands, narrow-band Hα and colour maps. This study revealed that starbursts occur in a variety of morphological environments. The galaxies in which the starburst phenomenon is seen can be broadly grouped into S0's/E's, spirals and irregulars. Starburst activity as indicated by blue colours and Hα emission is seen predominantly in the central region of the galaxies. However, activity is not only confined to the central kpc, but is also found in the form of circumnuclear rings, at the ends of bars or even globally. Except in the case of Mrk 439, the line emission and the blue regions are coincident indicating that the same episode of star formation is responsible for both these observed results.

- Structural properties

  The structural properties of the underlying galaxies were studied using ellipse fitting techniques.

  Isophotal twists were detected in all the S0's/E's galaxies in the sample. Signatures of dust were found in the central regions of Mrk 1379, Mrk 439 and

Mrk 1134. A strong dust lane was found in Mrk 449. Besides these, all the other objects appear to be relatively dust free along the line of sight. Ellipse fitting analysis reveals variety of fine structure indicative of mergers, hidden distortions like bars, rings of star formation, etc. Spiral arms extending right into the nuclear region were found in Mrk 363. We detect secondary bars in Mrk 213 and Mrk 1194.

- Age of the burst

  On the basis of composite models constructed we derive ages between 10^6 and 10^7 years for most of the sample objects. This is consistent with the fact that we observe Hα emission nearly coincident with the optically blue colours.

In general, we find that the sample of galaxies shows considerable extranuclear star formation. The Hα intensity is highest in the central regions but the induced star formation relative to the underlying population shows varying behaviour. In some cases like Mrk 363, Mrk 332 and Mrk 439, the nuclear pseudo E.W. is lower than its global value. This suggests that the induced star formation relative to the underlying population is higher at locations other than the nucleus. For galaxies with star formation confined to the central regions, it is seen that the half-light radii in B are smaller than the half-light radii in R. This is seen in case of S0's/E's in the sample. In case of spirals, the extranuclear star formation contributes to the B band and we find the half-light radii in B to be greater than those in R. The scale lengths of all the sample galaxies are comparable in B and R. All the galaxies in the sample get redder outwards. However, two galaxies namely, Mrk 708 and Mrk 602 get bluer outwards and these show blue scale lengths larger than the red scale lengths.

6.0.1 *Future work*

Near infrared imaging of these galaxies would prove to be very useful in probing the structure of the underlying galaxy better. Most of the mass of the galaxy is locked up in low mass stars and the near infrared wavelengths are the best tracers of this population. Since most of the mass of the galaxy is in this stellar population, it dictates the dynamics of the galaxy. It would be interesting to apply the methodology developed in this thesis to study the galaxies at near infrared wavelengths. Input from these studies will also help in further constraining the starburst models. In addition to this, kinematical studies of starburst galaxies will be very useful in understanding the distribution of gas.

Bibliography

[1] Aaronson M., Mould J., Huchra ., 1980, ApJ 237, 655

[2] Aguilar L.A., White S.D.M., 1986, ApJ 307, 97

[3] Arsenault R., 1989, A&A 217, 66

[4] Baade W., 1944, ApJ 100, 137

[5] Balzano V.A., 1983, ApJ 268, 602

[6] Barbon R., Benacchio L., Capaccioli M., 1976, A&A 51, 25

[7] Barnes J.E., Hernquist L., 1992, ARAA 30, 705

[8] Barth C.S., Coziol R., Demers S. 1995, MNRAS 276, 1224

[9] Bender R., Döbereiner S., Möllenhoff C., 1988, A&AS 74, 385

[10] Bender R., Möllenhoff C., 1987, A&A 177, 71

[11] Bertola F., Galletta G., Zeilinger W.W., 1985, ApJ 292, 51

[12] Bessell M.S., 1990, PASP 102, 1181

[13] Bica E., Alloin D., Schmidt A., 1990, MNRAS 242, 241

[14] Binney J., Petrou M., 1985, MNRAS 214, 449

[15] Borne K.D., 1984, ApJ 287, 503

[16] Boroson T., 1981, ApJS 46, 177

[17] Bothun R.D., Halpern J.P., Lonsdale C.J., 1989, ApJS 70, 271

[18] Bruzual G.A., 1996, in *From Stars to Galaxies*, ASP Conference Series, eds. Leitherer C., Fritze-v. Alvensleben & Huchra J., 98, p.14

[19] Burstein D., Heiles C., 1984, ApJS 54, 33

[20] Burstein D., Krumm N., Salpeter E.E., 1987, AJ 94, 883

[21] Bushouse H. A., 1986, Ph.D thesis, University of Illinois at Urbana-Champaign

[22] Buta R., 1986, ApJS 61, 631

[23] Charlot S., 1996, in *From Stars to Galaxies*, ASP Conference Series, eds. Leitherer C., Fritze-v. Alvensleben & Huchra J., 98, p.275

[24] Chini R., 1987, in *Starbursts and Galaxy Evolution*, eds Thuan T.X., Montmerle T. & Tran Thanh Van J. (Editions Frontières, Gif-sur-Yvette) p.193

[25] Combes F., 1987, in *Starbursts and Galaxy Evolution*, eds Thuan T.X., Montmerle T. & Tran Thanh Van J. (Editions Frontières, Gif-sur-Yvette) p.325

[26] Combes F., 1998, in *Starbursts Triggers, Nature and Evolution* eds. B. Guiderdoni, A. Kembhavi, Springer p.175

[27] Combes F., Gerin M., 1985, A&A 150, 327

[28] Condon J.J., Condon M.A., Gisler G., Puschell J.J., 1982, ApJ 252, 102

[29] Condon J.J., Dressel L.L., 1978, ApJ 221, 456

[30] Condon J.J., Huang Z.P., Yin Q.F., 1991, ApJ 378, 65

[31] Contini T., Considere S., Davoust E., 1998, A&AS 130, 285

[32] Contini T., Davoust E., Considere B., 1995, in *The World of Galaxies II*, Astro. Lett. & Communications, guest eds. Paturel G., Petit Chantal

[33] Contini T., Wozniak H., Considere S., Davoust E., 1997, A&A 324, 41

[34] Courteau S., 1996, ApJS 103, 363

[35] Coziol R., Demers S., Barneoud R., Pena M., 1997, AJ 113, 1548

[36] Cutri R.M., McAlary C.W. 1985, ApJ 296, 90

[37] de Jong R.S., 1996, A&A 313, 45

[38] de Mello D.F., Keel W.C., Sulentic J.W., Rampazzo R., Bica E., WhiteIII R.E., 1995, A&A 297, 331

[39] Deutsch L.K., Willner S.P., 1986, ApJ 306, L11

[40] Deutsch L.K., Willner S.P., 1987, ApJS 63, 803

[41] Devereux N.A., Hameed S., 1997, AJ 113, 599

[42] de Vaucouleurs G., 1953, MNRAS 113, 134

[43] de Vaucouleurs G., 1959, ApJ 130, 728

[44] de Vaucouleurs G., 1974 in *Formation of Galaxies*; Proc. IAU Symp, 58, Shakeshaft J.R. (ed), Reidel, Dordrect, p.335

[45] Donas J., Deharveng J.M., Laget M., Milliard B., Huguenin D., 1987, A&A 180, 12

[46] de Vaucouleurs G., Capaccioli M., 1979, ApJS 40, 699

[47] Doublier V., Comte G., Petrosian A., Surace C., Turatto M., 1997, A&AS 124, 405

[48] Dressler A., 1984, ARAA 22, 185

[49] Elmegreen D.M., Elmegreen B.G., Bellin A.D., 1990, ApJ 364, 415

[50] Faúndez-Abans M., de Oliveira-Abans M., 1998, A&AS 128, 289

[51] Fabbiano G., Feigelson, E., Zamorani, G., 1982, ApJ 266, L5

[52] Franceschini A., Danese L., De Zotti G., Toffolatti L., 1988, MNRAS 233, 157

[53] Franx M., Illingworth G.D., 1988, ApJ 327, L55

[54] Freeman K.C. 1987, ARAA 25, 603

[55] Friedli D., Benz W., 1993, A&A 268, 65

[56] Friedli D., Martinet L., 1993, A&A 277, 27

[57] Frogel J.A., 1985, ApJ 298, 528

[58] Geller M.J., Huchra J.P., 1983, ApJS 52, 61

[59] Gilmore G., King I.R., van der Kruit P.C., 1990, in *The Milky Way as a Galaxy*, ed. R. Buser, University Science Books.

[60] Guiderdoni B., Rocca-Volmerange B., 1987, A&A 186, 1

[61] Gunn J.E., Stryker L.L., 1983, ApJS 52, 121

[62] Haro G., 1956, Bol. Obs. Tonantzintla y Tacubaya 2, 8

[63] Hawarden T.G., Longmore A.J., Tritton S.B., Elson R.A.W., Corwin H.G.Jr., 1981, MNRAS 196, 747

[64] Heckman T.M., 1978, PASP 90, 241

[65] Heller C.H., Shlosman I., 1994, ApJ 424, 84

[66] Heraudeau P, Simien F., Mamon G.A., 1996 A&AS 117, 417

[67] Hernquist L., 1992, ApJ 400, 460

[68] Hernquist L., 1993, ApJ 409, 548

[69] Hodge P.W., 1975, ApJ 202,619

[70] Hodge P.W., Kennicutt R.C., 1983, ApJ 267, 563

[71] Hubble E., 1930, ApJ 71, 231

[72] Huchra J.P., 1977a, ApJS 35,171

[73] Huchra J.P., 1977b, ApJ 217, 926

[74] Hummel E., 1980, A&A 89, L1

[75] Hunter D.A., Gallagher J.S.III., 1986, PASP 98, 5

[76] Icke V., 1985, A&A 144, 115

[77] Ishizuki S., Kawabe R., Ishiguro M., Okumura S., Morita K., 1990, Nature 344, 224

[78] Jedrzejewski R.I., 1987a, MNRAS 226, 747

[79] Jedrzejewski R.I., 1987b, in *Structure and Dynamics of Elliptical Galaxies*, ed. Tim De Zeeuw, D. Reidel Publishers, p.37

[80] Joseph R.D., Meikle W.P.S., Robertson N.A., Wright G.S., 1984, MNRAS 209, 111

[81] Joseph R.D., Wright G.S., 1985, MNRAS 214, 87

[82] Jungwiert B., Combes F., Axon D.J., 1997, A&AS 125, 479

[83] Keel W.C., Kennicutt R.C., Hummel E., van der Hulst J.M., 1985, AJ 90, 708

[84] Keel W.C., van Soest E.T.M., 1992, A&AS 94, 553

[85] Kenney J.D.P., Koopmann R.A., Rubin V.C., Young J.S., 1996, AJ 111, 152

[86] Kennicutt R.C., 1983, ApJ 272, 54

[87] Kennicutt R.C., 1998, in *Starbursts Nature, Triggers and Evolution* eds. B. Guiderdoni, A. Kembhavi, Springer p.1

[88] Kennicutt R.C., Roettiger K.A., Keel William C., van der Hulst J.M., Hummel E., 1987, AJ 93, 1011

[89] Kent S.M., 1984, ApJS 56, 105

[90] King I.R., 1978, ApJ 222,1

[91] Knapen J.H., van der Kruit P.C., 1991, A&A 248, 57

[92] Kormendy J., 1982, in *Morphology and Dynamics of Galaxies*, Twelfth Saas-Fee Advanced Course, (Sauverny : Geneva Observatory)

[93] Landolt A.U., 1992, AJ 104, 340

[94] Larson R.B., 1987, in *Starbursts and Galaxy Evolution*, eds Thuan T.X., Montmerle T. & Tran Thanh Van J. (Editions Frontières, Gif-sur-Yvette) p.467

[95] Larson R.B., Tinsley B.M., 1978, ApJ 219, 46

[96] Leitherer C., Heckman T.M., 1995, ApJS 96, 9

[97] Leonardi A.J., Rose J.A., 1996, AJ 111, 182

[98] Li J.G., Seaquist E.R., Wang Z., Sage L.J., 1994 AJ 107, 90

[99] Liller M.H., 1960, ApJ 132, 306

[100] Liller M.H., 1966, ApJ 146, 28

[101] Lo K.Y., Berge G.L., Claussen M.J., et al., 1984 ApJ 282, L59

[102] Lonsdale C.J., Persson S.E., Matthews K., 1984, ApJ 287, 95

[103] Márquez I., Moles M., 1994, AJ 108, 90

[104] Malin D.F., 1979, Nature 277, 279

[105] Markarian B.E., 1983, Afz 19, 29

[106] Mass-Hesse J.M., Kunth D., 1991, A&AS 88, 399

[107] Massey P., Jacoby G.H., 1992, in *Astronomical CCD observing and reduction techniques*, ASP Conference Proceedings, ed. Steve B. Howell, San Fransisco, CA., 23 p.240

[108] Mazzarella J.M., Balzano V.A., 1986, ApJS 62, 751

[109] Mazzarella J.M., Boroson T.A., 1993, ApJS 85, 27

[110] Mihos J.C., Hernquist L., 1994, ApJ 425, L13

[111] Moorwood A.F.M., 1996, SSRv 77, 303

[112] Neff S.G., Hutchings J.B., 1992, AJ 104, 1

[113] Nieto J.L., Bender R., 1989, A&A 215, 266

[114] Noguchi M., Ishibashi S., 1986, MNRAS 219, 305

[115] O'Connell R.W., in *From Stars to Galaxies*, ASP Conference Series, eds. Leitherer C., Fritze-v. Alvensleben and Huchra J., 98, p.3

[116] Peletier R.F., Valentijn E.A., 1989, Ap&SS 156, 127

[117] Petrosian A.R., Burenkov A.N., 1993, A&A 279, 21

[118] Pogge R.W., Eskridge P.B., 1993, AJ 106, 1405

[119] Prieto M., Beckman J.E., Cepa J., Varela A.M., 1992a, A&A 257, 85

[120] Prieto M., Longley D.P.T., Perez E., Beckman J.E., Varela A.M., Cepa J., 1992b, A&AS 93, 557

[121] Reynolds J.H., 1913, MNRAS 74, 132

[122] Rieke G.H., Lebofsky M.J., Thompson R.I., Low F.J., Tokunaga A.T., 1980, ApJ 238, 24

[123] Rieke G.H., Low F.J., 1975, ApJ 197, 17

[124] Rocca-Volmerange B., Lequeux J., Maucherat-Joubert M., 1981, A&A 104, 177

[125] Sargent W.L.W., Searle L., 1970, ApJ 162, L155

[126] Scalo J.M., 1986, FCPh 11, 1

[127] Scalo J.M., Struck-Marcell C., 1986, ApJ 301, 77

[128] Schwarz M.P., 1984, MNRAS 209, 93

[129] Schweizer F., 1983, I.A.U. 100, 319

[130] Schweizer F., 1986, Science 231, 227

[131] Schweizer F., Seitzer P., 1988, ApJ 328, 88

[132] Schweizer F., Seitzer P., 1992, ApJ 104, 1039

[133] Scoville N.Z., Hersh K., 1979, ApJ 229, 578

[134] Searle L., Sargent, W.L.W., Bagnuolo W.G., 1973, ApJ 179, 427

[135] Seaton M.J., 1979, MNRAS 187, 73

[136] Sersic J.L., Pastoriza M., 1967, PASP 79, 152

[137] Sharp N.A., Jones B.F., 1980, Nature 283, 275

[138] Shlosman I., Frank J., Begelman M.C., 1989, Nature 338 45

[139] Silva D.R., Elston R., 1994 ApJ 428, 511

[140] Simkin S.M., Su H.J., Schwarz M.P., 1980, ApJ 237, 404

[141] Soifer B.T., Rowan-Robinson M., Houck J.R., et al., 1984, ApJ 278, L71

[142] Soifer B.T., Sanders D.B., Madore B.F., Neugebauer G., Danielson G.E., Elias J.H., Lonsdale C.J., Rice W.L., 1987, ApJ 320, 238

[143] Stine P., 1992, ApJS 81, 49

[144] Struck-Marcell 1986

[145] Sulentic J.W., Keel W.C., Telesco C.M., 1990, in *Paired and Interacting Galaxies*, International Astronomical Union Colloquim No. 124

[146] Telles J.E., 1995, Ph.D thesis, University of Cambridge

[147] Tinsley B.M., 1972, ApJ 178, 319

[148] Tinsley B.M., Danly L., 1980, ApJ 242, 435

[149] Toomre A., Toomre J., 1972, ApJ 178, 623

[150] Tully R.B., 1988, in *Nearby Galaxies Catalog*, Cambridge University Press

[151] Turner J.L., Hurt R.L:, 1992, ApJ 384, 72

[152] van Driel W., van Woerden H., 1991, A&A 243, 71

[153] van Moorsel G., 1988, A&A 202, 59

[154] van den Bergh S., 1980, PASP 92, 409

[155] van den Driel W., van den Broek A.C., de Jong T., 1991 A&AS 90, 55

[156] Vorontsov-Velyaminov B.A., 1977, A&AS 28, 1

[157] Weedman D.W., 1973, ApJ 183, 29

[158] Wiklind T., Henkel C., 1989, A&A 225, 1

[159] Williams T.B., Schwarzschild M., 1979, ApJ 227,56

[160] Worthey G., 1994, ApJS 95, 107

[161] Wozniak H., Friedli D., Martinet L.,Martin P., Bratschi P., 1995, A&AS 111, 115

[162] Wrobel J.M., Heeschen D.S., 1988, ApJ 335, 677

[163] Wrobel J.M., Heeschen D.S., 1991, AJ 101, 148

[164] Wunderlich E., Klein U., Wielebinski R., 1987, A&AS 69, 487

[165] Zepf S.E., Whitmore B.C., Levison H.F., 1991, ApJ 383, 524